LLB MICROMAGNETIC MODELS OF NANO-GRANULAR MAGNETIC THIN FILMS FOR ULTRA-HIGH DENSITY RECORDING MEDIA

LEWIS JACK ATKINSON

Doctor of Philosophy

University of York

PHYSICS

APRIL 2016

Abstract

The continuing need for increased information storage capacity has driven a remarkable increase in areal density over the lifetime of hard disk technologies, built on the physical principles of nano magnetic structures. Understanding how the component nano-granular magnetic recording media operates at ultra-high densities and how novel switching mechanisms, such as heat assisted magnetic recording (HAMR), impact the nature of magnetic data storage is essential. In this thesis current state-of-the-art macro scale modeling methods, built on the principles of the Landau-Lifshitz-Bloch equation, are developed and applied to better understand the physical principles that govern the ultra-high density recording media. The modeling method is shown to be in close agreement with experiment in a number of situations. The dependence of magnetic damping, the combination of intrinsic and extrinsic damping, due to inter-granular interaction is shown to be significant. The form of the damping arises due to a change in the degeneracy of the ferromagnetic frequency of spinwaves, as a function of both increasing magnetostatic and inter-granular exchange interactions. The observed damping results in a nontrivial dependence of the magnetic switching time on intergranular interactions, within the range for the intergranular exchange and saturation magnetisation that is likely in ultra-high density recording media. The nontrivial nature of the switching time should be taken in to consideration when selecting materials for the magnetic grains and inter-granular regions. A detailed investigation of the HAMR process is made, concentrating on the thermodynamic limits of the technology. The nature of HAMR is shown to be far more complex than simply magnetisation reversal over a thermally reduced energy barrier. It is shown that, to achieve the required level of magnetisation reversal a number of factors must be considered. The temperature rise must be to the Curie point or above, invoking the linear reversal mechanism, with a cooling rate that is sufficiently low to allow the temperature of the media to remain higher than the blocking temperature for a period of time significantly larger than the relaxation time of the material. Also, the write field must be sufficiently large not only to reverse the magnetisation, but also to ensure no thermally activated back switching of the magnetisation, as in the concept of thermal writability. Also a new method for approximating the magnetostatic field to a high level of accuracy with a computational runtime that is comparable with the tensor form of the dipole approximation has been developed and tested.

Table of Contents

List of Figures

Acknowledgements

I would like to take this opportunity to acknowledge and express my deepest thanks to all who have given help and advice and supported me throughout my doctoral studies.

First and foremost I would like to thank my supervisor, Professor Roy W. Chantrell, whom has made this work possible. Professor Chantrell has been an inspiration throughout my time studying at The University of York and without his help, support, advice and criticism I would not have achieved half of what I have to date.

I would also like to thank all the collaborative partners and colleague that have contributed to the research presented in this thesis. I would like to thank the collaborative researches, T.Y. Cheng and J. Wu at The University of York for the experimental work on continuous wave laser heating to induce magnetisation dynamics presented in chapter 6, B. Bergmans, J. Holhfeldt, B. Lu, KK Wang and GP Ju at Seagate Technologies for the experimental work on the damping dependence due to inter-granular interactions presented in chapter 4, T. Ostler for his work with the semi-analytical spinwave model in determining the source of the damping due to inter-granular interactions, R.W. Chantrell for his semi-analytical energy barrier approach to determining the switching time dependence due to damping as a function of the inter-granular exchange interaction and also S. Ruta for the use of his magnetostatic code that made the calculations possible in chapter 7.

I would also like to thank the people who gave excellent help and advice: R.W Chantrell, R.F.L. Evans, T. Ostler, S.Ruta and D. Serantes.

I would like to give a big thank you the advanced storage technology consortium (ASTC) for the funding that has made this research possible.

Finally I would like to thank Claire Sayers and Margaret Clegg for there administrative help throughout the period of my research studied at The University of York.

Declaration

The author of this thesis hereby declares that the following work is his own original work, excepting the work done in collaboration. The work done in collaboration includes experimental research done by T.Y. Cheng and J. Wu at The University of York, on continuous wave laser heating to induce magnetisation dynamics presented in chapter 6. Also, experiment research done by B. Bergmans, J. Holhfeldt, B. Lu, KK Wang and GP Ju at Seagate Technologies, on the damping dependence due to inter-granular interactions presented in chapter 4. Theoretical work by T. Ostler who developed and implemented the semi-analytical spinwave model for determining the source of the damping due to inter-granular interactions presented in chapter 4 and R.W. Chantrell for his semi-analytical energy barrier approach to determining the switching time dependence due to damping as a function of the inter-granular exchange interaction, also presented in chapter 4 and finally, S. Ruta for the use of his magnetostatic code that made the calculations possible presented in chapter 7. The author would also like to declare that the following work has not been submitted previously at this or any other university.

Published Papers

"Heat-Assisted Magnetization Dynamics in GdFeCo Using Field-Induced TR-MOKE", T. Y. Cheng and L. Atkinson and J. Wu and R. W. Chantrell and J. Sizeland and Y. M. Lu and J. W. Cai and Y. B. Xu, IEEE Transactions on Magnetics, 50(11):1-4, 2014.

Awaiting Publication

"Modelling the HAMR Process in a High Anisotropy FePt Granular Thin Film", Lewis J. Atkinson, Richard F.L. Evans and Roy W. Chantrell. Submitted.

"The effect of interaction on the relaxation processes in magnetic nanostructures", Lewis J. Atkinson, Thomas A. Ostler, O. Hovorka, K.K Wang, B. Lu, G.P Ju, J. Hohlfeld, B. Bergman, B. Koopmans and Roy W. Chantrell. Submitted.

1. Introduction

Magnetism is a physical phenomenon that was first recognised by Greek philosophers in approximately 600BC, when they noted that certain rocks, known as lodestones, would attract iron and other lodestones. Today the physics that governs magnetic materials is well understood and it is now possible to produce magnetic materials with a chosen set of properties that serve many modern day technologies, such as: computer chips, electric motors and magnetic data storage.

The following covers a brief introduction to the magnetic properties that are relevant to this research, an introduction to magnetic data storage, including the remarkable increase in data density over the lifetime of the technology which has resulted in current physical issues that must be understood if the technology is to continue, the exact motivation for research presented in this thesis and finally a brief outline of the thesis including the methods employed and the nature of the research covered.

1.1 Properties of Magnetism

Magnetism arises at the sub atomic level of matter as certain elements have an uneven number of electrons, which results in an unpaired electron in the outer electron shell. This unpaired electron causes a net polarisation of the electron cloud, resulting in an angular momentum on the electron that generates a magnetic moment perpendicular to the plane of average rotation of the net polarisation. This is generally called a magnetic or spin moment and the effective magnitude of the magnetic moment is a result of the exact structure of the atom in question. The spin moment associated with each atom interacts with the neighbouring atoms via the exchange interaction and exact nature of the exchange interaction dictates the way the magnetic moments align, resulting in a number different magnetic phenomenon that can be split in to categories known as: ferromagnetism antiferromagnetism and paramagnetism. Ferromagnetism and antiferromagnetism are a result of the magnetic moments aligning with each other; parallel in the case of ferromagnetism - which results in a net magnetisation of the material - and antiparallel for the antiferromagnetic case - which results in no overall magnetisation. In the case of paramagnetism there is no inter-atomic exchange interaction and the atomic magnetic moments are dispersed randomly, but will align in the presence of an applied magnetic field. However,

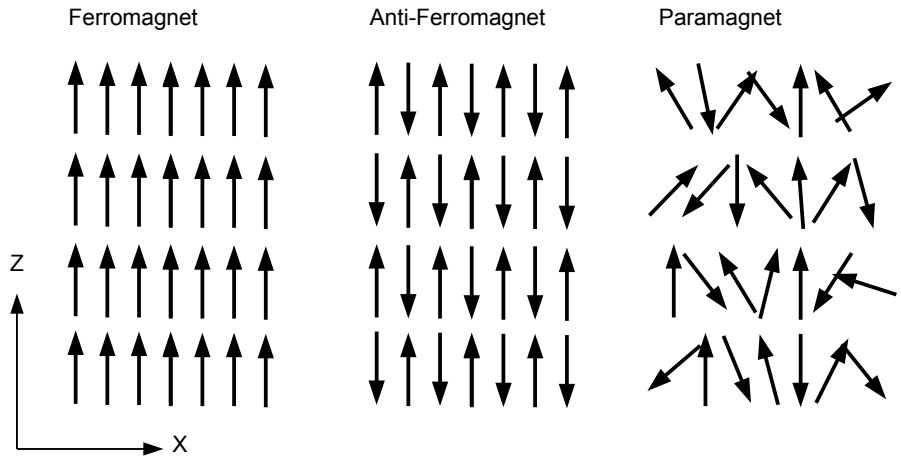

Figure. 1.1: Schematic representation of the three magnetic categories discussed in the above text: ferromagnetic, antiferromagnetic and paramagnetic. Each showing the orientation of atomic magnetic moments.

this alignment is only temporary and will disappear when the applied field is removed. The relative orientation of the atomic spin moments of these three magnetic categories are shown in figure 1.1.

Ferromagnetism is further discussed in this chapter as this has made the implementation and development of hard disk technologies possible and a better understanding of how ferromagnetic materials act in certain situations is essential to the research presented in this thesis.

1.1.1 Ferromagnetic Properties

For all magnetic categories the magnetisation (**M**) is the sum of the atomic magnetic moments per unit volume and is therefore the net magnetisation in a given direction per unit volume. For most magnetic materials, formed in the absence of an external magnetic field, there is no net magnetisation. In the case of ferromagnetism this is because the material is formed of distinct magnetic domains which each have an individual **M** but the magnetisation of the domains have no overall alignment. The concept of magnetic domains will be discussed further at a later stage. In the presence of an applied field (**H**) the magnetisation of

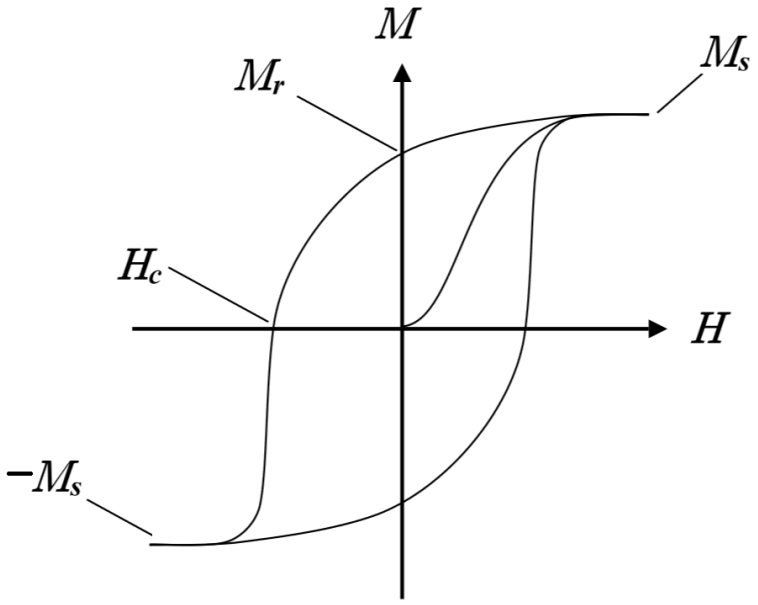

Figure. 1.2: A simple hysteresis diagram for a generic ferromagnetic material. Here are shown the key points on a hysteresis diagram: the saturation magnetisation, M_s, the remnant magnetisation, M_r, and the coercivity or coercive field H_c.

each domain will align causing a net magnetisation, and if the field is sufficiently large the value of the magnetisation vector will reach a maximum magnitude known as the saturation magnetisation ($\mathbf{M}_s$). This process is shown in figure 1.2. When the applied field is removed the magnetisation vector will reduce in magnitude, due to a number of effects which are also discussed further at a later point; the reduced magnetisation is known as the magnetic remanence ($\mathbf{M}_r$), also shown in figure 1.2. It is normal to measure the magnetic remanence by reducing the magnitude of the applied field slowly from a value where $\mathbf{M}_s$ is achieved to zero. If the applied field is then further reduced to a negative value the magnetisation is seen to switch orientation and $\mathbf{-M}_s$ is reached, see figure 1.2. At a certain point in the range of negative **H** the magnetisation vector will be zero and the applied field strength at this point is known as the coercive field or coercivity ($\mathbf{H}_c$) again see figure 1.2. This process is known as magnetic hysteresis and the characteristic pattern this generates on a **H** vs **M** graph is known as a hysteresis loop, see figure 1.2. Note it is normal practice to take the applied field from a value of **+H** to **-H** and then back to **+H** to complete the hysteresis loop. Note, it is often the case that the magnetisation vector shown on the hysteresis loop will be given as $\mathbf{M}/\mathbf{M}_s$ and will therefore always be stated as a value between -1.0 and +1.0.

The nature of ferromagnetic materials at the nano-scale is known to be

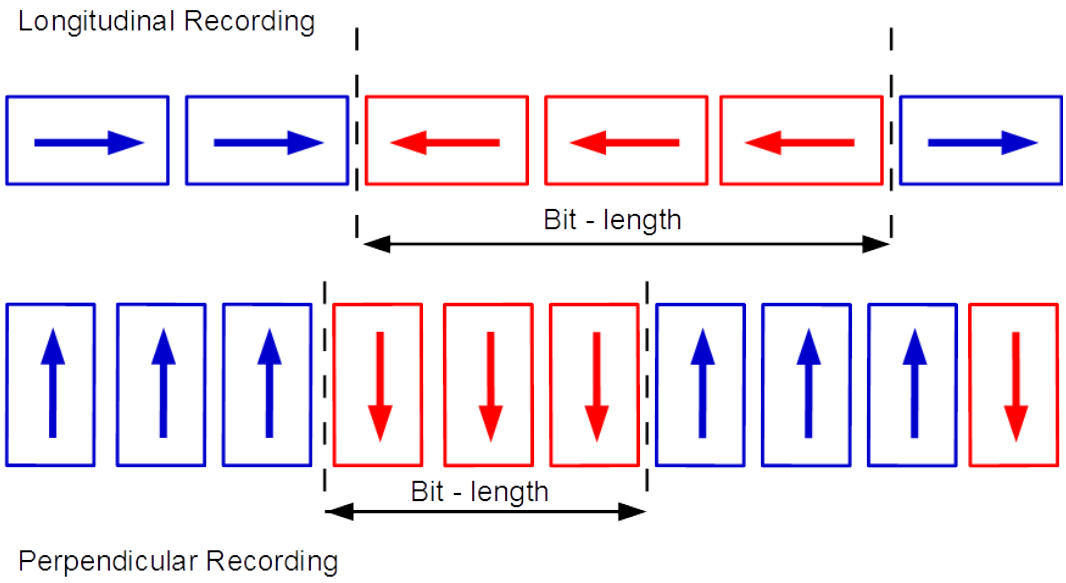

Figure. 1.3: A simple depiction of the component magnetic structure of hard disk recording media, showing the magnetic configuration of longitudinal and perpendicular recording media. Also showing the relative size of the bit length, for a comparable grain size, for the two media configurations. The north and south poles are depicted using the arrow, where the north pole is in the direction of the arrow and the south pole is at the opposite.

different from what is observed on a larger scale and for ferromagnetic nano particles below a critical volume it is energetically favourable to maintain a single domain [1], which results in a net magnetisation that is essential to magnetic data storage.

1.2 Magnetic Data Storage

Magnetic data storage was first proposed in 1887 by Oberlin Smith, although there is no evidence he produced a viable magnetic recording device. The first confirmed implementation of magnetic data storage was by Danish inventor Vladimir Poulsen, when in 1898 his device recorded sound onto a steel wire by setting the magnetic configuration of the wire using an applied field generated with an electromagnet. The stored information could then be read back by passing the same electromagnet over the steel wire which produced a current via induction, allowing the sound to be reproduced though a rudimentary speaker system. The technology progressed slowly over the next 40 years, producing systems for recording sound in an analogue format, where the magnitude and direction of the magnetisation both had a significant role to play in storing the information. Later technologies, such as the first computers, required

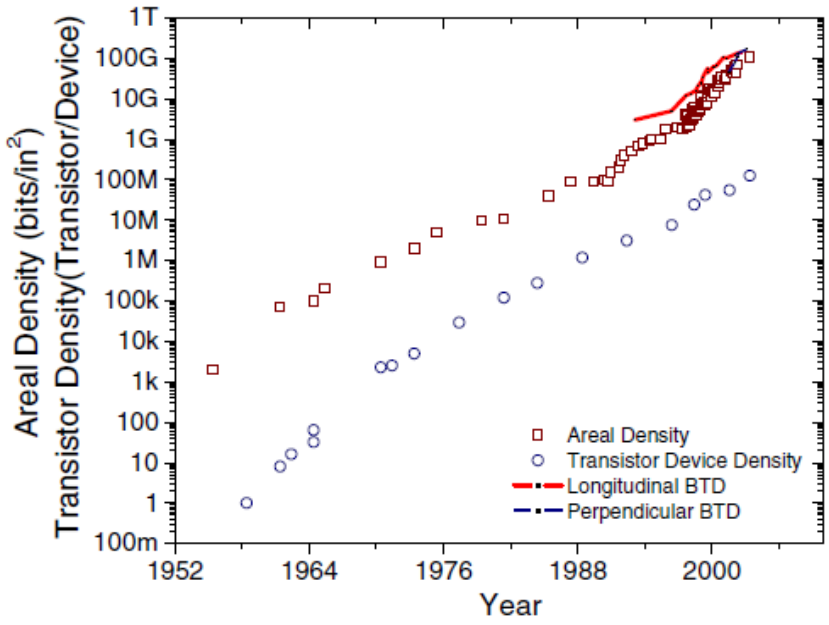

Figure. 1.4: The increase in areal density between the late 1950s and early 21st Century is comparable with the much quoted increase in transistor density.

information to be stored using a binary system and this requirement induced a significant progression in the technology. The binary system requires only two states to store information and therefore the properties of magnetic materials are well suited to such needs. It is well known that ferromagnetic materials, under certain conditions, exhibit what is commonly called a north (N) and south (S) pole (effectively positive and negative $\mathbf{M}_r$), which allow for materials to be manufactured which will exhibit properties that enable information to be stored using the binary system. Computers store information using a combination of 0s and 1s where a single piece of stored data, either 0 or 1, is called a bit; figure 1.3 gives a simple schematic of the cross section of hard disk recording media, showing the N and S pole configuration in two differing formats. Note that an individual bit is stored on multiple magnetic particles, in order to achieve adequate signal-to-noise ratio. One of the first computers to use the binary magnetic storage method was the ERA Atlas in 1950, which stored information with a data or areal density of approximately 400 bits/sqinch. Over the lifetime of magnetic storage technologies the increase in areal density has been truly remarkable and is of the same order as the much quoted increase in transistor density, known as Moore's Law, figure 1.4. A simple way to picture the increase in areal density is that it has effectively doubled every 18 months since the 1950s and today hard disk technologies have an areal density well in to the hundreds of Gbit/sqinch regime.

1.3 Research Motivation

The increase in areal density has resulted mainly from an adherence to geometric scaling, as the size of the recorded bit has been reduced over successive time periods [2, 3]. As previously mentioned a single bit is comprised of multiple magnetic particles which are called grains in hard disk recording media. The number of grains per bit, in part, dictates the level of single-to-noise ratio (SNR) on data read back. Other factors that contribute to SNR are the grain shape and interference from neighbouring bits and neighbouring tracks; that being said a good statistical estimate of SNR is that it scales with the number of grains (N) per bit, with the relationship $N^{\frac{2}{3}}$ to N^{1} [2]. Therefore if SNR is to be maintained, when reducing the size of the recorded bit, the grains that comprise the recording media must also be reduced in a similar manner. However, there has also been other factors that have contributed to the increase in areal density, such as altering the configuration of the magnetic materials that comprise the storage media. The most recent modification to the configuration occurred in around 2005 when the orientation of the N - S pole alignment was changed from a longitudinal to perpendicular format, figure 1.3. This change resulted in a significant increase in the areal density as the technology progressed, figures 1.3 and 1.4 [2].

Magnetic data storage has existed in many forms over its lifetime, but today the primary storage method is hard disk technologies. The storage media in hard disk technologies is a circular disk comprised of multiple layers of both non-magnetic and magnetic materials. The non-magnetic layers serve in multiple ways. The bottom substrate layer acts to support the additional layers and is usually made of ceramic, glass or aluminium. There are layers of non-magnetic metals deposited on the substrate to optimise the magnetic properties and size of the magnetic nano-particles that make up the recording layer. The granular magnetic recording layer is deposited on top of these layers. In current HDD's this process results in a recording media with component magnetic grains that have uniaxial anisotropy perpendicular to the plane of the thin film. These grains are spatially independent and are separated by a non-magnetic material.

Certain parameters that dictate the properties of magnetic materials have made the development of magnetic storage possible. These parameters include the macroscopic magnetisation (**M**), discussed above, the magnetocrystalline anisotropy (K_v) which dictates the preferred direction of **M** where the magnitude of K_v dictates the strength of that alignment and finally the volume (V) of the magnetic grains that comprise the recording media. These parameters have also been key to the remarkable increase in areal density. The magnetocrystalline anisotropy and volume, in combination, dictate the thermal stability of the

magnetisation and therefore the life span of the stored information. The Arrhenius-Néel law, equation 1.1, approximates the time between thermally activated magnetisation switching events, known as the relaxation time, τ_n. A simple analysis of the relationship between K_v, V and τ_n shows the critical nature of the volume and anisotropy dependance of the thermal stability of the magnetisation and the subsequent onset of superparamagnetic effects [4, 5].

$$\tau_n = \tau_o \exp\left(\frac{K_v V}{k_B T}\right). \tag{1.1}$$

Therefore, as the size of the constituent magnetic components that comprise the recording media are reduced, there must also be a complementary increase in K_v in order to maintain the desired thermal stability and consequently the lifespan of the written information. The required increase in K_v is normally achieved by developing new materials with a larger value of K_v. However, in more recent years this has also be achieved by developing complex media structures, such as exchange spring media [6] . To maintain the desired lifespan of stored information recorded on hard disk media the inequality given in equation 1.2 must be satisfied [2].

$$n_o = \frac{K_v V}{K_b T} > 60 \tag{1.2}$$

The historic increase in areal density has resulted in information being recorded on a length scales of nanometres; with the recorded bit being approximately 50nm - 100nm in size on media comprised of grains with an average diameter of approximately 10nm. There in lies the problem; any further reduction in grain volume will require an increase in K_v to a level that would prohibit the recording of information, as the field required to switch the magnetisation scales with K_v, as roughly $H_k = 2K_v/M_s$, whereas the maximum write field that is achievable with current write head technologies is held by the hard material limit of the highest saturation magnetisation found in magnetic solids, approximately 2.0 kemu/cc, which would produce a maximum write field of roughly 12.0 kOe [7]. Therefore, when using the standard recording method, K_v can not be scaled indefinitely with reducing grain volume.

These factors have all contributed to the 'magnetic recording trilemma' [2]. To increase the areal density any further this requires a smaller bit size and due

to the requirements of the SNR, this dictates a smaller grain volume and if the inequality given in equation 1.2 is to be satisfied there must be a consequent increase in K_v, which raises the switching field to a level beyond the physics of write head technologies due to the material limit of magnetic solids. These three requirements mean that any further increase in areal density will not be possible using current methods of magnetic storage in hard disk technologies.

Fortunately there may be a method for recording information on media with increasingly large anisotropy using the applied field strength that is available with current write head technologies. The parameters that govern magnetisation stability are not fixed and are thermally dependant. The temperature dependence of the magnetocrystalline anisotropy of ferromagnetic materials is well understood since the development of Callen-Callen theory which gives an approximate scaling for K_v(T) [8] as follows:

$$K_v(T) = K_v(0) \left(\frac{M_s(T)}{M_s(0)} \right)^n \tag{1.3}$$

where the exponent n is typically 3 for materials with uniaxial anisotropy and 10 for cubic anisotropy.

Therefore K_v can be thermally varied from a condition of media stability at ambient temperature, to approximately zero at temperatures approaching T_c. This approach could solve the problems of both writability and media stability as the same time, if temperature of the recording media was raised locally and momentarily, allowing data to be recorded in the low anisotropy regime with media stability returning as the temperature lowers to ambient. Heat assisted magnetic recording (HAMR) has been cited as a possible technology capable of exploiting this temperature dependent approach to recording information in hard disk technologies. The HAMR process coupled with high anisotropy materials, such as L_{10} ordered FePt, could allow for ultra high areal densities well into the Tbit/sqinch regime [9]. The HAMR process is more complex than simply magnetisation reversal over a thermally reduced energy barrier and research has shown additional challenges that must be overcome if the technology is to succeed, such as the problem of 'thermal writability' proposed by Evans et al. [10].

The physical structure of ultra high density recording media results in a system of strongly coupled nano particles which exhibits physical challenges

that must also be understood if hard disk technologies are to develop. The strong coupling can have a significant effect on the stability and dynamics of the magnetisation due to a demagnetising effect which is a result of the perpendicular orientation and the long ranged magnetostatic interaction and also the intergranular exchange interaction [11, 12]. Understanding how these interactions effect the magnetic damping and relaxation processes is becoming an increasingly important factor in hard disk technologies, as they play an important role governing the write speed and can affect the magnitude of both transition and dc noise during the recording process [13, 14, 15, 16, 17].

The body of work presented in this thesis concentrates on a computational study of the granular thin films that will be implemented in ultra high density recording media in hard disk technologies. Computational micromagnetics is the preferred method for studying the complex behaviour of magnetic materials on the sub-micrometer scale and has become an essential tool in current research. In recent years the Landau-Lifshitz-Bloch (LLB) equation has become the standard for modelling single domain magnetic nano particles on the sub-pico second timescale, especially in situations where the temperature of the system approaches the Curie point [18, 19]. This approach combined with additional modelling methods is implemented to construct a model which is capable of investigating the underlying physics that governs the magnetic processes that will dictate the future of hard disk technologies.

1.4 Thesis Outline

The following section gives a brief outline of the contents of this thesis. Chapter 2 covers the physics relevant to the ultra-high density magnetic granular thin films which has led to the implementation of the LLB granular model and also the research in this thesis. This includes a brief description of the properties of nano granular magnetic materials, including the temperature dependence of these properties and how these properties relate to hard disk recording media and magnetic data storage. Chapter 3 covers the methods used to implement the LLB granular model, including the simulation of the physical structure using a voronoi construction, how the model describes the internal and interaction fields acting on each grain that comprises the thin film and also how the magnetic configuration is evolved through time using the Landau-Lifshitz-Bloch equation coupled with the Heun integration scheme. The remaining chapters (4 - 7) cover the research that was accomplished with the LLB granular model and also newly developed discrete approximation (DA) method for describing the magnetostatic

field. Chapter 4 presents research on the dependence of the effective damping in high density granular thin films as a function of the interaction fields - the intergranular exchange field and magnetostatic field. This work includes both a numerical study, with supporting experimental results and also a study of how the damping dependence impacts the transition time. Chapter 5 presents a thermodynamic study of the HAMR process using the LLB granular model, including a study of the bulk properties, the role of the linear reversal mechanism in HAMR, the effects of 'thermal writability' and finally how these factors impact the HAMR process. Chapter 6 presents a collaborative study on the feasibility of using a continuous wave (CW) laser as a heating tool within the HAMR process. Chapter 7 describes and tests the proposed discrete approximation method for describing the magnetostatic field. Finally the thesis concludes with a summary of the main results and conclusions and also a discussion of any further work that has become apparent during this study.

2. The Physics of Ultra-High Density Recording Media and HAMR

As mentioned in the introduction the increase in areal density in hard disk technologies has been as a result of an adherence to geometric scaling; essentially the component magnetic particles (or grains) in the recording layer have been reduced in size over successive time intervals and the grains are now approximately 8.0 to 10.0 nanometres in diameter. This reduction in the particle size has been accompanied by a complementary increase in the magnetocrystalline anisotropy to give the required stability of the magnetisation in order to maintain the stored information for the desired lifetime. This increase in the areal density has resulted in a situation where any further reduction in the size of the magnetic particles and subsequent increase in the magnetocrystalline anisotropy will require significant changes in the methods used to record the data on the recording layer as the maximum applied field that write head technologies can achieve will be insufficient to reverse the magnetisation of the magnetic particles. The physics that governs the magnetic thin film used for the recording layer in hard disk technologies and the proposed methods for furthering the capabilities of the technology are discussed in this chapter.

The physical properties of magnetism are discussed and how these properties are used to implement the recording layer in hard disk technologies and how these properties may be used in future hard disk technologies. Firstly magnetic nano particles are introduced and how the magnetic properties of these particles differ from the bulk properties of like materials. Secondly the temperature dependence of these magnetic properties is discussed and how these properties may be beneficial to future hard disk technologies. Thirdly magnetic nano particles in a thin film ensemble are discussed and how understanding the inter-particle interactions are essential to the development of future hard disk technologies. Also magnetisation reversal is briefly discussed in terms of an energy barrier to reversal using the Stoner-Wohlfarth model. Finally the physics of the HAMR process is introduced and discussed, again in terms of the Stoner-Wohlfarth energy barrier model.

2.1 Magnetic Parameters

The key parameters that govern ferromagnetic materials and are also of importance when developing the model that has been implemented to complete this body of research are established and further discussed in this section.

2.1.1 Magnetic Anisotropy

An important parameter associated with magnetism is the magnetic anisotropy. This can generally be split in to two parts: the magnetocrystalline and shape anisotropy. The magnetocrystalline anisotropy has played a key role in the increase of the areal density and therefore in the development of hard disk technologies.

Magnetocrystalline Anisotropy

The magnetocrystalline anisotropy, K_v, given as an energy per unit volume, arises due to the spin orbit coupling of the electron being affected by the local atomic environment, which causes the magnetisation to align with a certain crystallographic axis. The simplest form of magnetocrystalline anisotropy is a uniaxial anisotropy where the magnetic moment aligns along a single axis usually referred to as the easy axis, $\boldsymbol{e}$. The effect of an easy axis gives rise to a hard plane, as the magnetic properties in this situation are rotationally similar around the easy axis. Note a uniaxial anisotropy will be the only form of the magnetocrystalline anisotropy implemented in this body of work.

When K_v is sufficiently large the magnetisation will remain relatively constant in an equilibrium position close to the anisotropy axis, although the magnetisation will precess around the easy axis with a superposed random walk due to thermal effects. The thermal effects are further discussed later in this chapter. The anisotropy energy is defined in equation 2.1 for a uniaxial particle, where θ is the angle between $\mathbf{M}$ and the easy axis. It can be seen from equation 2.1 that there is a maximum value for the anisotropy energy at $\theta = \pi/2$ and there are two energy minima at $\theta = 0$ spin up and $\theta = \pi$ spin down, enabling a two state system, where each state is equally likely, shown as a schematic representation in figure 2.1.

$$E(\theta) = K_v V \sin^2(\theta) \tag{2.1}$$

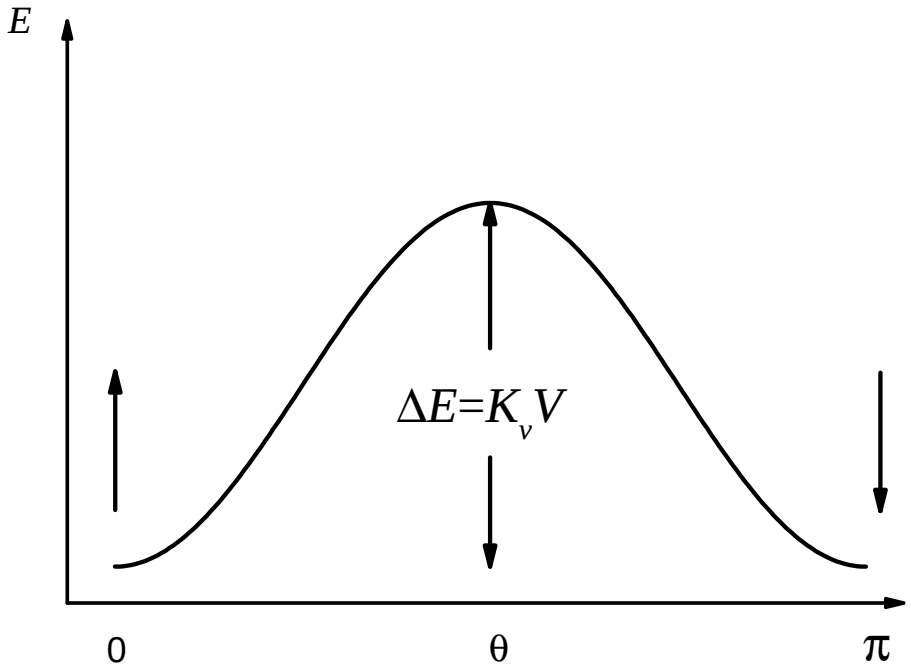

Figure. 2.1: A simple schematic representation of the anisotropy energy barrier to magnetisation reversal as a function of the angle between the magnetisation and easy axis. This shows the maximum height of the energy barrier at an angle of $\pi/2$ and the 2 energy minima at $\theta = 0$ and π. This diagram depicts the 2 state magnetic system that each grain within the recording layer of hard disk technologies exhibits.

The anisotropy energy gives rise to a contribution to the total field, acting on **M**, of the following form, equation 2.2.

$$H_k = \frac{2K_v}{M_s} \tag{2.2}$$

where H_k is the anisotropy field and the temperature dependent field contribution is a vector where the magnitude is a function of the temperature dependent magnetisation - $H_k(M(T))\mathbf{e}$, where **e** is the direction of the anisotropy axis.

Shape Anisotropy

The magnetic properties of materials deviate from the bulk properties when the characteristic dimension approaches the nano scale, these effects are further

discussed at a later stage in this chapter. In equilibrium conditions the build up of effective magnetic charge on the surface of the material will work to oppose the magnetisation that created it and this can contribute an effective shape anisotropy. If the magnetocrystalline anisotropy of the nano particle is sufficiently small and the shape is non-spherical, shape anisotropy can can become the limiting anisotropy. Here we are considering systems with large magnetocrystalline anisotropy and regular shape, so shape anisotropy is currently not included in this body of work.

2.1.2 The Exchange Interaction

The exchange interaction is of quantum mechanical origin and arises due to the probability of the exchange of electrons between neighbouring atoms. Since no two electrons of the same spin can occupy the same state simultaneously the Pauli exclusion principle is therefore satisfied. This exchange interaction generates an internal field known as the Weiss field which, in ferromagnetic materials, causes the atomic spin moments to align parallel. The exchange energy for an individual atom i is a function of the neighbouring atomic spin moments and is given by equation 2.3.

$$E(exch) = -J_{ij} \sum_{ij} \hat{\mathbf{S}}_i . \hat{\mathbf{S}}_j \tag{2.3}$$

where J_{ij} is the exchange field between the spins i and j, $\hat{\mathbf{S}}_i$ is the local spin moment and $\hat{\mathbf{S}}_j$ are the neighbouring atomic spin moments. If the exchange energy, J_{ij}, is positive this causes the atomic spin moments to align and the material will be ferromagnetic. If J_{ij} is negative then the atomic spin moments will attempt to align anti-parallel and the material will be antiferromagnetic and also if J_{ij} is approximately zero there will be no alignment of the atomic spin moments and the material will be paramagnetic.

2.1.3 Magnetic Susceptibility

Magnetic susceptibility is a measure of the response of the magnetisation to an external field and is a dimensionless vector quantity which is defined as:

$$\chi_{ij} = \frac{dM}{d\mathbf{H}_{H \to 0}} \tag{2.4}$$

where i and j are cartesian components, which can be split into two components; the parallel susceptibility (χ_{zz}) which dictates the response in the direction of the magnetisation and also the perpendicular susceptibility ($\chi_{xx} = \chi_{yy}$) which dictates the response perpendicular to the anisotropy axis, assumed directed along the z axis.

2.1.4 Damping

In all magnetic materials the magnetisation is subject to damping which acts as a resistance to dynamic motion of the magnetisation. In the situation where the magnetisation is perturbed from an equilibrium state the magnitude of the perturbation and the manner in which the magnetisation returns back to the equilibrium state is dictated by the relative damping of the material. The magnetisation of materials with relatively high damping will return to the equilibrium state quicker than in materials with relatively low damping. This is an important parameter to be considered when selecting materials to be used in hard disk recording media.

2.2 Temperature Dependence of the Magnetic Properties

The properties of magnetic materials, such as the equilibrium magnetisation, the magnetocrystalline and saturation magnetisation, are temperature dependent and are significantly reduced as the temperature is raised above zero Kelvin and effectively zero above the Curie point (T_c).

2.2.1 Temperature Dependence of the Magnetisation

As mentioned above the magnetisation, **M**, is the sum of the atomic magnetic moments per unit volume and for a ferromagnetic material this will give a net magnetisation. Therefore at zero Kelvin, when the atomic magnetic moments are at minimum energy, and with a perfect crystallographic structure the magnetic moment for each atom will be aligned and the magnitude of **M** will be at a maximum. As the temperature is raised the thermally activated motion of the atomic magnetic moments causes the loss of alignment between the atomic spin moments and the magnetisation is seen to reduce in magnitude.

The temperature where the magnetisation is seen to exhibit no magnetisation is known as the Curie temperature, T_c, at this temperature and above the

thermal energy is sufficient to overcome the energy of the exchange interaction and the atomic spin moments will be in a disordered state. The Curie point is material dependent and is approximately 750K for bulk FePt, although as the material dimensions approach the nano scale T_c has been observed at the lower temperature of 660K [20, 21, 22]. For a description of the temperature dependence of the magnetisation of FePt see figure 2.2, where the temperature dependence has been determined both experimentally, by Thiele et al. [21], and computationally using the constrained Monte Carlo method, by Asselin et al. [20].

2.2.2 Temperature Dependence of the Anisotropy

The temperature dependence of the magnetocrystalline anisotropy is key to the development of future hard disk technologies such as HAMR. As previously mentioned HAMR aims to exploit the fact that the magnitude of the magnetocrystalline anisotropy reduces in a known manner as the temperature of the magnetic material is raised towards T_c and is zero above this point.

The temperature dependence of the magnetocrystalline anisotropy of ferromagnetic materials has been well understood since the development of the $l(l+1)/2$ theory of Callen and Callen (C-C) who showed that $M(T)/M(0)=(K(T)/K(0))^n$, where n describes the form of the dependence [8]. However it is true that the $l(l+1)/2$ power law is only valid at temperatures far below T_c and not all ferromagnetic materials show a C-C dependence, such as FePt, in that they exhibit a non integer value for n. FePt has a relatively large anisotropy which arises from a combination of single and two ion anisotropy terms and as a result has a temperature dependence that does not conform to C-C theory [20]. The temperature dependence of the magnetocrystalline anisotropy of FePt has also been observed both experimentally, by Thiele et al. [21], and using the constrained Monte Carlo method, by Asselin et al. [20], and in both cases follows the form $K_v(T)=K_v(0)M(T)^{2.1}$, and is also shown in figure 2.2.

2.3 Magnetic Nano Particles

The magnetisation of magnetic nano particles is known to behave differently when compared to the magnetisation of the same magnetic material of a larger size. This is due to the relatively small particle size resulting in larger percentage of the atomic spin moments being at the surface and this leads a number of significant effects. Firstly for magnetic nano particles below a critical volume it is energetically favourable to maintain only a single domain, this effect was

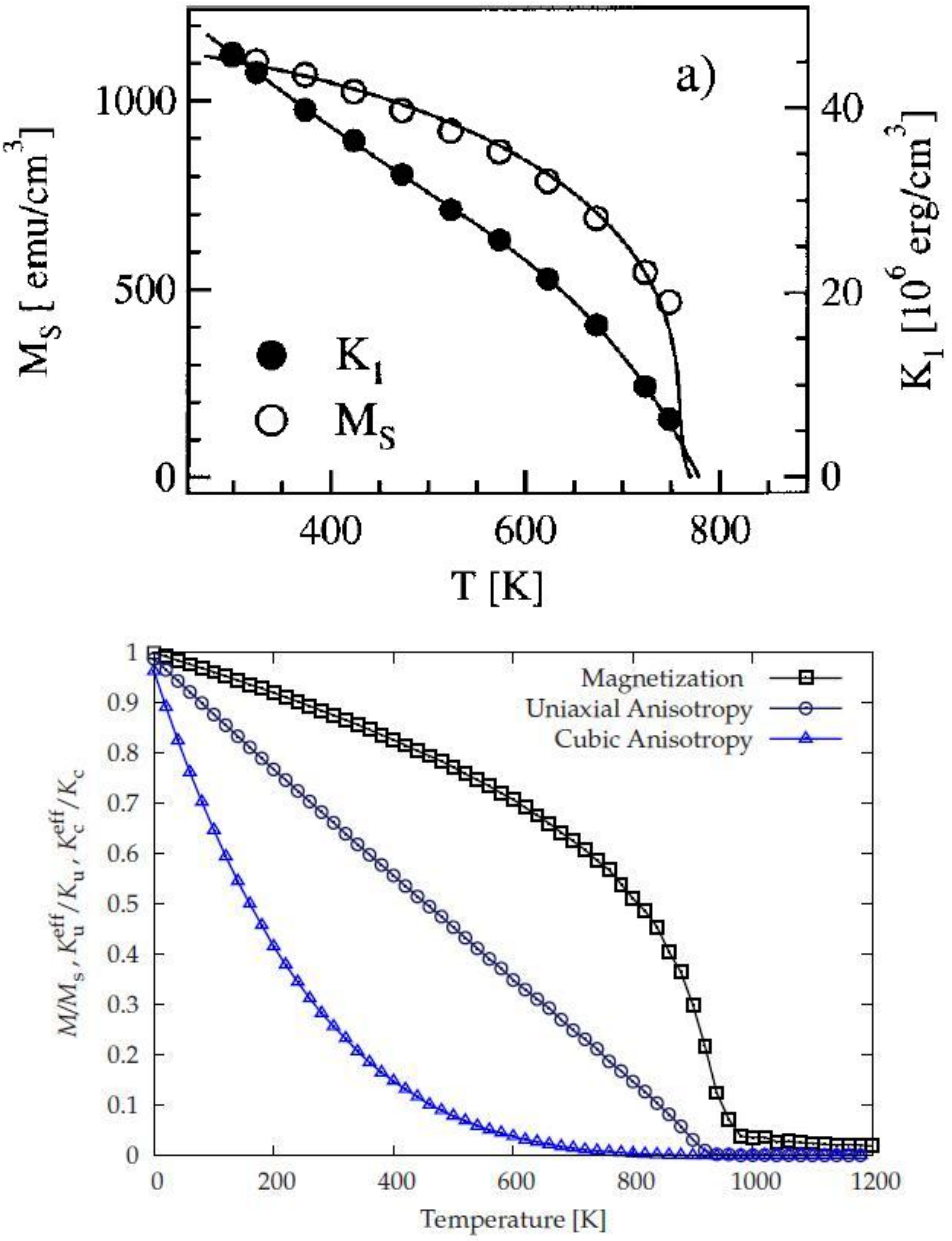

Figure. 2.2: Top: Experimental data, from Thiele et al. [21], showing the temperature dependence of the magnetisation and the subsequent relationship with K_v. The hollow circle line indicates the magnetisation and the black circle line indicates the anisotropy dependence. Bottom: The same information calculated with the constrained Monte Carlo method by Asselin et al. [20, 21, 22].

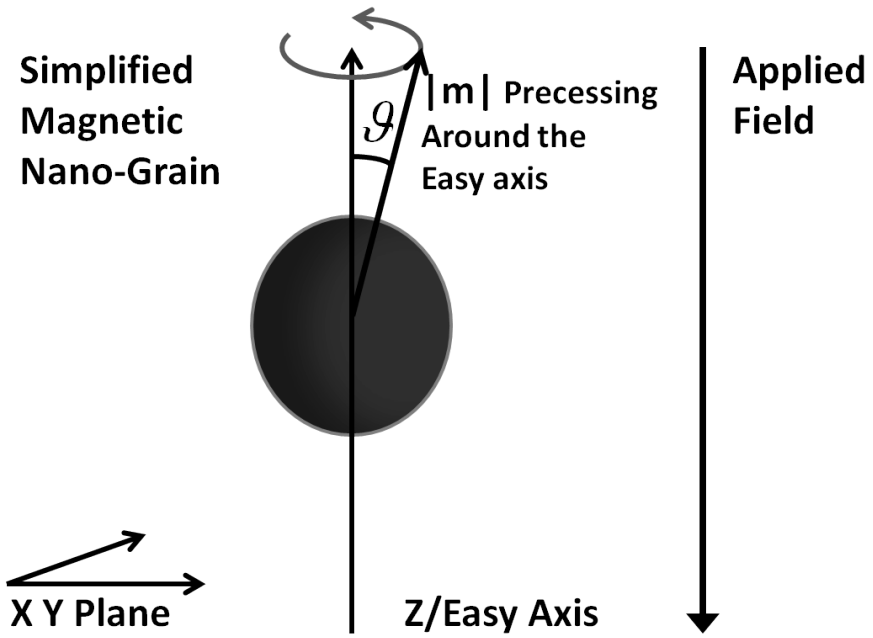

Figure. 2.3: A simplified picture of a magnetic nano particle with uniaxial anisotropy. The applied field direction is anti parallel to the easy axis of the nano particle. The magnetisation is shown precessing around the easy axis.

first predicted by Frenkel and Dorfman [1] and this phenomenon is essential to magnetic recording media. This effect also means all ferromagnetic nano particles below the critical volume will have a net magnetisation.

The stability of the magnetisation of magnetic nano particles is also affected by the small particle volume. This effect is characterised by the Arrhenius-Néel law, shown in equation 2.5, which gives the relaxation time of a material, τ_n (the average time between thermally induced switching events) and this is governed by the parameters: K_v, V, the particle volume, and T, the temperature of the material [4, 5].

$$\tau_n = \tau_o \exp\left(\frac{K_v V}{k_B T}\right) \tag{2.5}$$

Here τ_o is the attempt time, estimated using Brown's approximation of the attempt time, equation 2.6 [23, 24], to be between 10^{-10} and 10^{-11} seconds, and k_B is the Boltzmann constant.

$$\tau_0 = \frac{1}{f_0} = \left[\frac{\alpha\gamma}{1+\alpha^2} \sqrt{\frac{H_k^3 M_s V}{2\pi k_B T}} \left(1 - \frac{H}{H_k}\right) \left(1 - \frac{H^2}{H_k^2}\right) \right]^{-1} \tag{2.6}$$

The critical nature of the relaxation time, and therefore the stability of the magnetisation, due to particle size is apparent in equation 2.5 and is shown in figure 2.4. The granular thin films used in hard disk technologies do have a dispersion in the size of particles that comprise the thin film. This dispersion can affect the stability of the magnetic particles, which in turn could impact the lifetime of the stored data. For a given value of the magnetocrystalline anisotropy the volume is the critical parameter to maintaining the stability of the magnetisation. For a 6.0nm cubic particle and K_v equal to 1.15×10^7ergs/cc, the relaxation time is approximated to 1.14×10^{16}s or about 360 million years. Reducing the grain dimensions to 4.0nms reduces τ_n to less than 0.01 of a second, figure 2.4. This shows the critical nature of the volume dependence on the stability of the magnetisation of magnetic nano particles and the onset of superparamagnetic effects [4, 5].

The anisotropy dependence on the stability of the magnetisation is less critical than the size dependence, as the volume of particles are roughly the cube of the diameter, but this still has an exponential relationship, as in equation 2.5, and the high value must be maintained to ensure magnetisation stability. This relationship can be seen in figure 2.4, where reducing the anisotropy by 30% from 1.2x10^7 ergs/cc to 0.9x10^7 ergs/cc will reduce the relaxation time by 7 orders of magnitude.

Superparamagnetism is well understood and occurs in ferromagnetic nano particles that sustain a single domain, at temperatures much lower than T_c. If the time taken to measure the magnetisation of the nano particles is larger than the relaxation time then the particles are said to be superparamagnetic. The magnetisation of ferromagnetic nano particles can flip due to the thermal energy associated with the nano particle [4, 5].

2.4 Magnetic Interactions within Granular Materials

In an ensemble of magnetic particles there are additional fields acting on the magnetisation which alter the energy profile of the magnetic system and further perturb the motion of the magnetisation of the individual particles that comprise the material. Understanding the role these fields play in the magnetic thin

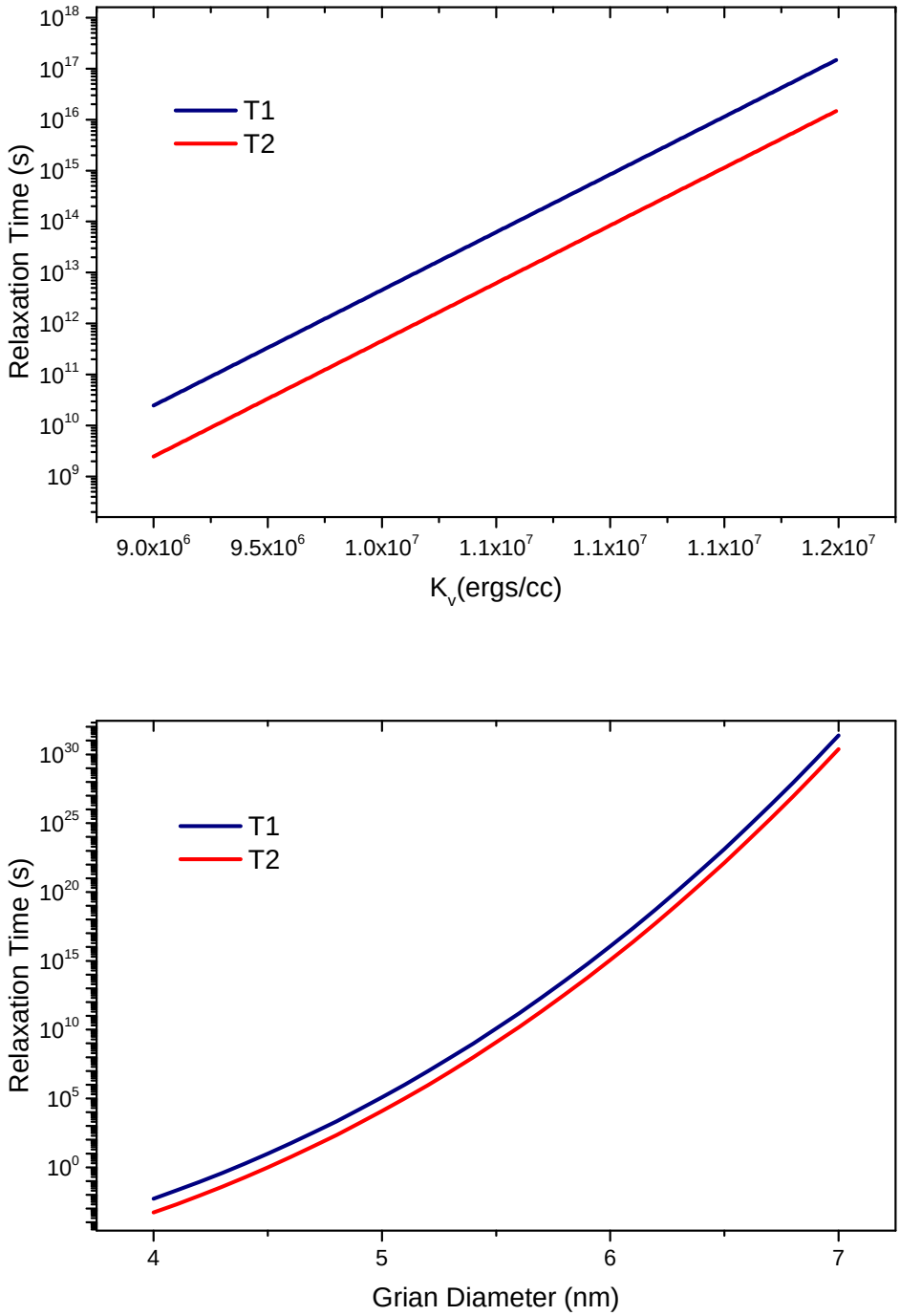

Figure. 2.4: Top: The anisotropy dependence of the relaxation time, τ_n, calculated for 6nm cubic grains at 300K. The relaxation time increases exponentially with increasing anisotropy. Bottom: The grain size dependence on the relaxation time, τ_n. The dimension given is 1 side of the cubic grain. The anisotropy was held at 1.15×10^7ergs/cc and the system temperature was 300K. T1 and T2 represent the different attempt times, τ_o, T1=10^{-10} and T2=10^{-11}.

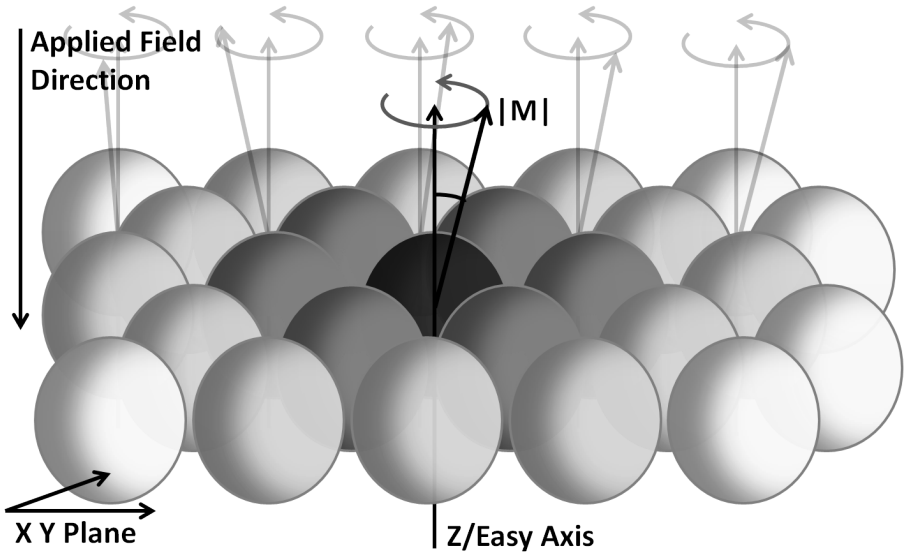

Figure. 2.5: A simple diagram of a single domain magnetic particle in the thin film environment where the anisotropy axis is perpendicular to the plane of the thin film. The black grain at the center is interacting, via the exchange field, with the neighboring dark grey grains. The black grain also interacts, via the magnetostatic ineteraction, with all the grains within a set radius from the black the grains, with diminishing effect.

films that are used for the recording layer of hard disk technologies is of critical importance. The thin films used in current hard disk technologies have all of the individual grains set in a plane, with the easy axis of each grain aligned perpendicular to the plane of the thin film. This format has a specific field arrangement which brings additional physical challenges when designing and implementing future hard disk drives. A simplified example of a section of a granular thin film is shown in figure 2.5. Not all of the grains are showing the magnetisation and easy axis, and the grey scale is to indicate the field interactions for later discussion. The grains in an actual thin film are not spherical, their shape is dictated by the boundaries they make with neighboring grains. The nature of the microstructure and the construction of the theoretical model is dealt with in a later section.

2.4.1 Inter Particle Exchange Interaction

As discussed above the exchange interaction is short ranged and exists between neighbouring atoms and in ferromagnetic materials this causes the spin on each atom to align parallel resulting in a net magnetisation on the material. It is also known that in an ensemble there is an exchange interaction between neighbouring ferromagnetic particles which are separated by a distance greater

than the inter-atomic distance. This effect, known on the macro scale as exchange coupling, is well documented and is known to act much like the inter-atomic exchange interaction and causes the magnetisation of the individual particles to align to varying degrees, dependent on the strength of the intergranular exchange coupling. As the inter-atomic exchange interaction is short ranged there must be another mechanism for the inter-particle exchange coupling. It is proposed that the interaction arises from impurity atoms in the boundary material between grains, as this material is an oxide, and this idea forms a basis for the theoretical model of the intergranular exchange [25].

2.4.2 The Magnetostatic Field

The magnetostatic field is generated by the magnetisation of the individual nano particles within the ensemble and therefore each particle is subject to the net field generated by all the other particles in the material. The net field acting on each particle i is a function of the position, shape and orientation of the magnetisation of both particle i and all the other particles j in the system. Therefore the magnetostatic field can take many forms. For a granular thin film the orientation of the anisotropy field, and therefore the orientation of the magnetisation in an equilibrium state, can significantly alter the effect of the magnetostatic field. For a thin film where the anisotropy is orientated perpendicular to the plane of the thin film and with the magnetisation aligned parallel the net magnetostatic field, acting on each grain, is in the opposite direction and works to oppose the magnetisation, with a field strength, at zero Kelvin, equal to -$4\pi \mathrm{M}_s$. For a similar thin film with the anisotropy axis orientated parallel to the plane the direction of the magnetostatic field lies in the same direction as the magnetisation and is therefore supporting the magnetisation. Given that these granular magnetic systems are dynamic in nature the magnetostatic field is therefore also dynamic; locally the strength and orientation of the magnetostatic field is dependent on the orientation of the neighbouring grains and also the temperature of the system, as this will reduce the magnitude of the magnetisation and therefore reduce the strength of the magnetostatic field generated by each particle. For systems with perpendicular magnetisation, where the magnetostatic field strength is of the same order as the magnetocrystalline anisotropy field the stability of $\mathbf{M}$ is effected by the magnetostatic interaction between neighbouring spins and can cause magnetisation switching in an otherwise thermally stable system. As a result, media with perpendicular magnetisation must satisfy the criterion $2\pi M_s^2 < K_v$[26, 27, 28].

As already stated the exact magnetostatic field is dependent on a significant

number of factors, including the shape, size of both interacting particles i and j also the separation distance between the particles. A standard approximation to the magnetostatic field is the dipole approximation, given in equation 2.7. The dipole approximation is limited in its scope as it does not account for the shape of the interacting particles.

$$\mathbf{H}^{i}_{mag} = \sum_{j} \frac{M^{j}_{s} V_{j}}{r^{3}_{ij}} (3(\hat{\mathbf{r}}_{ij} \cdot \mathbf{M}_{j})\hat{\mathbf{r}}_{ij} - \mathbf{M}_{j}) \tag{2.7}$$

where M^{j}_{s} is the saturation magnetisation and V_{j} is the volume of grains j and also r_{ij} is the distance between grains i and j.

2.4.3 The Effective Local Field

Therefore the total field H_{tot} acting on the individual grains within the granular material, when including an applied field, is equal to the sum of all the local field contributions.

$$\begin{aligned} \underline{H}_{tot} = \underline{H}_{applied} + \underline{H}_{anisotropy} \\ + \underline{H}_{exchange} + \underline{H}_{mag} \end{aligned} \tag{2.8}$$

2.5 Magnetisation Reversal

Data storage in magnetic hard disk technologies requires the switching of the orientation of the magnetisation of the magnetic nano particles that make up the recording layer. This is achieved by subjecting the desired area on the recording layer to an external applied field which is sufficient in magnitude to reverse the direction of the magnetisation, setting the direction of the magnetisation of a sufficient number of the grains to enable data read back.

The Stoner-Wohlfarth (S-W) model gives a simple energy description of magnetisation switching in single domain magnetic particles, such as those seen in the recording layer in hard disk technologies. The S-W model assumes coherent rotation of the magnetisation throughout the switching process;

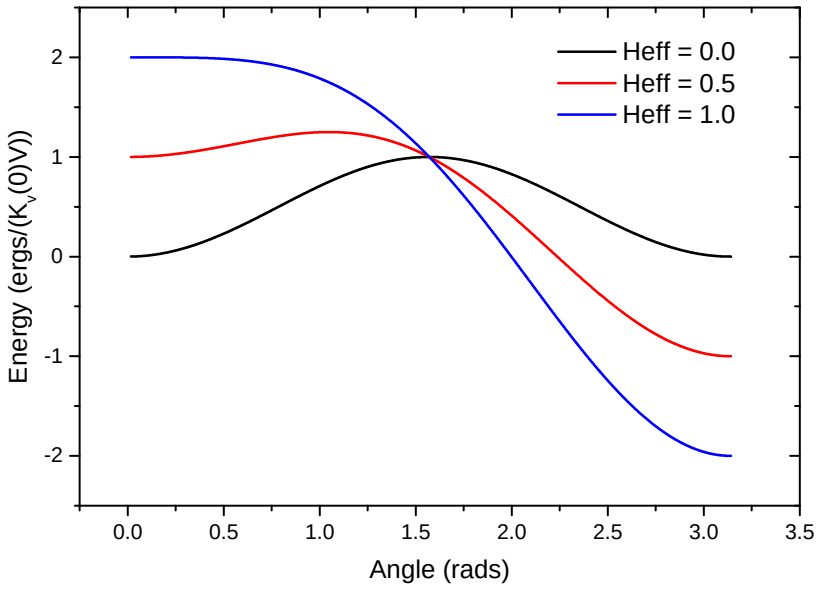

Figure. 2.6: A diagram showing the energy barrier for reversal as a function of the angle between the magnetisation and the easy axis, calculated using equation 2.9. H_{eff} is altered to simulate the effect of an applied field. Increasing the applied field raises the Zeeman energy, altering the energy profile of the system, causing a situation where magnetisation reversal is energetically inevitable.

essentially assuming a sufficiently large atomic exchange interaction. Also we are assuming no temperature effect in this simple description of the magnetisation reversal process. This being said the S-W model is very useful at describing the switching process in terms of the energy barrier for reversal.

The assumptions made by the S-W model imply that the energy surface for the reversal process is entirely a function of the anisotropy energy and the effect of the applied field and therefore the Zeeman energy and is here shown in equation 2.9.

$$E(\theta,\phi) = K_v V \left[\sin^2(\theta) - 2H_{eff}\cos(\phi-\theta)\right] \tag{2.9}$$

where the first term is the anisotropy energy as function of θ (where θ is the angle between the magnetisation and the easy axis) and the second term is the Zeeman energy as a function of θ and ϕ, where ϕ is the angle between the applied field. $K_v V$ is the anisotropy energy, H_{eff}=H/H_k, H is the applied field, H_k=2K_v/M_s is the anisotropy field and M_s is the saturation magnetisation.

It can be easily seen using equation 2.9 that the energy barrier restricting magnetisation is dictated by the magnetocrystalline anisotropy, K_v and the

particle volume, V, and this results in an energy barrier equal to $K_v V$ in zero field. It is also apparent using equation 2.9 that for magnetisation reversal to occur for particles with easy axes aligned with the field, at zero Kelvin, the applied field must be greater than the anisotropy field. This is shown in figure 2.6, where the energy is given in units of ergs/($K_v V$) so that the maximum energy barrier, without the presence of an applied field, is equal to 1. In the zero applied field case there are clearly two energy minima or energetically stable positions, at 0 and $\pi/2$ radians, which are both equally probable. If we assume that the magnetisation lies at $\theta = 0$, then increasing the strength of the applied field in the negative direction, to greater than zero but still less than $H_{eff} = 1.0$, causes the shape of the energy surface to change so that there are still two energy minima, but they are now not equally probable, the energy minima at $\theta = \pi$ is the more stable position with a metastable state at $\theta = 0$. It is also apparent that increasing the strength of the applied field has reduced the height of the energy barrier to magnetisation reversal. Further increasing the applied field strength so that H_{eff} is great than 1.0 changes the energy profile entirely and results in one stable position at $\theta = \pi$ and the energy barrier to reversal has been removed and we can say that the magnetisation has now switched direction. At finite temperatures reversal is possible due to thermal activation over the energy barriers leading to coercivities, H_c, less the the anisotropy field, H_k, for this reason thermal effects are included in the dynamic equation of motion that describes the magnetisation, to be described later.

2.6 Heat Assisted Magnetic Recording

As previously mentioned heat assisted magnetic recording (HAMR) is a proposed technology which may be capable of maintaining the historic increase in the areal density and achieve data density levels above 1 Tb/sqinch [9]. As mentioned above, further reducing the dimensions of the magnetic grains which make up the recording layer will require a consequent increase in K_v to maintain the inequality shown in equation 2.10, which in turn maintains the stability of written information. Any further increase in K_v will result in an energy barrier to magnetisation reversal that is far greater than the maximum write field is capable of overcoming due to the material limits of the magnetic components in write head technologies [7]. The proposed idea of HAMR makes use of the temperature dependence of K_v and would raise the temperature of the recording layer, locally and temporarily, to a point where the anisotropy has been sufficiently lowered to allow magnetisation reversal to happen in the low anisotropy regime and magnetisation stability is returned when the temperature returns to ambient

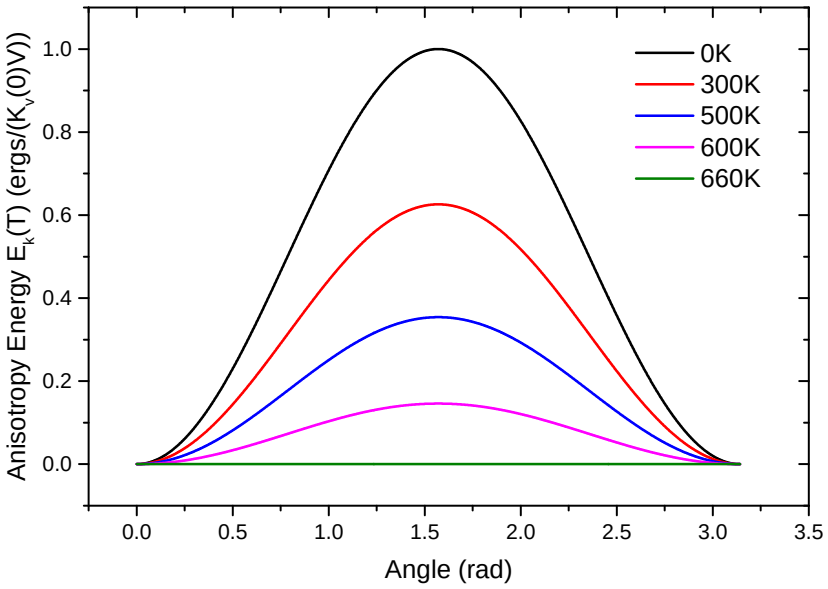

Figure. 2.7: The energy barrier for reversal calculated as a function of the angle between the magnetisation and the anisotropy axis, using equation 2.9, in the absence of an external field. The energy barrier is reduced to zero when the temperature is equal to or greater than T_c.

along with the high anisotropy regime [2].

$$n_o = \frac{K_v V}{k_B T} > 60 \tag{2.10}$$

The S-W simplistic energy barrier model can also be used to depict the HAMR process, although this simplistic analysis is at constant temperature the intention of the HAMR process is well displayed. As already mentioned, for a particle with uniaxial anisotropy, the magnitude of the anisotropy energy is a maximum at $\pi/2$ degrees, equal to $K_v V$. Also as previously mentioned the anisotropy reduces to zero as the temperature is raised towards the Curie point. This results in a reduction in the anisotropy energy as a function of the angle between **M** and the anisotropy axis, shown in figure 2.7, and therefore the energy barrier to reversal.

As the temperature of the grains is raised the magnitude of the energy barrier, when switching from 0° to 180°, is lowered and above T_c the energy barrier for reversal is removed entirely. This implies that the magnetisation can make the transition from 0° to 180° in zero field. This simply describes the HAMR process although not all factors have been included, as the increase in the energy of the

grains, due to the increased thermal energy (k_BT) has not been accounted for. The S-W description is only used to indicate the physical reduction in K_v that HAMR will exploit.

3. Modelling Magnetic Granular Systems

This chapter describes the methods and systems used to design and implement the model which forms the basis of the research contained within this thesis. This chapter will include a description of the systems being modeled and why the methods used have been chosen when implementing the model. The first section describes the purpose and also the capabilities of the model. The second section describes the modeling of the physical structure and why the correct description of physical structure plays an important role in describing the interactions between the magnetic elements. The third section describes the methods used to model the dynamics of the magnetisation of the individual magnetic elements and the final section describes the methods used to model the interaction between the magnetic elements.

3.1 An Overview of the Model

One of the main aims of the project was to design and implement a model of the granular recording media which are proposed for use in future hard drive technologies, such as the high anisotropy FePt granular media to be used for heat assisted magnetic recording (HAMR). This requires a model which can operate on a relatively large scale; in the nanometre to micrometre range and also should be capable of operating over a broad temperature range, from 0 Kelvin to above the Curie point. Beyond that the model should also be capable of describing a broad range of granular and domain based magnetic systems. The systems include standard single-layer granular media comprising single domain grains interacting via magnetostatic and exchange interactions and also multilayered systems such as exchange coupled composite media.

There are many options available to model magnetic systems and each has its benefits and short-falls and therefore each option should only be used in the correct circumstance. Atomistic spin and first principle models generate the magnetic system by simulating the atomic structure and are therefore desirable as they can give highly accurate results. But current atomistic spin and first principle models are relatively computationally expensive and can only be implemented for relevant systems, such as small clusters of atoms or translationally invariant systems [29]. Therefore this model implements a micromagnetic approach as this approach has been shown to be a powerful tool for modeling the magnetisation of 'single domain magnetic particles' and 'discrete magnetic domains' and at length

scales which are applicable for these systems.

The micromagnetic approach to modeling magnetic systems is to treat each magnetic element as a single magnetic object with an individual spin vector; the individual spins associated with each atom that comprise the domain are averaged and the magnetisation of the domain is treated as a single spin vector. Historically, micromagnetic models have implemented the Landau-Lifshitz-Gilbert (LLG) equation, which in the correct situations is capable of accurately describing the motion of the magnetisation vector and can be the preferable option in many cases due to the comparatively large integration step allowing large time frames to be investigated. The LLG equation treats the magnetic moment as a constant vector with a fixed magnitude, a unit vector, over the entire temperature range. The LLG approach is very successful in describing the zero Kelvin dynamics, but it has been shown that this method is restricted in accuracy at higher temperatures, close to and above the Curie point [30]. Due to the high temperature inaccuracy of the LLG equation this model implements the Landau-Lifshitz-Bloch (LLB) equation, as the LLB equation has been shown to be a realistic alternative to the LLG for micromagnetic simulation at high temperatures up to and above the Curie point[30]. The LLB equation differs from the LLG equation in that the magnetisation vector is not a constant magnitude and is set by the temperature.

As the model uses the micromagnetic approach, which is only capable of dealing with an ideal situation, a physical structure must be assigned to the system. In the case of granular and multi-domain structures a Voronoi construction is an ideal tool for simulating the physical structure as it is capable of giving a realistic dispersion in both the size and shape of the grain/domain structures.

The remainder of this chapter describes the methods used to model the granular thin film in more detail.

3.2 Building the Granular Structure

The modelling of magnetic materials requires precise knowledge of the physical structure of the system, as this is important to correctly describe the magnetisation and the magnetic fields that act upon the particles that comprise the system, this is true for both the external applied field and magnetostatic field.

On the nano scale the correct description of the thermal fluctuations of the

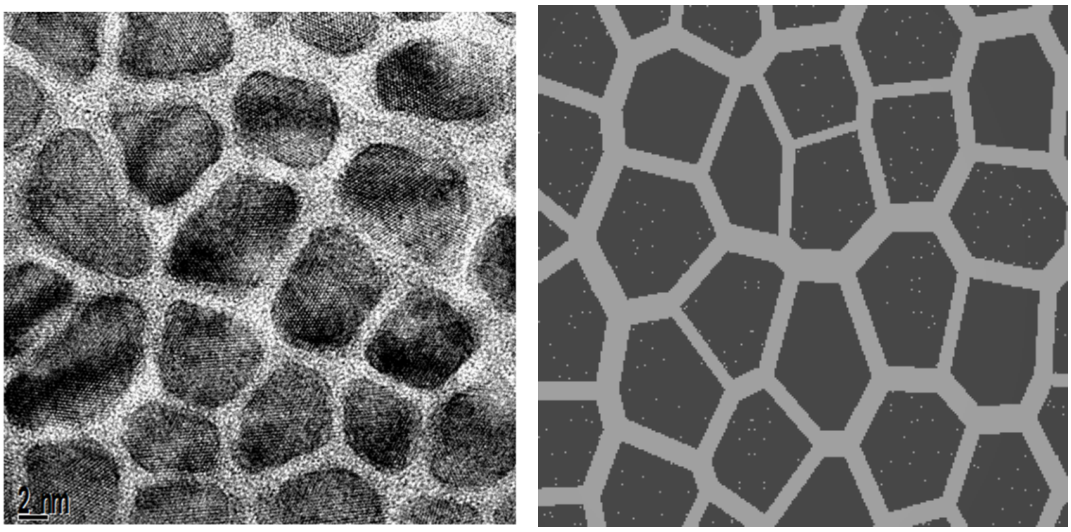

Figure. 3.1: On the left: An image of a $CoCrPtSiO_2$ granular thin film for advanced recording media showing the granular structure, taken using a high resolution transmission electron microscope [31]. On the right: An image of the simulated advanced recording media generated using a Voronoi construction.

magnetisation at a given temperature requires precise knowledge of volume of the element.

When considering the internal field, shape anisotropy is a direct attribute of the particle shape and only exists if the particle is non-uniform in shape; i.e. a sphere will have no shape anisotropy whereas a column will have a shape anisotropy along the direction of the long axis, if the long axis is significantly larger than the width of the column. In this body of research shape anisotropy is not considered as the simulated particles that make up the thin films used for the research all approximately uniform and can be considered to have no limiting shape anisotropy. A particle is considered uniform if the particle height is the same as the average particle width. The intention is to include shape anisotropy at a later stage.

When considering inter-particle interactions, such as the intergranular exchange field and the magnetostatic interaction, an exact knowledge of granular structure is essential to correctly describe these fields. To determine the intergranular exchange field, for a thin film environment, precise knowledge of the individual grain's surface is required, including the contact length between neighbouring grains and the area of the grain in plan view. The exact form of the intergranular exchange field must also give the correct dispersion over the structure of the system, due to the variation of particle size. How this information is applied, when determining the intergranular exchange field, is described later in this chapter. The correct approximation to the magnetostatic

field also requires knowledge of the system structure, not only the shape and volume of the interacting magnetic elements, but also the relative position of those elements.

For all of these reasons a Voronoi construction has been implemented to set the physical structure of the magnetic systems. With the correct input information a Voronoi construction is capable of producing a simulated granular structure and determining all the required information by computation of Voronoi tessellation of the system. To simulate the granular thin films used for hard disk recording media the input required for the Voronoi construction is the position of an approximate two dimensional hexagonal grid. This is achieved by generating a hexagonal grid and moving each point on the grid by a random value, where the magnitude of the maximum value of the random move determines the disorder in the system, resulting in a dispersion of the grain size and a microstructural disorder, which can be controlled to give the desired dispersion of the grain size. The result of this approach can be seen in figure 3.1, which compares images of granular thin film used in advanced recording media [31], taken with a high resolution transmission electron microscope, and also an image of a granular thin film produced with the Voronoi construction.

3.3 LLB Equation of Motion

The Landau-Lifshitz-Bloch (LLB) equation, equation 3.1, coupled with a Huen integration scheme has been chosen to model the time evolution of the magnetisation of each of the ferromagnetic elements within the granular systems. The LLB equation has been implemented as it is capable of correctly describing the magnetisation of single domain magnetic particles over a broad temperature range, from zero Kelvin up to and above the Curie temperature, which is essential for simulating high temperature processes such as heat assisted magnetic recording. The LLB equation was first derived by Garanin from the classical Fokker-Planck equation within the meanfield approximation, based on the thermal averaging of many exchange coupled atomistic spins interacting with the heat bath [18]. Initial investigations (by Kazantseva et al. and Chubykalo-Fesenko et al.) have shown the LLB equation is in agreement with atomistic calculations relating to linear domain wall type and relaxation time [29, 32, 30].

The model uses the stochastic form of the LLB equation proposed by Evans et al. [33] which is written in the following form, equation 3.1:

$$\dot{\mathbf{M}}_i = \gamma[\mathbf{M}_i \times \mathbf{H}^i_{eff}] + \frac{|\gamma|\alpha^i_{\parallel}(T_i)}{M_i^2}(\mathbf{M}_i \cdot \mathbf{H}^i_{eff})\mathbf{M}_i$$
$$-\frac{|\gamma|\alpha^i_{\perp}(T_i)}{M_i^2}[\mathbf{M}_i \times [\mathbf{M}_i \times (\mathbf{H}^i_{eff} + \eta^i_{\perp})]] + \eta^i_{\parallel} \tag{3.1}$$

The free energy of the system for the LLB equation, not including the anisotropy, is conventionally defined as:

$$f(m) = \begin{cases} M_s(0)V\frac{(m^2-m_e^2)^2}{8\chi_{||}m^2} & T \leq T_c \\ \\ M_s(0)V\frac{3}{20\chi_{||}}\frac{T_c}{T-T_c}\left(m^2 + \frac{5}{3}\frac{T-T_c}{T_c}\right)^2 & T > T_c \end{cases} \tag{3.2}$$

where m is the magnitude of the individual grains $\mathbf{M}$ and m_e is the equilibrium magnetisation. The temperature dependant damping terms are:

$$\alpha^i_{\parallel} = \lambda\frac{2T_i}{3T_c^i}, \quad \alpha^i_{\perp} = \lambda(1 - \frac{T_i}{3T_c^i}) \qquad T_i \lesssim T_c^i$$
$$\alpha^i_{\parallel} = \alpha^i_{\perp} = \lambda\frac{2T_i}{3T_c^i} \qquad T_i \gtrsim T_c^i \tag{3.3}$$

where $\mathbf{M}_i$ is the magnetisation of the ith ferromagnetic element, $\alpha^i_{\perp}$ and $\alpha^i_{\parallel}$ are perpendicular and parallel temperature dependent damping parameters, given in equation 3.3, where λ is a general damping term which describes the coupling of the atomic spins to the heat bath, γ is the gyromagnetic ratio and $\mathbf{H}^i_{eff}$ is the effective field acting on $\mathbf{M}_i$. The effective field, $\mathbf{H}^i_{eff}$, is the sum of the intrinsic LLB field, the anisotropy field, the inter-element exchange field and the magnetostatic field.

The LLB equation is set out in three parts. The first term describes the precession of the magnetic moment, the second term describes the damping of

the magnitude of the magnetisation (the damping of the magnetisation is where the LLB differs from the LLG) and the third term describes the damping of the precessional motion of the magnetic moment.

In order to introduce finite temperature effects perpendicular and parallel noise parameters are introduced, $\eta_\perp$ and $\eta_\parallel$ respectively, which have the following properties:

$$\begin{aligned}
\langle \eta_i^\mu \rangle &= 0, \\
\langle \eta_i^\perp(0)\eta_j^\perp(t)\rangle &= \frac{2k_\mathrm{B}T_i(\alpha_\perp^i - \alpha_{||}^i)}{|\gamma|M_s^i(0)V^i(\alpha_\perp^i)^2}\delta_{ij}\delta(t), \\
\langle \eta_i^{||}(0)\eta_j^{||}(t)\rangle &= \frac{2|\gamma|k_\mathrm{B}T_i\alpha_{||}^i}{M_s^i(0)V_i}\delta_{ij}\delta(t), \\
\langle \eta_i^{||}\eta_j^\perp\rangle &= 0
\end{aligned} \tag{3.4}$$

where μ, $\nu = \parallel, \perp$ and i,j represent the x,y,z components, $\mathrm{M}_s^i(0)$ is the saturation magnetisation of element i at 0K, T_i is the temperature of element i, V_i is the volume of element i and k_B is the Boltzmann constant.

These two parameters simulate the thermally activated random nature of the magnetisation in a different manner. It can be seen in equation 3.1 that $\eta_\perp$ is an additive field that contributes a randomness to the damping of the precessional motion and $\eta_\parallel$ acts as a random torque working on the magnetisation as a whole.

3.3.1 The Temperature dependence of the LLB Equation

As mentioned above the LLB equation correctly describes the magnetisation over a broad temperature range. It achieves this by effectively interpolating the LLG equation at low temperature and the Ginzburg-Landau theory of phase transition at high temperature[33]. The LLB approach treats the magnetisation of single domain particles as single macro-spins, similar to the LLG equation, but the two methods differ in that the LLB equation includes a longitudinal damping parameter which results a in reduction in the magnitude of $\mathbf{M} = m$ with increasing temperature. Therefore the magnetisation is treated as a dynamic temperature dependant variable and this approach correctly describes the magnetisation dynamics at high temperatures approaching T_c, $\mathrm{T} \gtrsim 3\mathrm{T}_c/4$ [29]. When combined

with the temperature dependent noise parameters this results in the correct dispersion in the magnitude of **M** at a given temperature.

At higher temperatures the atomic spin moments, that comprise the macroscopic magnetisation, are in a disordered state and the degree of their alignment varies from instant to instant. This affects the nature of the magnetisation causing it to vary in magnitude, resulting in a known dispersion in the magnitude of **M** at a given temperature. Here it is shown, figure 3.2, that the LLB approach exhibits the correct dispersion of m at a given temperature. The LLB equation has been used to determine the magnitude of the magnetisation and is shown to be in agreement with the analytic solution, equation 3.5. In figure 3.2 the dispersion of the magnetisation is given as a probability of the magnetisation having a certain magnitude at a given temperature. The spread for the magnitude of **M** was calculated using an ensemble of non-interacting hexagonal elements at a temperature of 650K. The magnetisation length was captured at each time step (over a 1.0ns simulation) and the spread in the magnetisation length determined. Figure 3.2 compares the analytic solution (obtained using equation 3.5, the Boltzmann distribution for the temperature dependent magnetisation as a function of the free energy f(m), equation 3.2) to the result determined with the LLB model, which are in close agreement.

$$F(x) \propto m^2 \exp\left(\frac{-f(m)}{k_B T}\right) \tag{3.5}$$

The dispersion in the magnitude of **M** varies over the temperature range, from 0K to T_c, the bottom of figure 3.2 shows the dispersion of the magnitude of **M** over a broad temperature range. Note, the peak of each curve in figure 3.2 has been set to 1 to highlight change in spread of the magnitude of **M**. Had the data been represented as a probability, as in the 650K example, the peak would have been at different heights making the data difficult to interpret. At higher temperatures the magnetisation is not well defined, as the individual atomic spin moments the comprise the magnetisation are thermally activated disordered state which results in a broad broad spread in the dispersion of m. At lower temperatures the magnetisation is well defined and therefore the spread in the magnitude of **M** is much less.

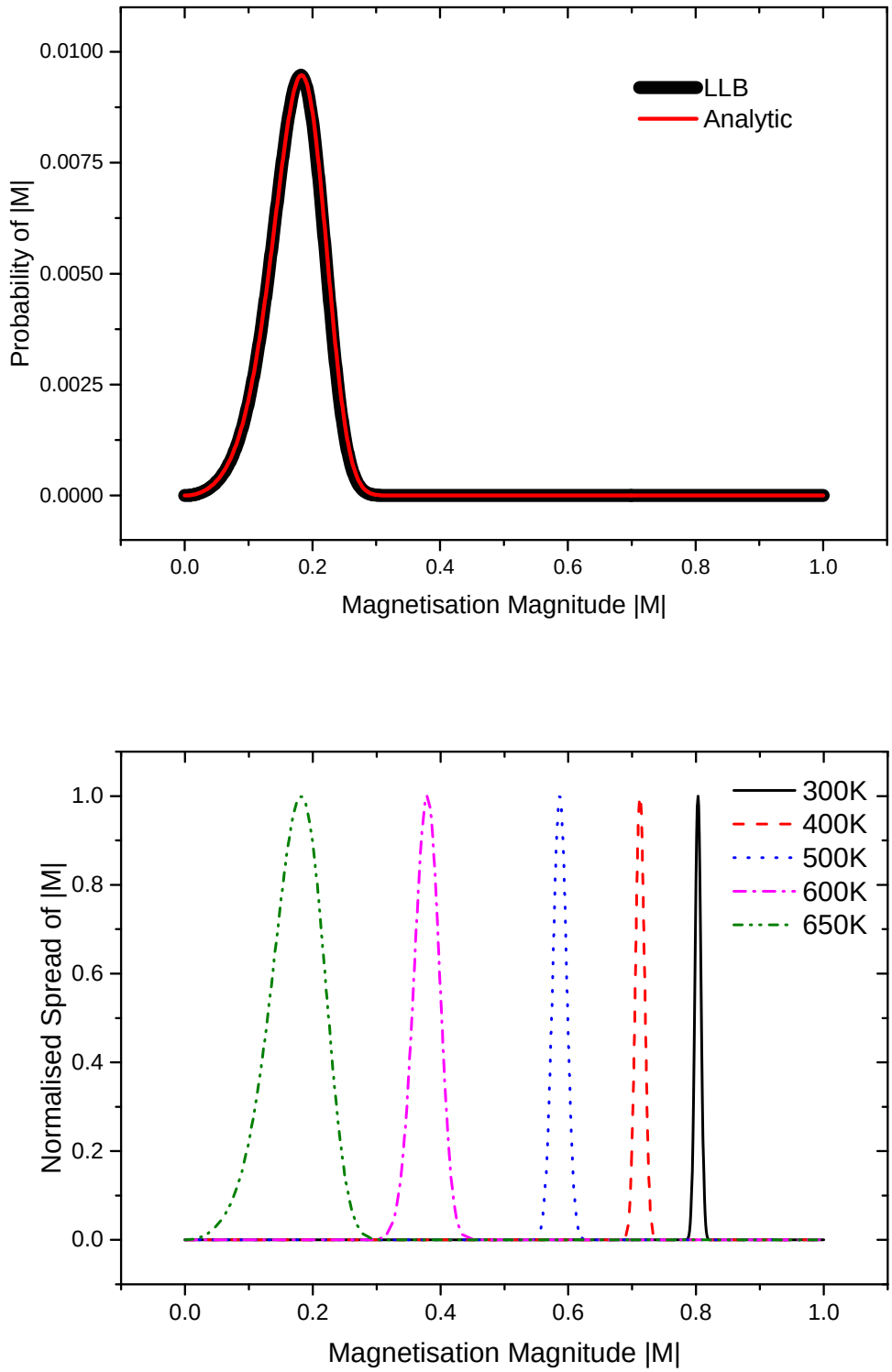

Figure. 3.2: Top: The probability of having a given magnitude for the magnetisation at elevated temperature calculated with the LLB equation also showing the comparison with the analytic solution. Bottom: A comparison of the relative spread in the magnetisation magnitude for a range of temperature from ambient to marginally below T_c where T_c is set to 660 Kelvin.

3.4 The Effective Magnetic Field Acting on Each Magnetic Element

The effective field acting on each magnetic element is the sum of the internal and interaction fields. As already mentioned the internal fields are those generated within the magnetic element and are due to the atomic structure and shape of the element. The internal fields, in a physical sense, are the sum of the anisotropy fields - the magnetocrystaline and shape anisotropies. In the case of the LLB equation there is an intrinsic field, that is unique to the LLB approach, which accounts for the effects of the inter-atomic exchange resulting in the correct magnitude of **M** at a given temperature

3.4.1 The Form of the Internal Fields

Below the form of the internal fields is given in equations 3.6 and 3.7:

The intrinsic LLB field, given in equation 3.6, acts to damp the magnitude of **M** to give the correct average magnitude at a given temperature and to achieve this damping at the correct rate.

$$\mathbf{H}^i_{intrinsic} = \begin{cases} + \frac{1}{\tilde{\chi}^i_{\parallel}} \left(1 - \frac{M_i^2}{(M_e^i)^2}\right) \mathbf{M}_i & T_i \lesssim T_c^i \\ - \frac{1}{\tilde{\chi}^i_{\parallel}} \left(1 + \frac{3}{5} \frac{T_c^i}{T_i - T_c^i} M_i^2\right) \mathbf{M}_i & T_i \gtrsim T_c^i \end{cases} \tag{3.6}$$

The form of the anisotropy field given below, in equation 3.7, is for a uniaxial anisotropy with the easy axis aligned in the z direction. It is written in the form of a hard plane, as this minimises any effect on the magnitude of **M** due to the strong anisotropy field which the magnetisation would be subject to if the anisotropy was given in an easy axis form. This is due to the longitudinal damping component of the LLB equation dictating the magnitude of **M**. The easy axis alignment can be easily changed by modifying the form of the denominator of equation 3.7.

$$\mathbf{H}^i_{anisotropy} = -\frac{(M_x^i e_x + M_y^i e_y)}{\chi^i_{\perp}} \tag{3.7}$$

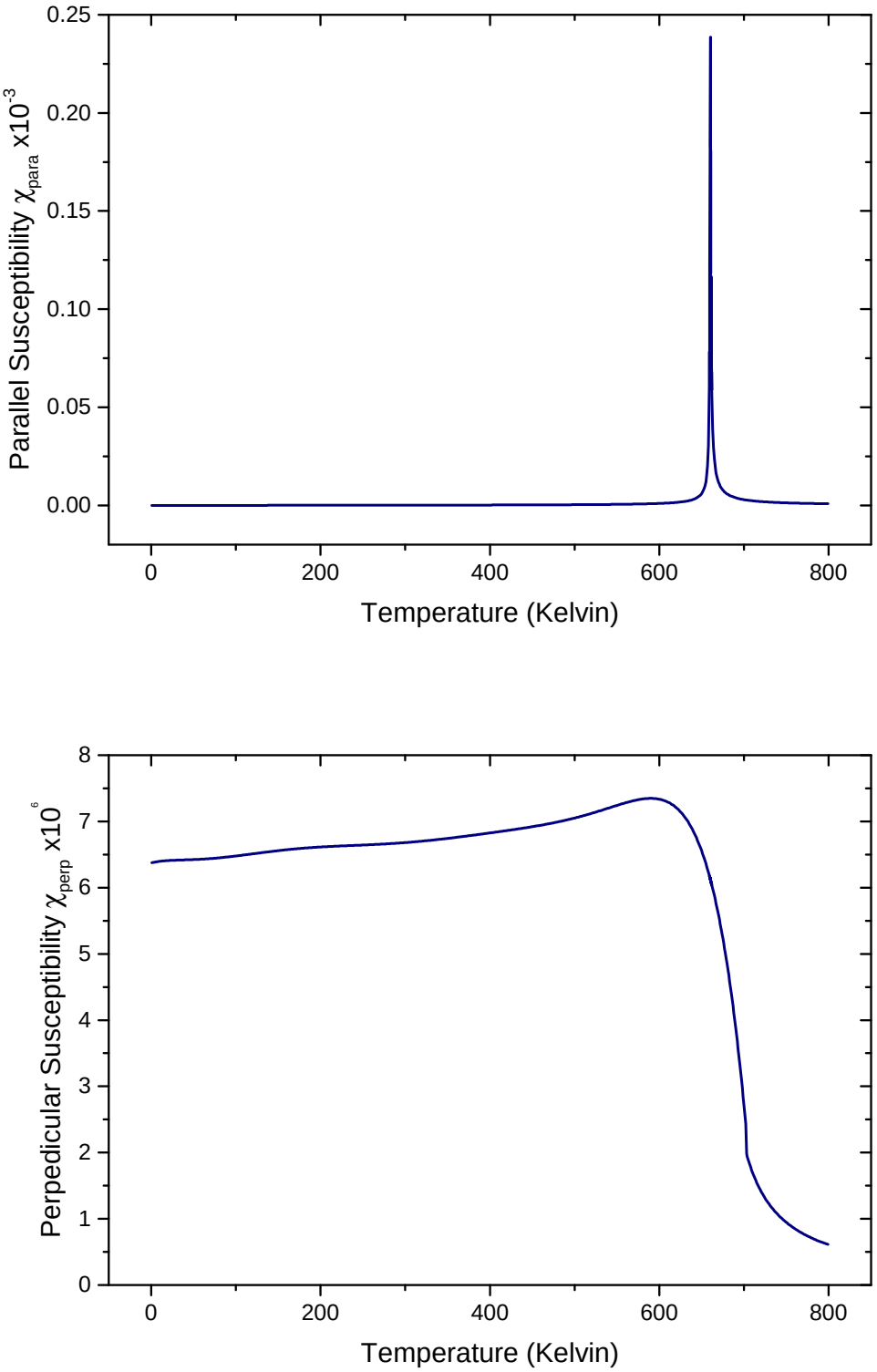

Figure. 3.3: Top: The temperature dependent form of the parallel susceptibility with a Curie temperature of 660K, used as an input parameter for the macrospin LLB model. Bottom: The temperature dependent form of the perpendicular susceptibility with a Curie temperature of 660K, used as an input parameter for the macrospin LLB model.

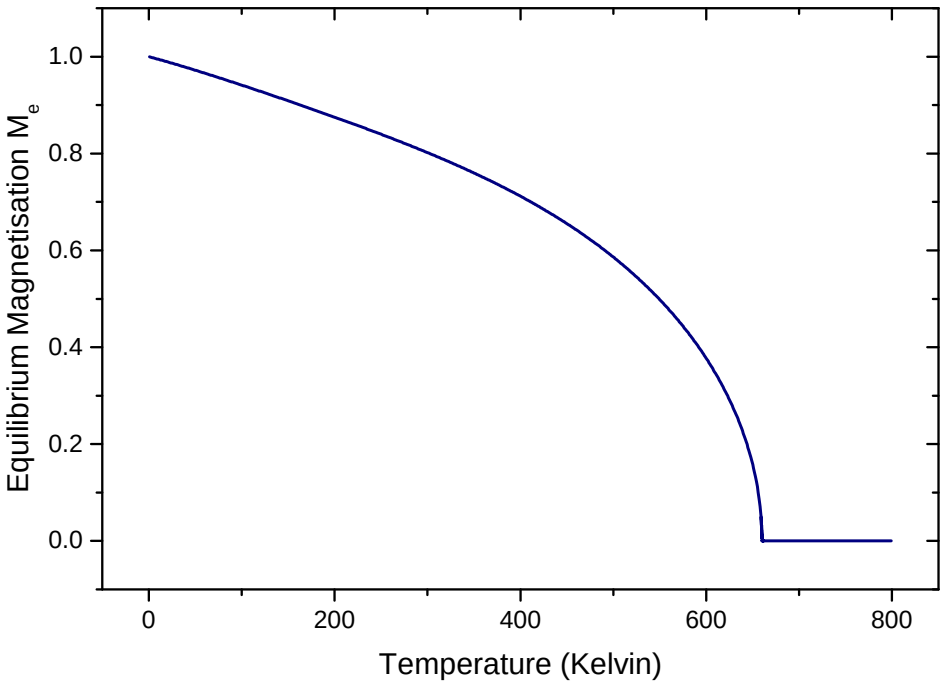

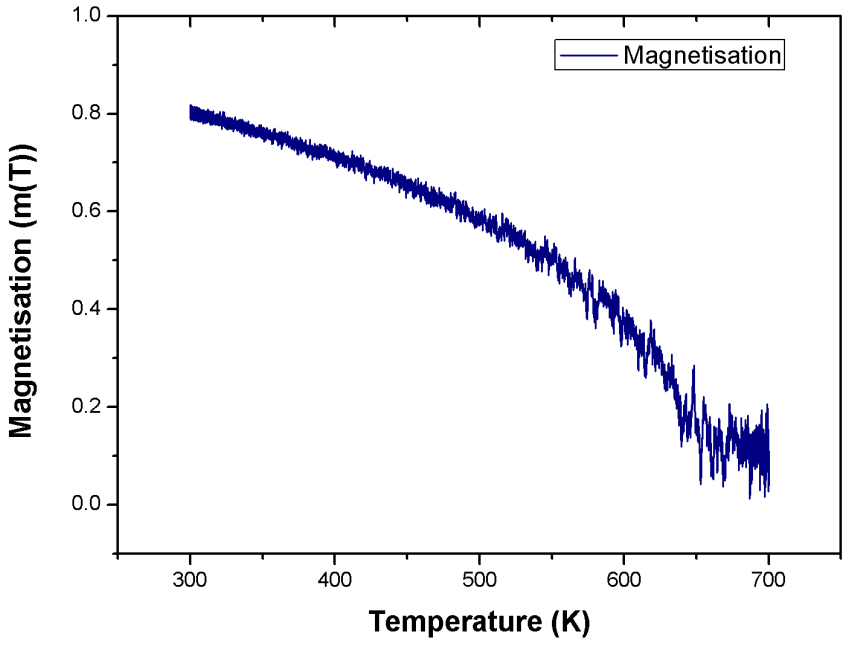

Figure. 3.4: Top: The equilibrium magnetisation (m_e) calculated for the LLB model within the mean field approximation with a Curie point of 660K, for further calculation within the model. Bottom: The temperature dependent magnetisation (m) for a single grain determined with the LLB model.

To correctly describe these fields certain information about the material properties is required, the parallel and perpendicular susceptibilities ($\chi_{||}$(T)) and ($\chi_{\perp}$(T)) respectively, and also the equilibrium magnetisation (m_e(T)). These parameters were determined with a mean-field approach (MFA) [34] and are used as an input to the model. The specific temperature dependent form of these parameters are shown in figures 3.3 and 3.4.

The susceptibility parameters and equilibrium magnetisation are used to determine the relative magnitude of these fields and rate of change of the magnetisation due to these fields, as these parameters dictate how the magnetisation responds to these fields at a given temperature. The intrinsic LLB field is a function of the parallel susceptibility and equilibrium magnetisation, these two parameters work to dictate the strength of this field and also the relative rate of change of the magnetisation due to this field. The parallel susceptibility determines the fluctuations of **M** and is essential to the linear reversal mechanism.

Figure 3.4 shows the temperature dependant equilibrium magnetisation (m_e) calculated for the model for use in the motion calculations and the temperature dependant magnetisation (m), calculated by the LLB model, is also shown for comparison with m_e. Both m_e and m were calculated by setting the temperature to 700K at the start of the simulation and allowing the system to equilibrate. After sufficient time the system was cooled from 700K to 300K over a 10ns simulation time. The temperature dependence of the spontaneous magnetisation is more noisy than that of m_e. This is caused by the stochastic nature of the LLB equation. The spontaneous magnetisation is a result of many interacting temperature dependant factors which gives rise to a dynamic magnetisation which arises from the finite size of the grains, whereas m_e is essentially for an infinite system.

3.4.2 The Interaction Fields

The interaction field experienced by an element in an ensemble is due to the other elements that comprise the material. In this body of work two forms of interaction are considered: the intergranular exchange interaction and the magnetostatic interaction. As mentioned in a previous chapter the exchange interaction is short ranged and occurs between neighbouring atoms, far smaller than the intergranular distance, although it is known that an exchange interaction does happen between neighbouring elements in granular materials, due to an interaction between the material that comprises the grains and the impurities

in the layer between the grains. Therefore in the model developed here the only exchange interaction is between neighbouring elements since the grains are assumed single domain.

The Inter-Element Exchange Fields

The form of the inter-element exchange interaction is dependant on whether the material is domain based or granular and whether the contribution to the field is from within the grain, as in multi-layer media, or external to the grain, as from a neighbouring grain. This body of work exclusively considers granular thin films comprised of a single material, therefore the form of the exchange field described here is only applicable to that format.

The intergranular exchange field in this model is given in the form as that of Peng et al.[35] under the assumption that the exchange energy is proportional to the contact area between neighboring grains. This approach allows for a realistic dispersion in the exchange field due to a variation in the grain boundary thickness and composition. This form of the exchange field is a function of the median values of the contact length between the grains, L_m, the area of the grain surface which is parallel to the plane of the surface, A_m, and also the coupling constant, J_m.

$$\mathbf{H}^i_{exch} = H_{exch} \left(\frac{J_{ij}}{J_m}\right) \left(\frac{L_{ij}}{L_m}\right) \left(\frac{A_m}{A_i}\right) \mathbf{M}_j \tag{3.8}$$

where $H_{exch} = J_m L_m/(a^2 M_s A_m)$, where L_{ij} is the contact length between grains i and j, A_{ij} is the surface area of grain i and a is the lattice constant of the material. In practice H_{exch} is set by the requirement that the average exchange field at saturation is given a certain value H^{sat}_{exch}, that is;

$$H^{sat}_{exch} = H_{exch} \sum_{i}^{N} \sum_{j \in n.n} \left(\frac{J_{ij}}{J_m}\right) \left(\frac{L_{ij}}{L_m}\right) \left(\frac{A_m}{A_i}\right) \tag{3.9}$$

The Dipole Approximation to the Magnetostatic Field

The correct calculation of the magnetostatic field, using the charge sheet approach, is computationally expensive and the runtime for this scales as N^6, where N is the number of magnetic elements within the system, and is therefore not a desirable approach. There are multiple methods of approximating the magnetostatic field and this model applies two of these approaches which are used depending on the physical structure of the granular material simulated for the experiment. The dipole approximation is used for systems where the grains are approximately uniform in shape, and a method designed specifically for this model should be applied where the grains are not uniform in shape. The grains are considered approximately uniform if the height of the grain is the same as the average grain width.

The dipole approximation treats each magnetic element as a point particle and is given in equation 3.10. The dipole approximation is very successful in situations where the magnetic elements, i and j, are uniform in shape and the elements, j, are at a sufficient distance from the element i. This approach can also be computationally expensive as the runtime scales with N^2 and therefore for relatively large systems the dipole calculation can becoming a limiting factor to the calculation. Therefore we have chosen to only include contributions to the field from elements, j, within a chosen distance from element i, as the magnitude of the contribution reduces with distance, where r_{ij} is the distance between element i and j. The cutoff distance is chosen to maintain accuracy while also limiting runtime, within this model it is 8 average element diameters from element i, as contributions from grains beyond this distance do not significantly change the magnitude on grain i.

$$\mathbf{H}^i_{dip} = \sum_j \frac{M_s^j V_j}{r_{ij}^3}(3(\hat{\mathbf{r}}_{ij} \cdot \mathbf{M}_j)\hat{\mathbf{r}}_{ij} - \mathbf{M}_j) \tag{3.10}$$

The accuracy of the dipole approximation can be low in situations where the elements within the system being modelled are not uniform in shape. In many granular systems the elements within the grains can often approximate columns and discs, therefore a method for approximating the magnetostatic field, the discrete approximation (DA) method, has been designed specifically for this situation. The DA method is an approximation of the magnetostatic field and is more time consuming than the dipole approximation, as the method requires a number of coefficients to be predetermined, since all the coefficients are

precalculated they can be stored and read in; therefore the runtime is as efficient as the dipole approximation. The DA method is described in more detail and the requirements to ensure accuracy are investigated in a later chapter.

4. The Effects of Interactions on the Relaxation Processes in Granular Thin Films

Over the history of hard disk technologies the demand for data storage has increased at unprecedented levels, consequently the advances in the areal density of hard disk technologies have encountered numerous physical barriers and subsequent technology changes. The increase in areal density has resulted in recording media comprised of grains with a significantly reduced volume with an increased packing density. These physical changes in the recording media have resulted in physical challenges which must be overcome for the technology to continue.

The current physical structure of hard disk recording media results in a system of coupled magnetic nano-particles with the anisotropy axis and magnetisation orientated perpendicular to the plane of the thin film. The coupling arises from two main mechanisms; the magnetostatic interaction, which is long ranged and has a significant effect on the stability of the magnetisation due to the perpendicular orientation of the magnetisation, which results in the magnetostatic field having a demagnetising effect; and also via the intergranular exchange field (IGE) through the magnetic impurities in the boundary layer [11]. In the ideal situation the grains would have no magnetic coupling and the direction of the magnetisation could be controlled without any effects from these interaction. But, due to the structure of the media, at the nanoscale, this is not possible. The effects of these granular interactions in relaxation process in magnetic materials has been studied for a long time [13, 14, 15, 16, 17], but the individual mechanisms that dictate these relaxation processes has proved difficult to determine.

The speed at which the data is written in hard disk technologies can be significantly affected by the effective damping of the recording media and due to the nature of current media formats it is becoming an increasingly important parameter. Ideally a larger intrinsic damping is desirable as this increases the speed of precession of the magnetisation in the reversal process and therefore the write speed. Also a higher intrinsic damping will reduce both transition noise and dc noise arising due to thermally induced back-switching during the heat assisted magnetic recording (HAMR) process.

The effects of damping on recording performance are significant, but as already stated the origins of this damping is not well understood. A detailed analysis of ferromagnetic resonance (FMR) data for CoCrPt perpendicular recording media was carried out by Mo et al.[17] and it was concluded that the value for the experimentally measured value of damping of the overall system was an order of magnitude lager than what was predicted from the mechanism of magnon-electron scattering, determined to be 0.004. Mo et al. assign the major contribution to the damping as arising from inhomogeneity line broadening and grain boundary two magnon scattering. However, another extrinsic candidate contribution to damping arises from the effects of intergranular interactions.

In this work the dependence of the damping on the intergranular exchange and magnetostatic fields is determined, numerically using the LLB granular model and also experimentally by a number of collaborative partners, and theory and experiment are shown to be in close agreement. The extrinsic damping is seen to reduce with increasing exchange, due to an increasingly coherent precession of the thin film magnetisation and in the case of the numerical model the value of the extrinsic damping reduces towards that of the input value. Also it is shown that increasing the magnitude of the magnetostatic interaction, as a result of a larger saturation magnetisation, gives rise to an increase in damping, which is ascribed to the presence of magnetostatic spin wave modes. Furthermore, a simplistic spin wave model [13] is used to show that the interplay between the magnetostatic interactions and intergranular exchange determines the number of spinwave modes with finite k-vectors that share the ferromagnetic resonance, k=0, frequency, which is where the degeneracy occurs. This degeneracy is well known to affect the damping arising from inhomogeneities [13].

Also the effect on the switching time is determined due to an increase in the intergranular exchange and the consequent decrease in the extrinsic damping and is shown to have an unexpected non-trivial relationship, which is not consistent with the macrospin picture where the magnitude of the damping is used to determine the switching time. At present the exact cause of this non-trivial relationship is not known and is considered an area for further investigation.

4.1 Optical Ferromagnetic Resonance (FMR) Method

The damping has been determined using an optical ferromagnetic resonance (FMR) method for both the experimental results and those obtained with the

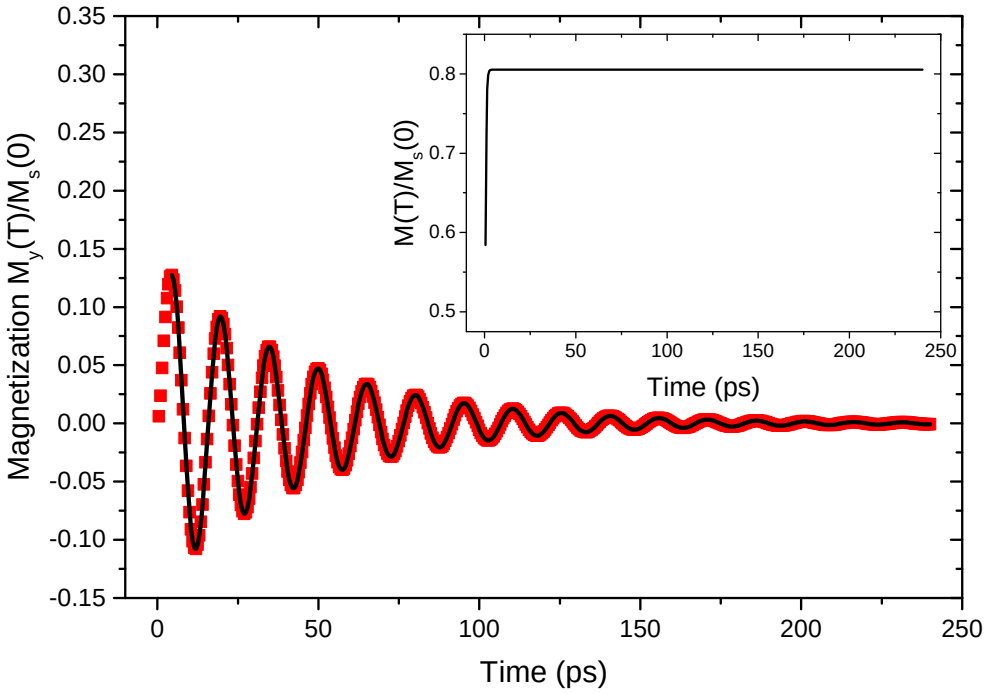

Figure. 4.1: A component of the transverse magnetisation dynamics after a heat pulse (points) with a fit to the dynamics (line) using equation 4.1. The inset shows the magnitude of the magnetisation, which demonstrates that the longitudinal dynamics occur on a much faster time-scale than the precessional dynamics.

numerical LLB granular model. Interestingly, the optical FMR method was shown to give the same values of the damping by Clinton and co-workers in using a numerical and experimental approach [36]. An optical FMR experiment is performed by first altering the equilibrium state of the sample by firstly allowing the system to achieve an equilibrium configuration with an applied field set at an angle from the anisotropy axis, let it be called the set configuration. This generates an equilibrium state due to the competing magnetocrystalline anisotropy, magnetostatic, intergranular exchange and Zeeman energies. The system is then subjected to a significant temperature rise, due to an ultrafast laser pulse, which produces a rapid temperature rise and decrease. The temperature rise lowers the magnetisation and anisotropy, shifting the magnetisation to a new equilibrium position. After the disappearance of the laser pulse the magnetisation and anisotropy recover rapidly and the magnetisation begins to precess back to its original direction. The magnetisation and anisotropy recover at a rapid rate, on the picosecond time scale, which has been observed experimentally [37, 38, 39] and numerically [40, 41, 39]. The quenching and recovery of the magnetisation and anisotropy field is much faster than the

timescale of the precessional dynamics, which allows for the resulting dynamics of the magnetisation to be analysed to determine the effective parameters governing the relaxation process. The analysis of the magnetisation dynamics is achieved by fitting a decaying oscillatory function, equation 4.1, to a transverse component of the magnetisation time sequence, say M_y.

$$M_{fit}(t) = A\cos(\omega t)\exp(-t/\tau) + B \tag{4.1}$$

where A is the initial amplitude of the oscillation, ω is the resonance frequency of the oscillation, τ is the relaxation rate for the system, t is the time and B is a parameter that accounts for any shift in the magnetisation trace away from an oscillation around a zero point. These fitting parameters can then be used to determine the effective damping, $\alpha_{eff} = 1/(\omega\tau)$.

A typical magnetisation trace with fitted data is shown in figure 4.1. The data shows the y component of the magnetisation oscillating around the zero point in the x axis. Also the data shown in the inset demonstrates the different time scales on which precession and longitudinal relaxation occur, showing that throughout the time period where the fitting is done the magnitude of the magnetisation is constant. The data shown in figure 4.1 is taken from the numerical results and in a situation where after the drop in temperature the temperature was constant during the period where the fitting was performed. This is explained in great detail at a later point in this chapter.

The optical FMR method is the preferred approach when determining the parameters that govern relaxation processes in high anisotropy materials [42], as the high fields that would be required to drive the system in to precession are not accessible with a typical resonance experiment[43]. This being said the optical FMR approach is still applied to a wide range of materials and structures [36, 44, 45, 46].

4.2 Experimental Results

Firstly a set of experimental results are presented for comparison and further discussion in the later sections where the numerical results are presented and discussed. The section contains experimental data obtained by colleagues at Seagate Technology (Dr's B Bergmans, J Holhfeldt, B Lu, KK Wang and GP Ju).

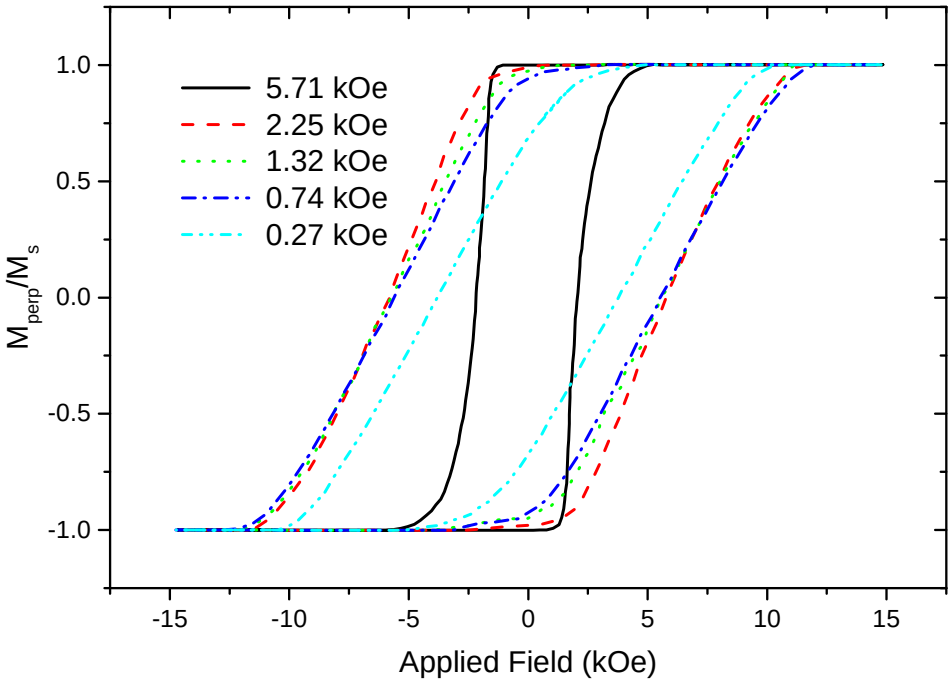

Figure. 4.2: A series of hysteresis loops determined using the CoPt granular thin films with variable intergranular exchange field strengths. Increasing exchange leads to increasingly square loops as expected.

To determine the effects of the intergranular interaction on the effecting damping, a series of experiments were undertaken, using a number of CoPt granular thin films equivalent to those used for perpendicular recording media. The exchange coupling was varied by altering the oxygen content within the intergranular layers. The increase in the intergranular exchange coupling is confirmed by the changing shape of the hysteresis loops given in figure 4.2, where reducing the oxygen content causes the hysteresis loops to become increasingly square, as the increase in the exchange coupling opposes the effect of the demagnetising field and causes the magnetisation of the film to rotate overall in a more coherent manner, with nucleation/propagation mechanisms setting in for large exchange.

The hysteresis calculations were used to determine the magnitude of the intergranular exchange field, using H_{exch} = N4πM$_s$ - H_{in} [47] where N is a demagnetising factor, usually anywhere between 0.75 to 0.85, and H_{in} is the mean interaction field which is measured using first order reversal curves (FORC). The size of the local interaction zone (D_n) is given as the cluster size in figure 4.3.

In order to study the damping dependence due to the intergranular exchange the damping was measured experimentally using an optically-pumped FMR

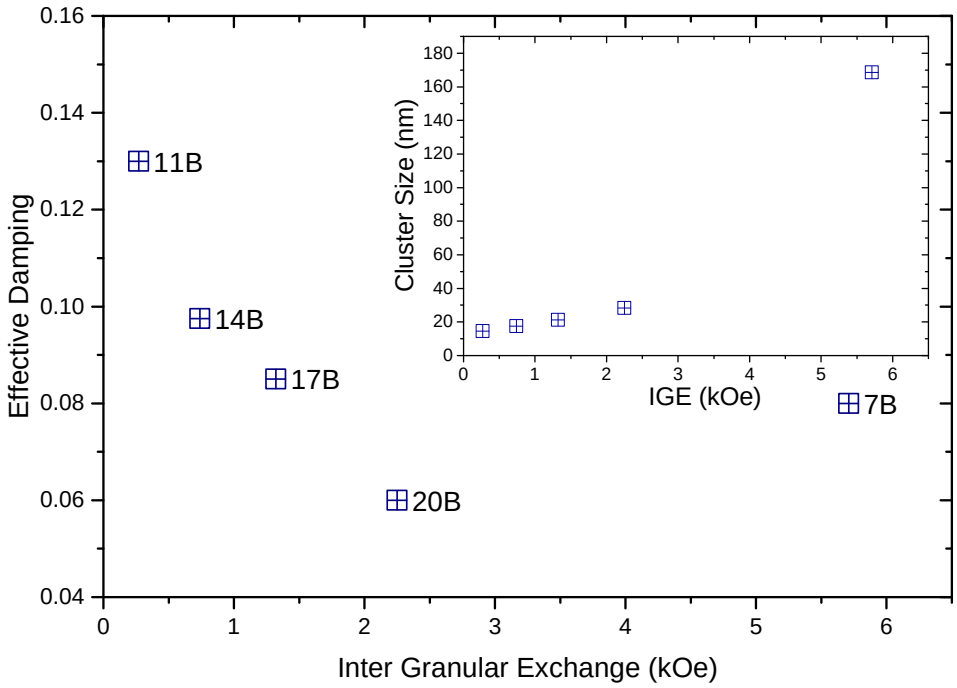

Figure. 4.3: The dependence of the measured damping constant on the exchange field. A non-monotonic dependence of α on the exchange field is clear. (Inset) The variation in the cluster size with increasing exchange field determined using the method given in reference [47].

technique on the series of thin films described above. The results obtained show a non-monotonic decrease in the damping for an increased intergranular exchange coupling, figure 4.3. The

In order to interpret the experiments in terms of the intergranular interactions the zero field cluster size was measured using the method of Nemoto et al. [47]. The results are given in the inset of figure. 4.3. Importantly, it is found that for the sample with the highest exchange coupling, there is a large increase in the cluster size. This is consistent with the form of the hysteresis loop shown in figure. 4.2, where the sample with the highest exchange exhibits a very square loop consistent with magnetisation reversal by nucleation and propagation of quasi-domains.

4.3 Numerical Results

The Landau-Lifshitz-Bloch granular model has been used in order to corroborate the experimental results and further investigate the extrinsic damping

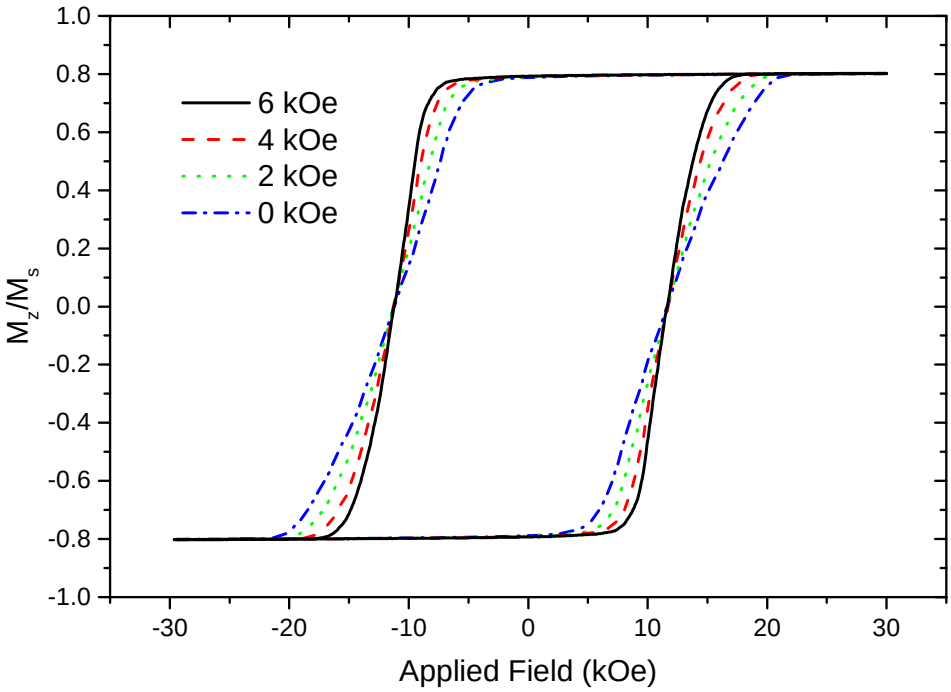

Figure. 4.4: A series of hysteresis loops determined with the granular model for a range of intergranular exchange field strengths. The results show a similar trend to what was seen experimentally, figure 4.2.

dependence on the intergranular interactions.

Firstly, in order to verify that the LLB granular model is giving static results that are consistent with those observed experimentally, the model was used to determine a series of hysteresis loops that approximate those observed experimentally, figure 4.4. These hysteresis loops were obtained for a system with K_v=1.38x10^{7}ergs/cc and M_s=1150emu and with a sweep rate of 10Oe/ns. The hysteresis loops show a similar dependance as a function of the intergranular exchange interaction; for an increasing intergranular exchange field the loops becoming increasingly square. However, there is a significant change in behaviour seen in the experimentally observed results for the highest exchange case, which we attributed to a change in the reversal mechanism due to formation of domain structures and the expansion of these domains via domain wall motion. Also, there are some expected quantitative difference between the numerically and experimentally determined results, as the numerical simulations do not take into account the magnitude of anisotropy and saturation magnetisation; as the aim was to show a qualitative comparison only. If these parameters were correctly input in to the computational model a more exact representation of the experimentally observed hysteresis results would be

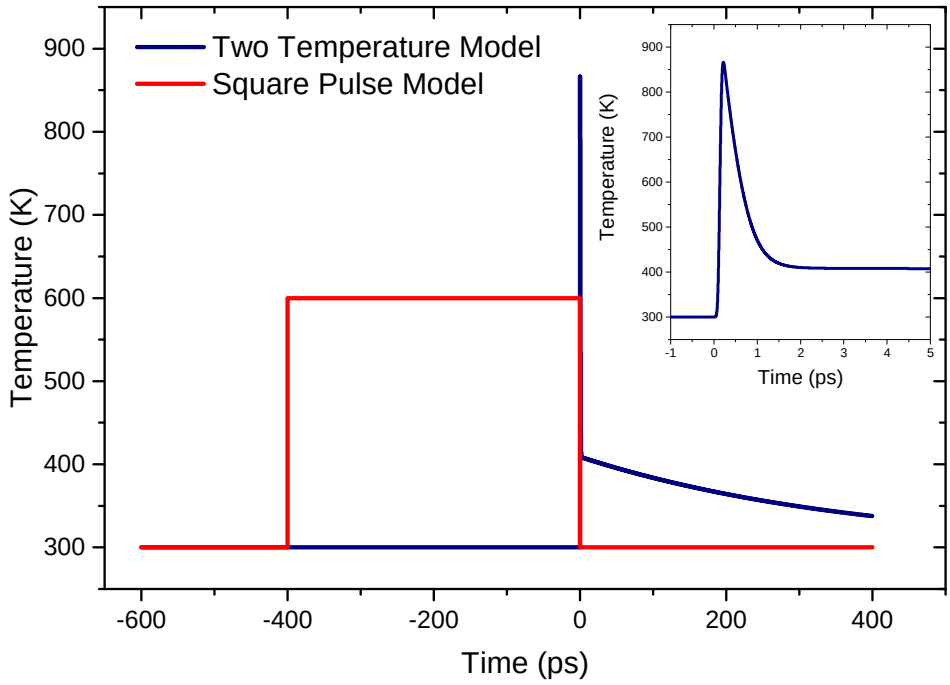

Figure. 4.5: A graphic showing the two different temperature profiles used to induce precession in the magnetisation as with optical FMR, the two temperature model and a simplistic square pulse model. The inset shows the temperature change given by the two temperature model over a narrower time range to better show the temperature profile.

found. Also, the numerically determined results do not show the same degree of squaring off for the highest exchange case.

4.3.1 Simulated Optical Ferromagnetic Resonance (FMR)

In optical FMR experiments the laser excitation of the system generates hot electrons which can reach temperatures as high as a thousand degrees Kelvin [48]. After this initial extreme heating process the electron and phonon temperatures reach a quasi-equilibrium state. The spin system will also reach an equilibrium state within this time frame, which depending of the relaxation time of the magnetic system will take around 0.1 - 1 picoseconds [49]. This form of heating is best approximated by the two temperature model (TTM), which was the first approach used to simulate the temperature profile for the numerical investigation, but this proved to have limited success. The TTM method proved difficult to accurately fit equation 4.1 to a component of the transverse magnetisation trace, as the data was sensitive to the constantly changing temperature during the period of time where the fitting was done. Secondly a far

simpler temperature profile was used to induce precession, that allowed for the fitting to be done during a period of constant temperature. Here both methods are described for completeness, with the results obtained with both methods presented later in this chapter.

Two Temperature Model

The variation in temperature associated with the heating due to a femtosecond laser pulse is described using the semi-classical two temperature model (TTM). The TTM defines the temperature of both the free electrons and the phonons. These two equations 4.2 and 4.3 are coupled with the pumping power which is assumed to heat the electrons and also induce a significant increase in the temperature of the phonons. For the purpose of this work the heating profile is assumed to be spatially uniform and also is not dependent on the thickness of the thin film, which is a reasonable assumption if the thin film is significantly thinner than the penetration depth of the laser, therefore the TTM is reduced to:

$$C_{el}(T_{el})\frac{dT_{el}}{dt} = -G_{el-ph}(T_{el} - T_{ph}) + P(t, \mathbf{r}) \tag{4.2}$$

$$C_{ph}(T_{ph})\frac{dT_{ph}}{dt} = -G_{ph-el}(T_{ph} - T_{el}) - C_{ph}\frac{(T_{ph} - T_0)}{T_{th}} \tag{4.3}$$

where T_{el} and T_{ph} are the temperature of the electrons and phonons respectively, C_{el} and C_{ph} are the specific heat capacity of both and G_{el-ph} is the electron - phonon coupling constant and T_{th} is a parameter that governs the rate of cooling of the temperature back to T_0. The spin system is assumed to be coupled to the electron temperature, T_{el}, which progresses as seen in figure 4.5

4.3.2 Square Pulse Model

As mentioned above the fitting process proved difficult using the magnetisation trace that was generated using the two temperature model to excite the system in to precession; as a larger temperature change was necessary with the model to achieve a sufficient precession angle and therefore the temperature remained above ambient during the period where the magnetisation trace was captured for the fitting process. Therefore a more simple temperature profile was applied,

to allow the capture of the magnetisation trace during a period where the temperature remained at ambient throughout. This was achieved using the square pulse temperature profile shown in figure 4.5. The square pulse model allows the system to equilibrate for 200ps at 300K, then the temperature increases as a step change to 600K and remains at the high temperature for 400ps to allow the system to equilibrate at this temperature, then the temperature drops back to ambient via a step change. It is after this point that the fitting process is applied. Although this approach is not realistic and could not be repeated experimentally, due to the instant change in temperature, the temperature change is only used to excite the system in to precession and the method is only used as a probe to determine the relaxation processes of the system, therefore the method is valid.

4.4 Numerically Determined Damping

The LLB granular model has been used to investigate the effects of the intergranular interactions, both the magnetostatic interaction, as a function of the saturation magnetisation, and intergranular exchange, on the damping of the ensemble of interacting grains. The granular system implemented is approximately 700nm x 700nm in the x-y plane and 8nm thick, with an average grain volume of $5.12\text{x}10^{-25}\text{m}^3$. The system is comprised of 7558 grains, with an average K_v=$1.35\text{x}10^7$egs/cc. The input damping is always set to 0.05 throughout the numerical investigation. The intergranular exchange and saturation magnetisation are varied for each experiment.

As mentioned above, at first the two temperature model was used to excite the system and induce precession as this better approximates the method used to determine the damping experimentally. Although the results generated using the TTM show a similar trend as the results obtained experimentally the data was insufficient to extrapolate any additional information that was required for use at a later stage of the investigation, so that process was repeated with the square pulse model. The results of both temperature models are presented and discussed in the following section.

4.4.1 Damping Dependence as a Function of IGE

At first the damping dependence as a function of the intergranular exchange was investigated for a range of values for the saturation magnetisation, figure 4.6. The results obtained with the LLB granular model are consistent with the experimentally observed decrease in the extrinsic damping with increasing IGE,

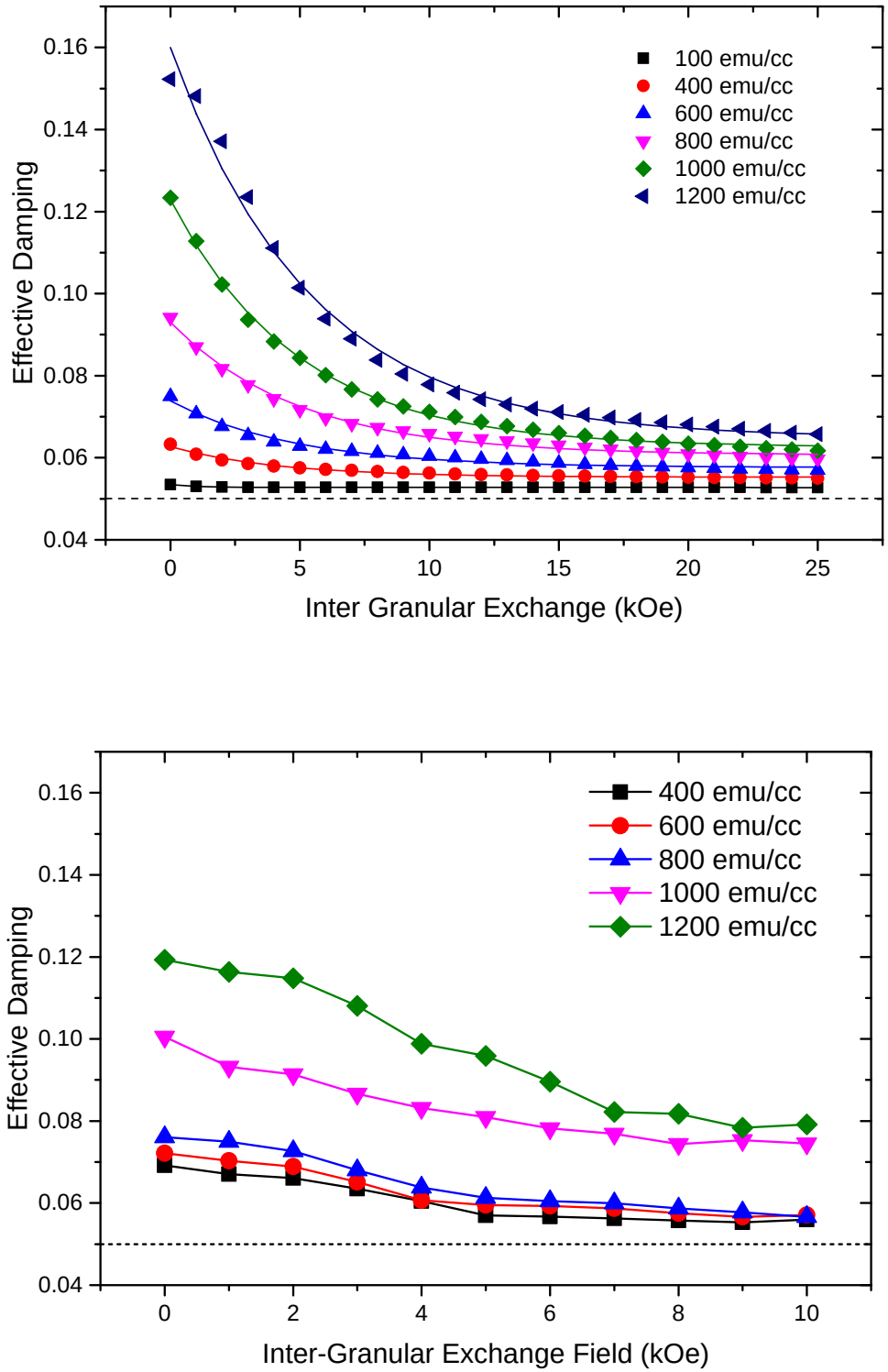

Figure. 4.6: The dependence of the extrinsic damping as a function of increasing IGE, determined using both the two temperature model (TTM) and the square pulse temperature model. Top panel: The square pulse model. Bottom panel: The TTM. Both models show a similar trend, although the square pulse model shows a more consistent decease in the extrinsic damping with increasing exchange.

for both the TTM and square pulse model. However, the square pulse model gives a much more consistent trend as a function of increasing IGE. As mentioned previously, the TTM gives rise to a highly elevated temperature during the precessional motion. Consequently the square pulse, although idealised, is adopted as the best procedure to obtain the damping constant from the model calculations. The results presented in the top panel of figure 4.6, determined with the square pulse model, show both the damping data points that were generated using equation 4.1 and also fits to those data points using equation 4.4. The fitted data (α_{Ex} vs IGE) is used, at a later stage of this investigation, as an input parameter for the semi-analytical model of transition time as a function of the IGE.

The fits shown in figure 4.6 are generated using equation 4.4.

$$\alpha_{Ex} = \alpha_0 \exp(H_e/H_0) + \alpha_\infty \tag{4.4}$$

where α_0, H_0, α_∞ are dependent on the value of the intergranular exchange and the saturation magnetisation and are determined by fitting equation 4.4 to the data points shown in figure 4.6.

Overall the LLB granular model is in agreement with the results obtained experimentally, for both the hysteresis loops and the damping calculations. For small values of the IGE the numerical results are consistent with the experimental data, where the damping decreases with increased IGE. However, for large values of exchange the model does not reproduce the significant increase in the damping seen experimentally. The increase in the damping for high levels of exchange seen experimentally can be attributed to the dramatic increase in the cluster size for the particular sample, shown in the inset of figure 4.3. It is possible that the interranular exchange field determined for this sample was an underestimate. The change in shape of the hysteresis loop obtained with this sample is consistent with a change in the magnetisation reversal mechanism, to the nucleation of domains that propagate via domain wall motion. For systems with strongly exchange coupled grains it is likely that an additional mechanism is responsible for the increase in the damping due to an interaction between the domain walls and defects. It is assumed that the granular model is not capable of exhibiting this kind of interaction, at the levels of IGE investigated, and therefore does not show the increase in the extrinsic damping for high IGE.

The saturation magnetisation, M_s, has a significant effect on the dependence of the extrinsic damping as a function of the intergranular exchange. For low

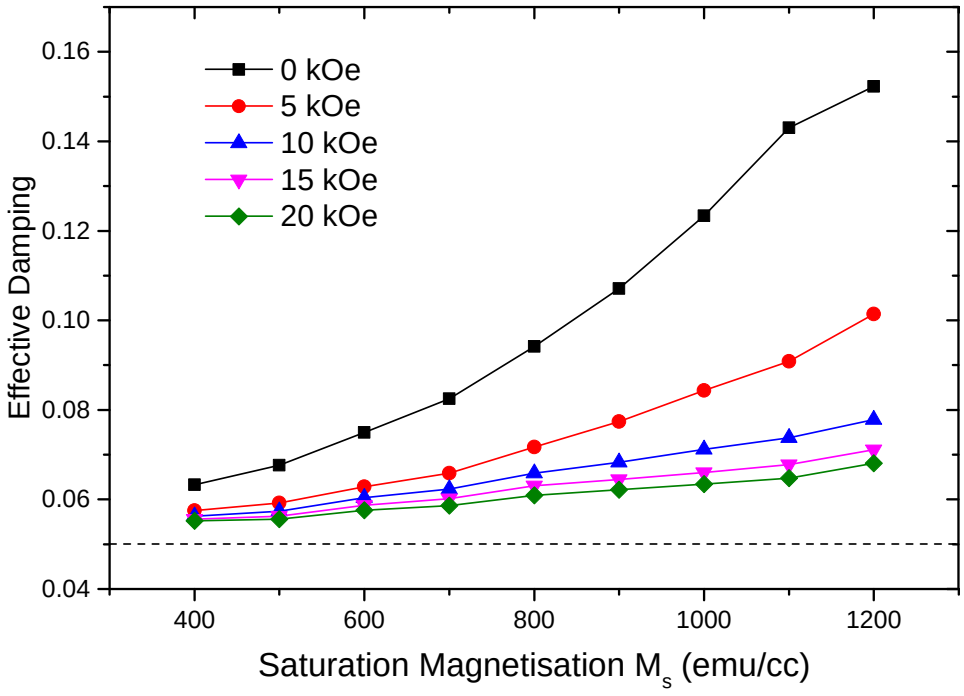

Figure. 4.7: The dependence of the extrinsic damping as a function of increasing IGE, determined using the square pulse temperature model.

levels of M_s the damping is approximately equal to the input damping for all values of the exchange. For larger values of M_s there is a much greater variation in the damping which is seen to reduce towards the input value for increasing IGE. This effect is due to the interplay between the two competing interactions. For low levels of M_s the magnitude of the magnetostatic field is relatively smaller and therefore has a reduced contribution to the dynamics of the thin film magnetisation. For higher levels of M_s the magnetostatic field has an increased effect on the dynamics of the individual grains, which causes the magnetisation of each grain to precess in a perturbed fashion, resulting in a significant increase in the damping above the input value. The intergranular exchange field works to mediate the effect of the increased magnetostatic field by inducing a coherent precession between the individual grains, which has the effect of reducing the extrinsic damping towards the input damping. This is discussed later in terms of the excitation of spin waves. In the following we just use the step temperature approach which gives the most reliable value of the damping parameter.

4.4.2 *Damping Dependence as a Function of the Magnetostatic Interaction*

To further the understanding of the effects the interaction fields have on the damping, the dependance as a function of magnetostatic field (due to increasing the saturation magnetisation), for a number of values of the intergranular exchange, was determined, figure 4.7.

The dependance of the extrinsic damping shows strong variation due to an increase in the magnetostatic and exchange field, figure 4.7. If the zero exchange interaction case is considered there is a large increase in the damping for increasing M_s, of around a factor of 3, due to the increased effect of the magnetostatic field causing the system to enter a disordered state at an increased rate. For low values of M_s the damping for all values of the IGE converge to the value of the input damping, due to the very low contribution from the magnetostatic field.

4.5 Semi-analytical Spinwave Model

So far the dependance of the damping has been determined as a function of the intergranular interactions, both numerically - with the LLB granular model - and experimentally and are shown to be in close agreement. But the underlying mechanism that governs the observed dependance is somewhat unknown. However, the reduction in the extrinsic damping can be explained as arising from a reduction in the degeneracy of the finite k-vectors with a frequency of the k=0, ferromagnetic resonance, mode shown in the inset in figure 4.8.

The presence of inhomogeneities within the thin film, such as lattice defects and grain boundaries, can act as a source for spin wave scattering which leads to the transfer of energy from uniform magnetisation precession into degenerate spin wave modes. Therefore a reduction in the degeneracy will reduce the number of possible spin wave modes where scattering can occur. This process involves a change in the wave number magnon, due to the annihilation of a zero-wavenumber magnon and the creation of a nonzero-wave number magnon, which causes the magnetisation precession to undergo a rapid relaxation / damping [50]. Therefore any reduction in the degeneracy will have a consequent reduction in the damping.

A simple model based on the methods of McMichael [13, 14, 51] for determining the frequencies of the spin wave modes has been developed and implemented by Dr T. Ostler. For a more complete description of the method see Appendix 1 - Spinwave Model.

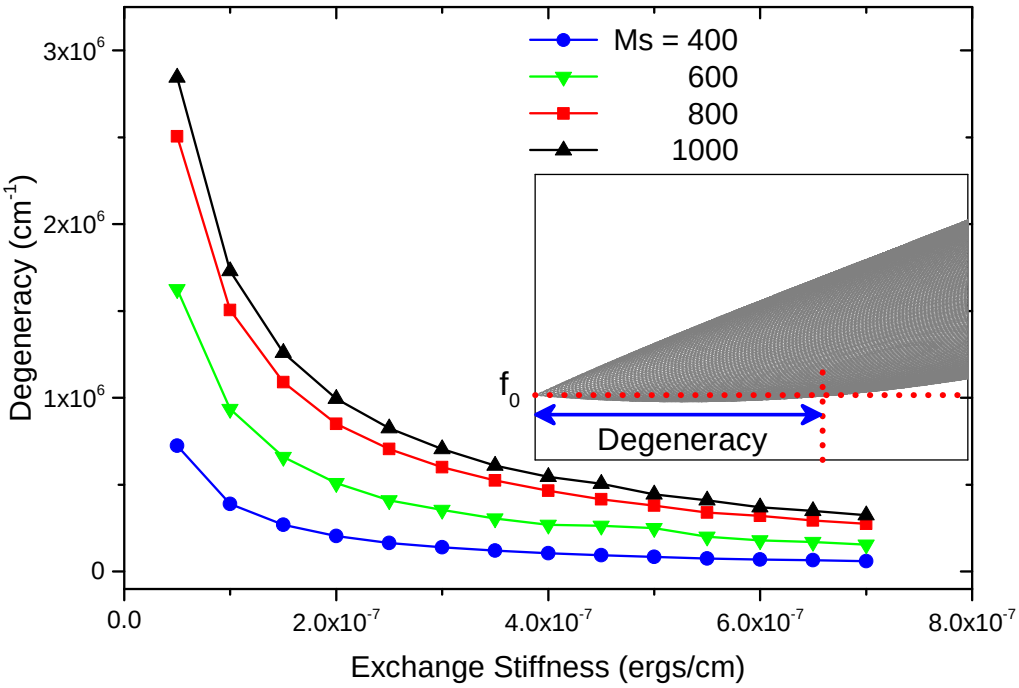

Figure. 4.8: Spinwave degeneracy as a function of exchange stiffness for a range of values of saturation magnetisation. There is clearly a direct correlation between the degeneracy and the damping shown in figure 4.6 and a similar trend for fixed exchange stiffness and varying M_s.

For consistency between the two approaches, the LLB granular model and the spin wave model, the same values for the saturation magnetisation, magnetocrystalline anisotropy, applied field and the average angle between the applied field and magnetisation are used in both cases. The average angles the magnetisation makes with the plane of the thin film are taken from the numerical simulations when the system is in equilibrium. Using these values the spin wave properties are calculated and the degeneracy of these modes, with the k=0 mode, is determined. Also it should be mentioned that the range of values used for the exchange stiffness for this investigation is in the correct range [15].

The number of modes having the same frequency as the ferromagnetic mode, the k=0 mode, - i.e. the degeneracy - is seen to reduce with in increasing exchange stiffness, figure 4.8. There is clearly a direct correlation between the degeneracy shown in figure 4.8 and the extrinsic damping shown in figure 4.6.

It is likely, based on the results determined with both the spin wave and LLB granular models, that the enhanced damping, seen in both the numerical calculations and experimentally, is due to the two-magnon scattering

process. Specifically, the introduction of the magnetostatic interaction introduces magnons with a degeneracy which increases with M_s. The introduction of exchange coupling decreases the degeneracy leading to a reduction in the damping. This is partly evident due to the form of the LLB granular model, as it does not allow for scattering due to impurities and both the LLB and spin wave models do not include any specific detail regarding grain boundaries, but both models do account for a grain size distribution and therefore a varying magnetostatic field which results in a distribution in the precession angle of the macro-spins. Also, in the LLB granular model the anisotropy axes for the individual grains are assumed to be perfectly aligned, therefore there is no dispersion in the anisotropy axes, which does not allow for any grain to grain scattering to occur. Similarly each grain is a single domain particle and therefore there is no contribution to the two-magnon scattering process from grain boundary scattering.

In terms of a macrospin picture, the decreased damping can be explained by a stiffening of the system resulting in a more coherent precession so that demagnetising effects become less important and the system as a whole acts more like a single macrospin.

4.6 Transition Time Calculations

The results presented in figures 4.3, 4.6 and 4.7 demonstrate the importance of interaction effects on the relaxation dynamics. As mentioned above effective damping can have a significant effect on the write speed in hard disk technologies. Over the damping range observed in figures 4.6 and 4.7 and within the single-domain macrospin limit the observed decrease in damping with increased intergranular exchange would lead to an increase in the switching time from one energy minima to the other, slowed by the decrease in damping [52]. However, this theory neglects the effects of the inter-particle interactions and therefore does not apply over the full range for the IGE investigated. The LLB granular model has been used to determine how the transition time varies over the range of IGE used for the above calculations. As is shown in figure 4.9, the simple macrospin picture does not hold and a non-trivial dependence between the transition time and the intergranular exchange is found.

To determine the reversal time numerically the system is allowed to equilibrate at 300K without the addition of an applied field. When the magnetisation has relaxed to its equilibrium value, an applied field of 20.0 kOe

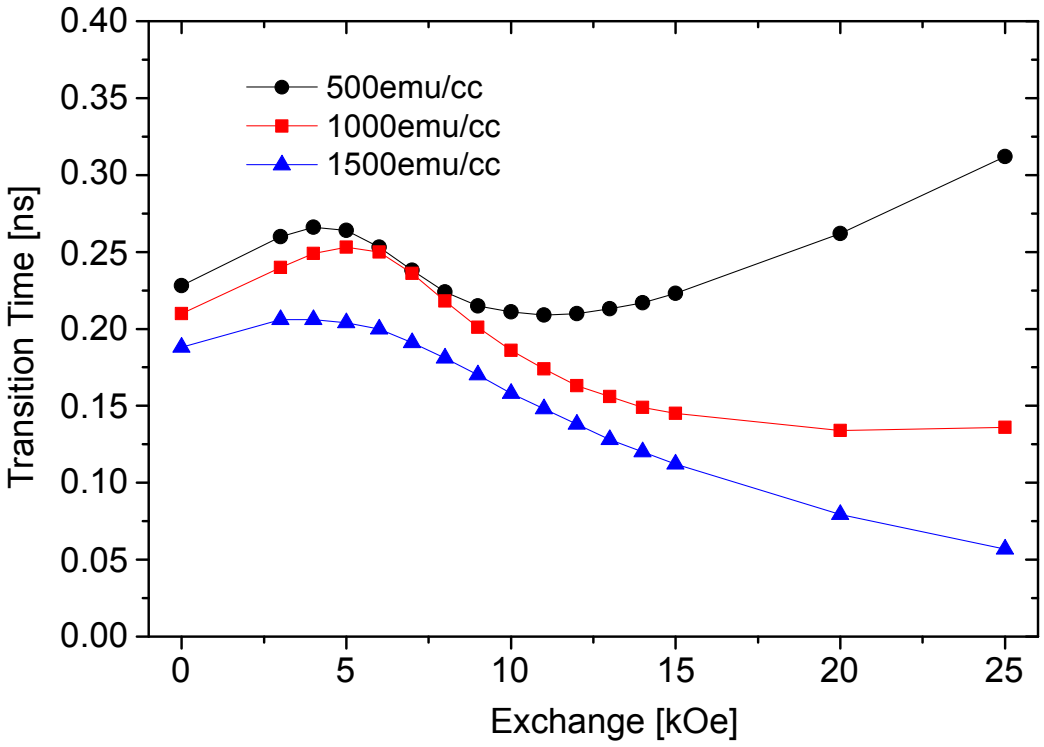

Figure. 4.9: Transition times as a function of intergranular exchange for a range of values of saturation magnetisation. Initially the system is relaxed to equilibrium at T=300K at which point a reversing field of 20kOe is applied. The transition time is taken when M_z¡0 and the data points are averaged over 10 instances with different random number seeds.

is applied in the negative z direction. As the magnetisation of the thin film crosses the $M_z = 0$ point [53], the associated transition time is captured. These results are averaged over 10 runs with different seeds for the random number generator, which was sufficient to reduce the standard deviation in the transition times to 0.1% of the value measured. The measured transition time exhibits a non-trivial dependence on the intergranular exchange field, figure. 4.9. Initially, for low levels of exchange (0 - 4 kOe), the transition time increases linearly with increasing IGE, as expected, but the increase slows and stops entirely as a local maximum is reached at approximately 5kOe. The transition time is then seen to decrease with increasing intergranular exchange. This result is not consistent with the standard single domain macrospin picture, as a decrease in the damping is expected to result in an increase in the transition time. In the high exchange regime the transition time follows the simple single domain macrospin picture, in which the decrease in damping shown in figure. 4.6 leads to an increase in transition times. This increase occurs for large values of the exchange, beyond typical values seen in granular media [11]. In the intermediate region there is a local maximum around 5kOe that cannot be simply explained using the macrospin picture. The cause of the non-trivial relationship between the

transition time and the intergranular exchange is currently unknown, but appears to arise due to a subtle interplay between the inter-particle interactions. This non-trivial relationship is of significant consideration for hard disk technologies and the cause of this relationship is an area for further investigation.

4.7 Summary

To surmise, the LLB granular model has been used to determine the dependence of the damping constant on the intergranular interactions; the intergranular exchange and magnetostatic fields. The results obtained with the LLB granular model are consistent with those obtained experimentally by colleagues at Seagate Technology. The effects of interaction on the damping was determined using an optical ferromagnetic resonance technique to probe the relaxation processes. Both the LLB granular model and the experimental results are consistent in the low exchange regime and show a decrease of effective damping with increasing exchange. The LLB model and experiment show a different trend for the higher exchange case and it is argued that the increase in the damping for the highest exchange case, seen experimentally, is due to a change in the reversal mechanism involving the formation and propagation of quasi domain structures. The ideal scenario for perpendicular recording is an ensemble of weakly exchange coupled grains, therefore any increase in the exchange strength is likely to see a subsequent decrease in the damping as predicted by the model.

To gain further insight into the mechanism responsible for the observed variation in the damping a further investigation using spin wave theory has been undertaken. The results of this investigation assign the reduction in the damping due to increasing intergranular exchange to a reduction in the degeneracy of the finite k-vectors with the frequency of the ferromagnetic resonance mode, k=0. The spin wave calculations show a direct correlation between the damping shown with the LLB granular model and the degeneracy, with a similar trend for a fixed exchange stiffness and varying M_s. It is concluded that the two-magnon scattering process is the dominant term in the reduction in damping with increasing intergranular exchange.

A study of the switching time dependence on the intergranular exchange field and consequently the effective damping is also undertaken and is shown to have a non-trivial relationship which is not consistent, in the low-medium exchange regime, with the simple macrospin picture, where the changes in the damping are used to determine the subsequent changes in the switching times. Importantly,

the simple macrospin picture breaks down for exchange values that are seen in high density magnetic recording media. The cause of this non-trivial relationship is currently unknown, due to the significance in hard disk technologies, this should be considered an area of further investigation.

5. Heat Assisted Magnetic Recording

Information has been stored magnetically for over 60 years and during that period the technology has taken many forms; from early magnetic drum technologies, through many forms of magnetic tape and now in its current form - hard disks. Over that period the demand for greater data storage has increased at an unprecedented rate, with data densities now well in to the Gbit/sqin as standard. This increase in areal density has encountered numerous technological and physical barriers that have been overcome to allow the technology to continue developing.

Hard disk technologies are now in a situation where information is stored at a length scale of nanometres, with a recorded bit being approximately 40nm in size, stored on media comprised of grains with an average diameter of roughly 10nms. The current state of hard disk technologies has presented an additional physical barrier in the form of the 'magnetic recording quadrilemma', which must be overcome to further develop the technology.

A possible solution to the physical barrier presented by the 'magnetic recording quadrilemma' is heat assisted magnetic recording (HAMR). As mentioned in a chapters 1 and 2, K_v is temperature dependent and tends toward zero as the temperature approaches the Curie point (T_c) [2, 54]. Therefore the thermal stability criterion n_o, given in chapter 1 - equation 1.2, can be varied from a relatively high value at ambient temperature, maintaining media stability, to a relatively low value by raising the temperature locally and momentarily removing the problem of writability via the low anisotropy state. This technique could maintain the historic increase in the areal density into the Tbit/sqin, by allowing for increasingly smaller grains to be used in the storage media [54]. HAMR is currently moving towards a practical realisation; recent work has demonstrated an areal density of 1.4 Tbit/sqin, for the rst time exceeding the data densities achieved with by conventional hard disk technologies[55].

A promising candidate for HAMR recording media is L_{10} ordered FePt as it has a high bulk magnetocrystalline anisotropy of $K_v(0) = 9.0 \times 10^7$ ergs/cc [9] allowing for a thermally stable grain as small as 3.3nm in diameter, generating a possible areal density well into the Tbit/sqin regime. Also L_{10} FePt has a relatively low Curie temperature, roughly 660K, which reduces the maximum temperature required to enter the low anisotropy state, where writability may be possible.

In this chapter many aspects of the the HAMR process are discussed. Firstly the constant temperature bulk properties of the FePt high anisotropy granular thin films, that are proposed for use in HAMR, are examined for comparison with the dynamic properties of the HAMR process. A new measurement technique similar to magnetic hysteresis is used to show the possible benefits of HAMR, this is achieved by determining the bulk properties of the HAMR process, including the demagnetising and also reversal fields[56]. These properties are studied over a range of values for the intergranular exchange field (IGEF) and also a the full range of magnetocrystalline anisotropy that is applicable to the HAMR process and can be physically achieved with L_{10} ordered FePt.

The practical requirements of the HAMR process are further examined; concentrating on the thermodynamic properties during the magnetisation reversal process. Here it is shown that conventional picture of HAMR as magnetisation reversal over a thermally reduced energy barrier is only true below a certain anisotropy dependant temperature rise and through this process the desired level of magnetisation reversal is never achieved. For practical levels of magnetisation reversal the linear reversal mechanism is required,[29, 57] which means that the temperature must be raised to a minimum of T_c during the HAMR process.

Also the limits of the HAMR process, regarding maximum areal density, are discussed in terms of 'thermal writability' as the limiting factor rather than the criterion of thermal stability given by the inequality shown in equation 1.2.

5.1 Simulation Parameters

The aim of this study is not to investigate the HAMR process by modelling the recording of bits; but rather the intention is to study the physics of the HAMR process as a field cooled magnetisation process. In doing this knowledge is gained regarding both the dynamics of the HAMR process and also the thermodynamic aspects which will limit the maximum areal densities achievable with HAMR. Due to this investigation approach both the applied field and temperature profile are spatially uniform. The time evolution of the temperature increase associated with the laser heating is simulated as a step change from ambient (300K) to a maximum value, returning to ambient following a Gaussian profile in a characteristic time. Throughout this study the cooling rate is set to 0.5ns unless otherwise stated; this brings the temperature back to ambient in approximately 1.2ns, shown in figure 5.1. All temperatures stated in this chapter

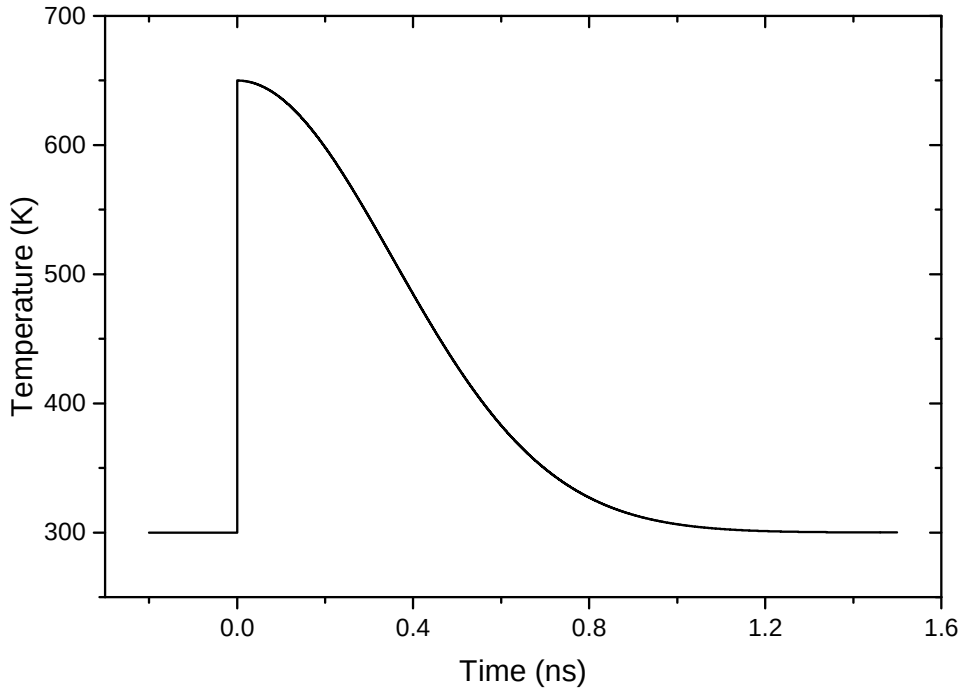

Figure. 5.1: A graphic depiction of the time evolution of the temperature, implemented in the model, to simulate the temperature rise associated with the HAMR process. Here the maximum temperature reached is 660K which is the Curie temperature of bulk FePt and the temperature reduces to ambient with a cooling rate of 0.5ns.

are given as the maximum temperature reached during the simulation of the HAMR process.

The FePt granular thin film simulated for this investigation in to the HAMR process is approximately 600nm by 600 nm in the x y plane and is comprised of 7558 grains, which for the majority of the investigation have and average volume of $2.16 \times 10^{25} m^3$, where each grain is separated by approximately 1nm.

The magnetocrystalline anisotropy of the individual grains is stated as a percentage of the bulk value for L_{10} ordered FePt, 9×10^7 ergs/cc. This simulates a system of grains that are partially L_{10} ordered, as it is not currently possible to produce fully ordered L_{10} FePt. Therefore the granular media used for early versions HAMR will have a lower anisotropy than that of fully L_{10} ordered FePt.

All input parameters have the same value for each grain, which include, the temperature, the applied field, the magnetocrystalline anisotropy (K_v), the saturation magnetisation (M_s), the damping constant (α) and the transverse and longitudinal susceptibilities ($\chi_\perp$) and ($\chi_{||}$) respectively.

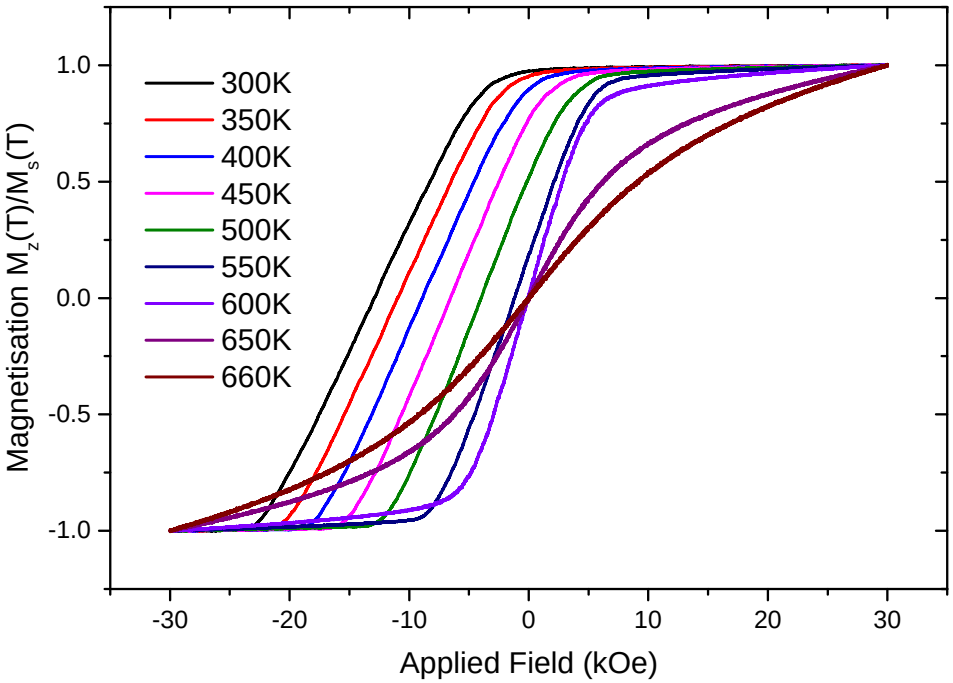

Figure. 5.2: A series of hysteresis curves determined over a broad temperature range from ambient to T_c. The magnetocrystalline anisotropy is 20% of L_{10} FePt. The data shows the reduction in the coercivity, H_c, and therefore the reduction in the anisotropy associated with the raised temperature.

5.2 Constant Temperature and Bulk Properties

The initial study concentrates on the minimum value of K_v that will ensure the desired thermal stability of the magnetisation for an ensemble of grains with an average diameter of 6.0nm. This equates to $K_v(0) = 1.8\text{x}10^7$ ergs/cc or approximately 20% of fully L_{10} ordered FePt. The saturation magnetisation, M_s was set to 1150 emu/cc, the average intergranular exchange field was set to 4kOe and the input damping parameter was set to 0.1.

To investigate the effect of increased temperature on the anisotropy, a series of hysteresis curves were generated to observe the reduction in the coercivity, H_c, and therefore the reduction in K_v, figure 5.2. The hysteresis curves where obtained using a sweep rate of 10Oe/ns, which was sufficient to approximate static hysteresis, as with a sweep rate of less than 10Oe/ns the observed coercivity was practically the same. As expected H_c reduces towards approximately zero as the Curie temperature is approached. In the lower temperature cases (300K - 600K) these results are in support of the conventional picture of HAMR as

magnetisation reversal over a thermally reduced energy barrier. In the ambient temperature case magnetisation reversal (we define magnetisation reversal as greater than 95% of the magnetisation being in the opposite orientation after the process) is achieved with an applied field strength in the region of 25kOe; clearly in this case the magnetisation of the media can not be switched using conventional methods. However, at higher temperature the field required to reverse the magnetisation is much reduced to approximately 10kOe. The higher temperature cases (greater than 600K) show a more complex picture, as the field required to reverse the magnetisation is of the same order as the ambient temperature case. This is due to the superparamagnetic effects as these high temperatures[5], requiring increasingly large applied field to induce the magnetisation to align with the applied field direction. This effect is also in support of thermal writeability introduced by Evans et al.[58, 59], which quantifies the tendency of backswitching of magnetisation at elevated temperatures and therefore the requirement of a higher applied field strength to achieve the desired level of magnetisation reversal. The concept of thermal writeability is discussed further later in this chapter.

Although the results given in figure 5.2 are in support of the conventional picture of HAMR, the nature of the HAMR process is sufficiently different from these hysteresis experiments as these are undertaken at constant temperature. The temperature rise associated with HAMR is only momentary and the reversal of the magnetisation occurs during the period of high temperature and subsequent cooling. The HAMR process is better observed with an alternative measurement technique first proposed and performed by Liu et al.[56], where the magnetisation is observed with a photomagnetic synchronised TR-MOKE technique, where the magnetisation is reset to remanence between each pump-probe experiment. In this case the technique determines only the effect on the magnetisation due to the current laser pulse and applied field, independent of the measurement history. Effectively the technique records the final state of the magnetisation of the thin film due a specific set of conditions, after a set period of time, and is therefore an excellent technique for observing the HAMR process. This technique has been used to generate the result shown in figure 5.3, where magnetisation state was recorded after a time period of 1.7ns, this includes a 0.2ns equilibration period before the temperature rise and then an additional 1.5ns to allow the magnetisation to react to the change in temperature from ambient to a maximum and back to ambient and also due to the external applied field. This time scale was used for all experiments of this type.

The results observed using the alternate hysteresis technique, figure 5.3,

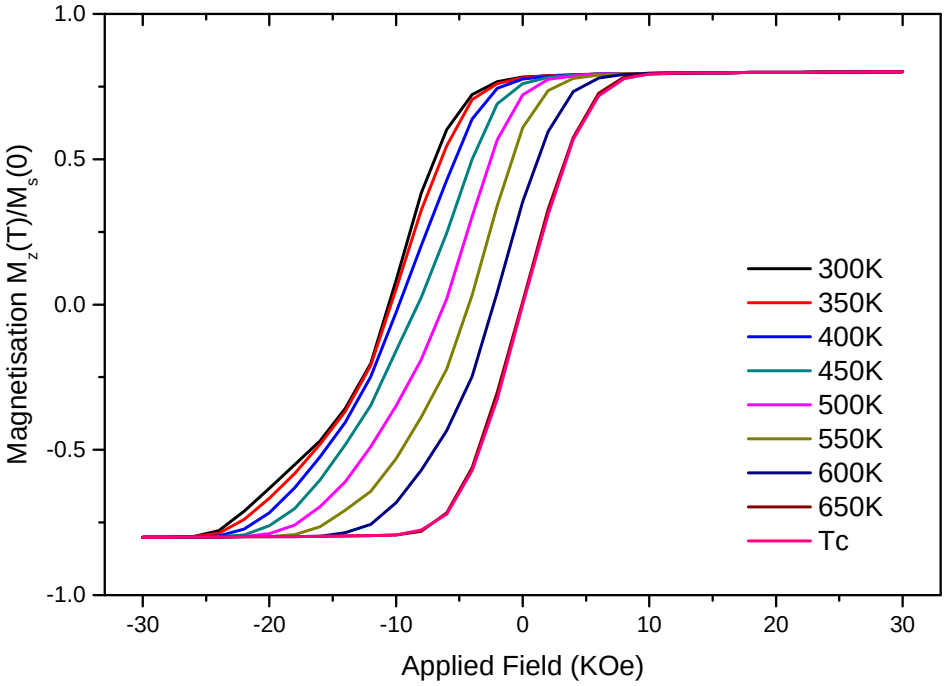

Figure. 5.3: A series of hysteresis curves, using the alternate measurement technique developed by Liu et al., over a broad temperature range from ambient to T_c, for the 20% L_{10} FePt case. The results show a decrease in the applied field strength required to reverse the magnetisation of the thin film as a function of the maximum temperature rise during the HAMR process.

well describe the HAMR process. From the results presented it is possible to determine both the temperature rise and applied field strength required to reverse the magnetisation of the thin film to the desired level. In the specific case shown in figure 5.3 to achieve magnetisation reversal the temperature must reach a minimum of 650K and the applied field strength must exceed 6kOe. Also a reduction in the effects of the intergranular interaction can be seen for the maximum temperature cases. For the lower temperature cases and in high negative field the curves exhibit a change in gradient. This effect can be attributed to the exchange and magnetostatic interactions, which can drive the system in to relatively stable low energy states and this can slow and prohibit the reversal of the magnetisation and can result in the reduced magnetisation seen in figure 5.3. This effect can be overcome in a number of ways. The conventional technique is to use a large field strength to drive the magnetisation to negative saturation within the desired time frame or as can be seen in figure 5.3 the effects of the intergranular interactions are reduced with increasing temperature and are not present in the highest temperature cases.

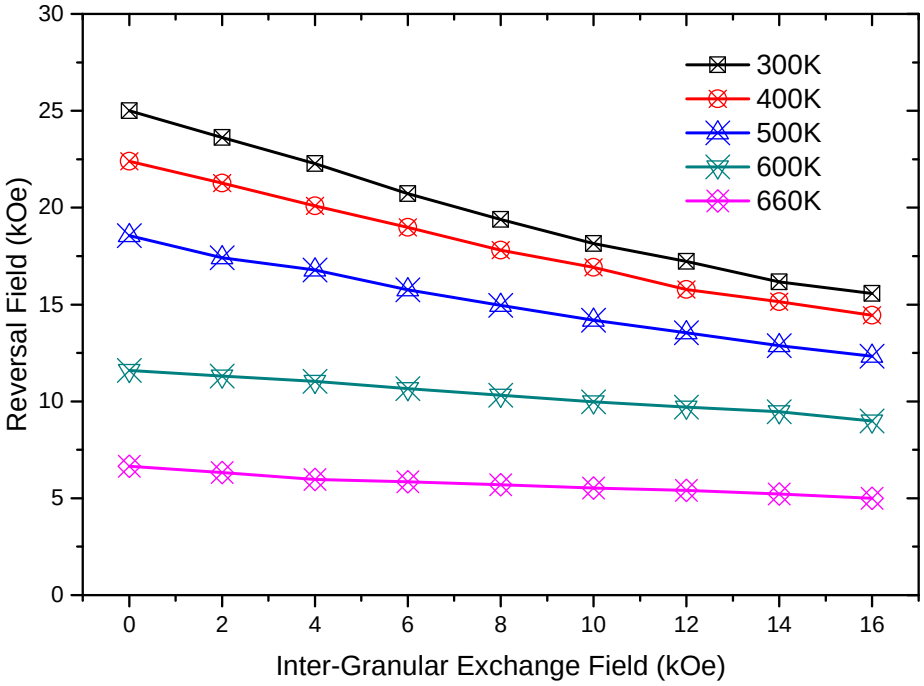

Figure. 5.4: The effect on the reversal field as a function of the the intergranular exchange field (IGEF) and the maximum system temperature during the HAMR process. There is a significant change in the effect of the IGEF on the reversal field with increased temperature; with a low temperature rise the increase in the IGEF reduces the reversal field significantly, whereas this effect is mediated with a higher temperature increase.

To further investigate this effect a further series of alternate hysteresis curves were generated over a range of intergranular exchange field (IGEF) strengths from 0 - 15 kOe and in each case the reversal field was determined, figure 5.4. At low temperature an increase in the IGEF reduces the reversal field significantly, from 25.0kOe with no IGEF to 15.6kOe with an IGEF of 15kOe, this suggests that the effect of the magnetostatic interaction, which has been shown to slow the approach to negative saturation, is being mediated by a larger IGEF. It is known that large IGEFs alter the dynamics of the reversal process, causing the magnetisation of the entire thin film to act a single macrospin, which would account for the observed change in the reversal field. Also the reduction in the effects of the intergranular interactions at high temperature are further demonstrated. In the case where the temperature rise was to the Curie point an increase in the IGEF has a less pronounced effect on the reversal field, changing by less than 1.6kOe from 6.6kOe to 5.0kOe over the complete range of IGEFs investigated. These results suggest that the intergranular interactions do not

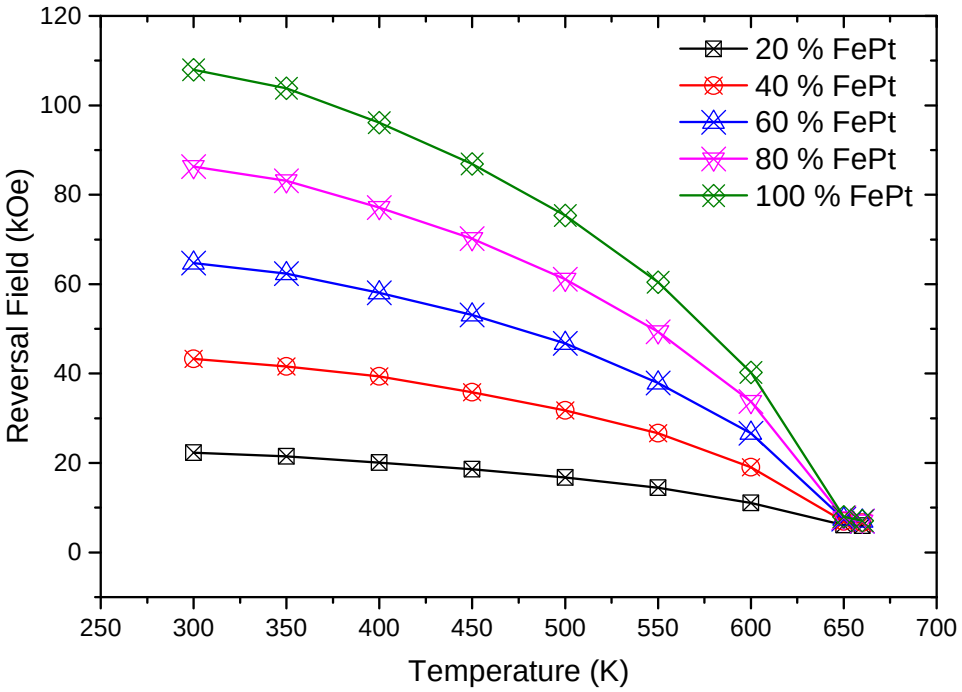

Figure. 5.5: The effect on the reversal field as a function of the magnetocrystalline anisotropy, K_v, and the maximum system temperature during the HAMR process. As expected the field strength required to reverse the magnetisation is reduced with increasing temperature rise. For the highest temperature case, a temperature rise to T_c, the reversal field is similar for all anisotropy case, approximately 6 - 7kOe.

contribute a significant contribution to the magnetisation dynamics during the HAMR process.

To achieve the highest levels of areal density possible with FePt granular thin films the fully L_{10} ordered highest anisotropy state must be implemented. To investigate the increase in the magnetocrystalline anisotropy on the effectiveness of the HAMR process a further series of the alternate hysteresis loops were generated and again the reversal field was observed, figure 5.5. It is clear that an increase in the anisotropy has a significant effect on the reversal field at low temperature, increasing approximately linearly with the increase of K_v. For all values of K_v investigated raising the temperature during the reversal process lowers the observed reversal field, as seen in the relatively low anisotropy case shown in figure 5.3. The effect of the anisotropy is minimised with a temperature rise to T_c where all cases are seen require a similar applied field strength, 6kOe - 7kOe, to reverse the magnetisation, figure 5.5. This result is encouraging for HAMR, as the anisotropy is not the limiting factor in the magnetisation reversal

process.

5.3 Magnetisation Dynamics of the HAMR Process

The thin film magnetisation dynamics during the temperature rise and subsequent cooling process give further insight into the HAMR process. The thin film magnetisation time sequence is used to give further insight into the progression of the magnetisation during the HAMR process. Figure 5.6 shows the M_z time sequences for the 20% and 100% L_{10} ordered FePt cases; during the simulation the applied field strength was held constant at 6kOe in the negative z direction. For the two cases shown in figure 5.6 the temperature rise affects the magnetisation dynamics in a markedly different manner. For the higher anisotropy case, 100% L_{10} ordered, the temperature rise must exceed 600K for any magnetisation switching to occur. However, for the lower anisotropy case, 20% L_{10} ordered, a degree of magnetisation switching is seen for all temperature cases. This was expected as the higher anisotropy case requires a significantly higher reversal field to switch the magnetisation, when compared with the lower anisotropy case for a given temperature, in all temperature cases below T_c. Whereas with a temperature rise to T_c an equal applied field strength will achieve a similar level of magnetisation reversal, figure 5.6.

For the low anisotropy case, at ambient temperature the applied field strength is sufficient to reverse a significant amount of the magnetisation, as the relatively smaller grains are seen to reverse the magnetisation (this effect is shown in greater detail at a later stage in this chapter). An increasing number of grains will switch the magnetisation for the higher temperature cases due to the reduction in the value K_v. At a temperature well below T_c there are three distinct time regimes for the progression of the magnetisation during the simulations. Firstly there is an initial rapid reduction of the magnetisation of the thin film, driven by the rapid increase in the temperature. This process is as a result of thermally activated longitudinal relaxation of the magnetisation, this causes a reduction in the magnitude of the magnetisation of each grain. This reduction happens in only a few hundred fs as shown by Chubykalo-Fesenko et al.[30] and as a result the changes in the magnetisation rapidly follow the temperature increase. Secondly, after the reduction in the magnetisation and consequent reduction in the magnetocrystalline anisotropy, the magnetisation of each grain proceeds by precessional switching over a thermally reduced energy barrier. Finally, as the temperature slowly lowers towards ambient there is a slow change in the magnetisation caused by thermally activated switching events which can

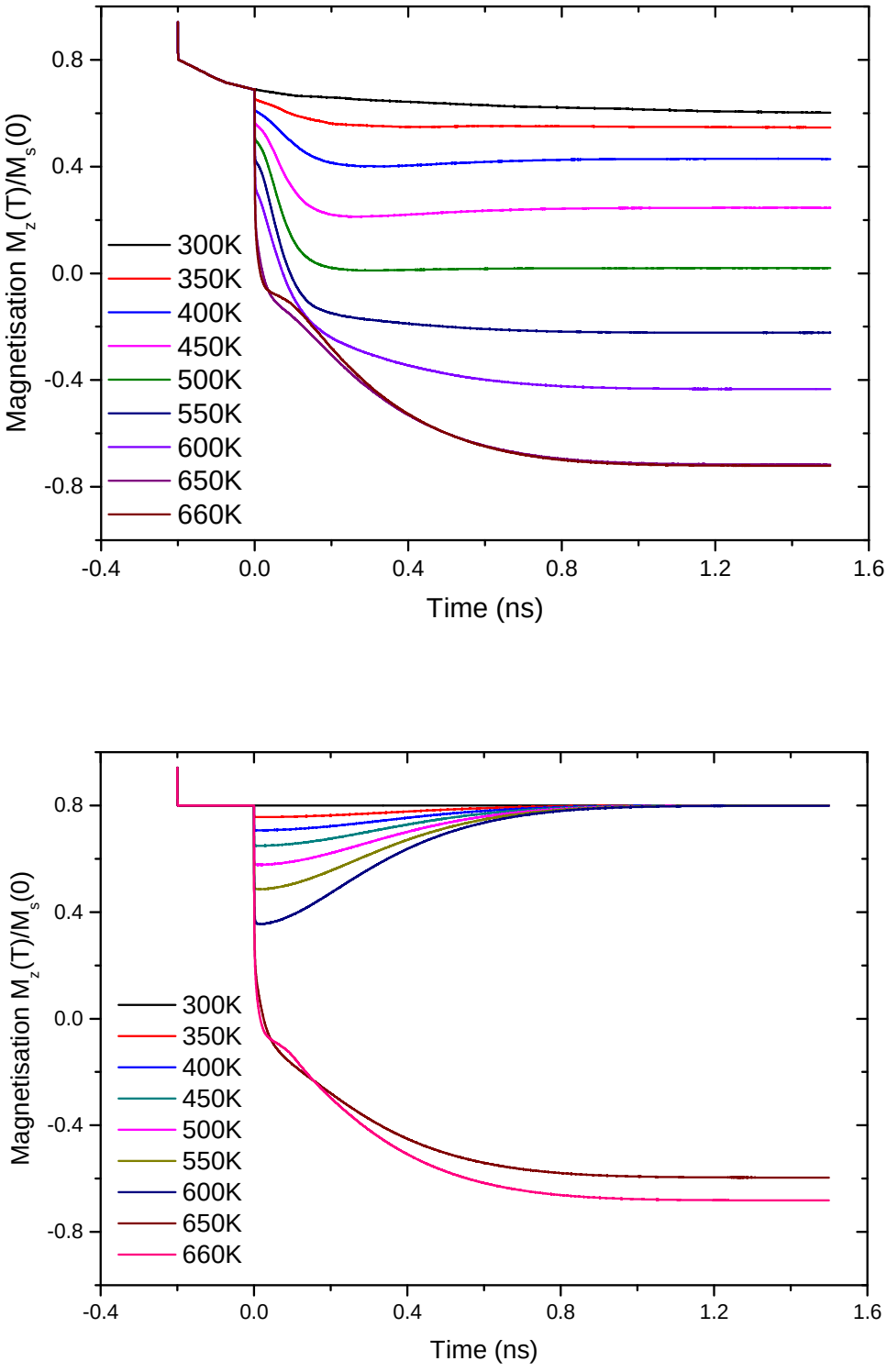

Figure. 5.6: Top: The M_z time sequence for the 20% L_{10} case, with a 6kOe applied field. The time sequence shows the effect of applying a temperature increase during the magnetisation reversal process and it also shows that the temperature must be increased to T_c to fully reverse the magnetization. Bottom: The M_z time sequence for the 100% L_{10} case again with a 6kOe applied field. Note the higher anisotropy simulation requires a higher temperature increase to achieve the same level of magnetisation reversal.

continue for a relatively long period dependent on grain size.

These lower temperature cases, for the low anisotropy case, support the conventional picture of HAMR, as magnetisation reversal over a thermally reduced energy barrier, as an increasing portion of the magnetisation is switched for a larger increase in the temperature. This conventional picture of the HAMR process is true for all cases up approximately 600K. However it is important to observe that in all these cases the magnetisation of the thin film is never completely reversed and to achieve the desired level of reversal the peak temperature must reach or exceed the Curie point. This effect is even greater for the 100% L_{10} ordered FePt case, figure 5.6.

As expected the high anisotropy case requires a much larger increase in the temperature, when compared with the low anisotropy case, to achieve magnetisation switching and due to this the conventional picture of HAMR does not apply in these extreme anisotropy cases. In these extreme anisotropy cases a larger component of the anisotropy remains even with a significant rise in the temperature, figure 5.6 shows that virtually no switching is seen with a temperature rise to 620K, but with a marginal increase in temperature of only 40k to T_c the magnetisation of the thin film reverses entirely. This suggests that for all anisotropy regimes the linear reversal mechanism is essential to the HAMR process.

The HAMR process is more complicated than simply magnetisation reversal over a thermally reduced energy barrier. The high temperature switching and the subsequent freezing of the magnetisation at lower temperature is best characterised as a field-cooled magnetisation process (FCM), albeit at relatively extreme rates of temperature reduction and also with spatially varying temperature and field profiles. Thermally activated switching is possible at temperatures below the Curie point, as shown by Evans and Fan[10], but for switching to occur the temperature must remain high for a prohibitively long period of time, which would be highly restrictive for HAMR, as this would put a limit on the minimum time frame for the recorded bit. It is suggested by Evans and Fan that for reliable magnetisation reversal the temperature rise must be to at least T_c in order to invoke the linear reversal mechanism and also that the applied field strength must be sufficient to overcome any thermally activated back switching of the magnetisation[10].

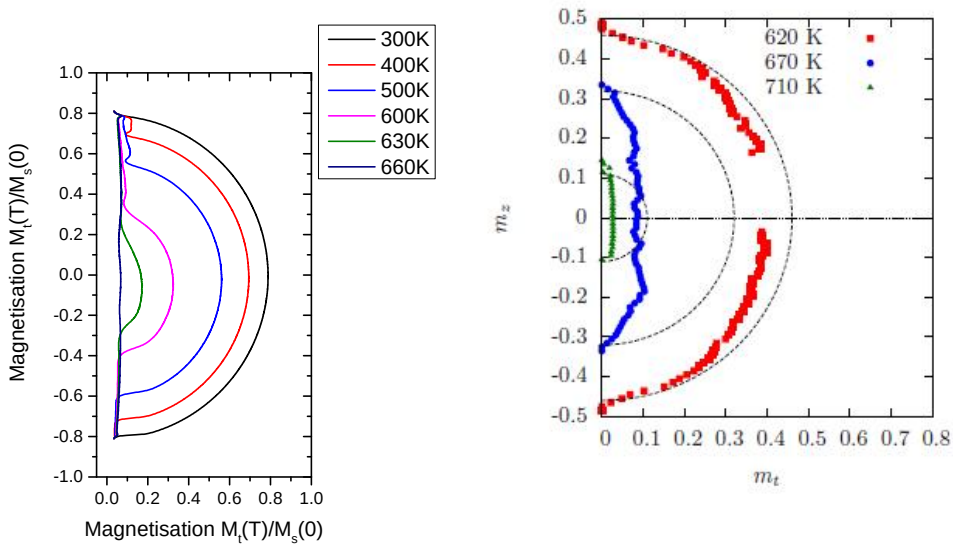

Figure. 5.7: Left: The position averaged reversal for the magnetisation of an individual grain with an anisotropy of 100% L_{10} ordered FePt. The data shows the reversal mechanism over a range of maximum system temperatures from ambient to T_c. The change in reversal modes is clearly displayed, from a strictly precessional type with a maximum temperature below 550K, through the elliptical mode between 550K to approximately 640K, and onto the linear reversal mode at temperatures above T_c. Right: Data showing the linear reversal mechanism determined Barker et al.[57] using atomistic spin model approach. The results show the same linear reversal mechanism as is observed with the LLB macro-spin approach.

5.4 The Linear Reversal Mechanism

As mentioned in the last section of this chapter the linear reversal mode is essential to achieve the required level of magnetisation reversal for the HAMR process. This effect is well demonstrated by the significant change in behaviour in the high anisotropy case, shown in figure 5.6, with a temperature rise of between 620K and 660K. This significant change in behaviour is due to the onset of the linear reversal mechanism as the temperature rise approaches T_c[29, 57].

The linear reversal mechanism is characterised by rapid longitudinal changes in the magnetisation as the macroscopic magnetisation of each individual grain is destroyed due to the high temperature state, figure 5.7. The data presented in figure 5.7 shows the position averaged magnetisation in the z axis verses the magnetisation in the transverse plane for a single grain, shown for the entire reversal process for the high anisotropy 100% L_{10} ordered FePt case. For the lower temperature cases, below a temperature rise to approximately 550K, the

magnetisation of each grain switches via coherent rotation. In this case the magnetisation rotates by precessing from the local energy minimum to the global energy minima characterised by a constant magnitude throughout the process, where the magnitude of the magnetisation is seen to decrease with increasing temperature. In this precessional regime the characteristic switching time is of the order of hundreds of pico seconds.

However, for the higher temperature cases the reversal mechanism is seen to change to a non-precessional type, termed elliptical and linear reversal. For these high temperature cases the switching occurs on faster time scale where the magnetisation is still in a transitional state. For both the elliptical and linear cases this means that the magnitude on the magnetisation is seen to vary during the reversal process.

The increased thermal energy counteracts the exchange forces, allowing the magnetisation to shrink when approaching the hard direction. This is the elliptical reversal mode, which has a lower energy barrier than coherent rotation. At higher temperatures close to T_c it is energetically favourable for the magnetisation to reverse via a collapse to zero magnetisation and then rebuild in the applied field direction; this is the linear reversal mode.

The elliptical reversal mechanism occurs within the temperature rise range between 600K and 640K, where the magnetisation is seen to decrease to a minimum magnitude in the anisotropy hard plain and is then seen to increase as the reversal process continue to completion, giving the characteristic elliptical pattern shown in figure 5.7 and importantly this mechanism results in a reduced energy barrier relative to coherent reversal. The linear reversal mechanism is introduced at temperature above 640K; where the macroscopic magnetisation of the individual grains are effectively destroyed due to the high temperature and is then seen to rebuild in the direction of the applied field as the temperature returns to ambient. These results are consistent with the atomistic simulations given by Barker et al.[57] also shown in figure 5.7. The linear reversal mechanism is known to be extremely fast acting with characteristic times of the same order as the longitudinal relaxation time associated with FePt, of approximately 100fs.

5.5 The Effect of Cooling Rate on the HAMR Process

Although the switching is very fast with linear reversal the cooling rate is much slower so complete reversal and recovery of the magnetisation, in the opposite direction, is dictated by the cooling rate. The dynamics of the reversal process

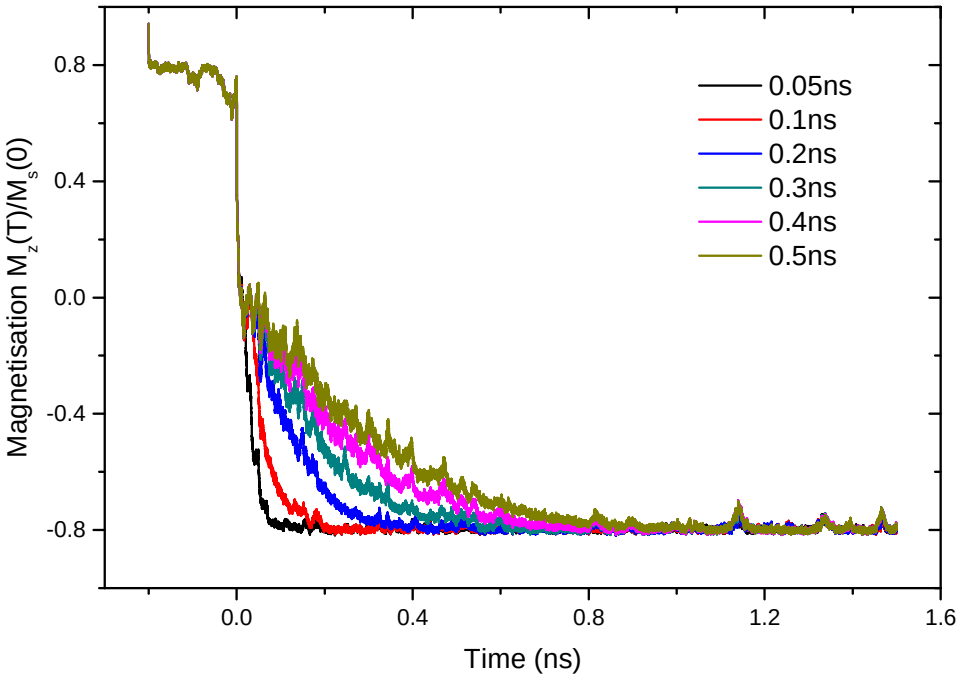

Figure. 5.8: The time evolution of the magnetisation, M_z, of a single grain undergoing switching via the linear reversal mechanism, where the maximum temperature was T_c, for a range of cooling rates. Magnetisation reversal, for the single grain, happens increasingly quickly with faster cooling rates, as the increase in the magnitude of the magnetisation follows the time evolution of the temperature profile.

are illustrated in figure 5.8, which shows the progression of the magnetisation in the z axis, M_z, of an individual grain undergoing switching via the linear reversal mechanism, for a range of cooing rates from 0.05ns to 0.5ns. In each case the magnetisation is destroyed and vanishes entirely and is seen to reverse rapidly. But, as the progression of the magnetisation follows the time evolution of the temperature profile during the cooling process, the time scale for magnetisation switching, via the linear reversal mode, is dictated by the cooling rate of the system.

When considering an ensemble of interacting grains the cooling rate of the system effects magnetisation reversal in a more subtle manner than in the single grain case. The time evolution of the magnetisation for the entire thin film, undergoing heating to T_c, is shown in figure 5.9. For the lower cooling rate cases, 0.3ns and above, the magnetisation of the thin film is fully switched via the linear reversal mechanism. But the situation is not as simple for the higher cooling rate

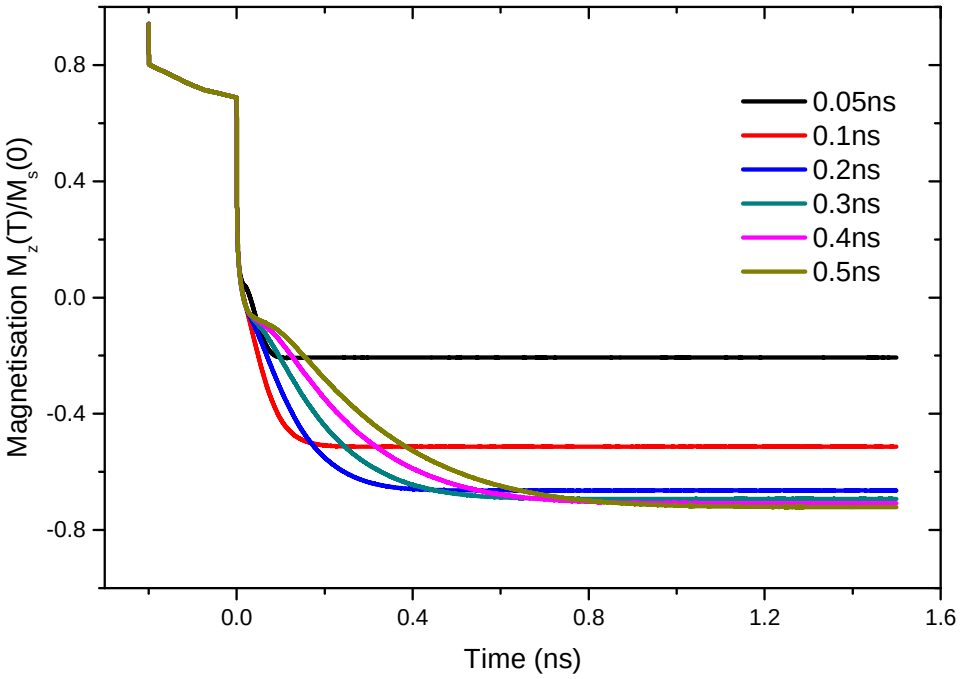

Figure. 5.9: The time evolution of the magnetisation, M_z, undergoing the HAMR process with a maximum temperature of T_c for the thin lm magnetisation with an anisotropy of 100% L_{10} FePt, over a range of cooling rates. For a cooling rate below 0.2ns the level of magnetisation reversal is signicantly reduced due to the reduction in the 'switching window' which results in a portion of the individual grains magnetisation to remaining in the initial orientation after the HAMR process.

cases, 0.2ns and below, as the magnetisation of a number of the grains are in the initial orientation, after the HAMR process, which results in a reduced overall magnetisation in the negative direction. The reduced magnetisation is a result of an apparent 'switching window' defined as the time between the appearance of the magnetisation as the temperature cools through T_c, and the time at which the temperature of the system drops below the blocking temperature, after which any further switching events are prohibited and the magnetisation of the individual grains freezes in orientation.

The approximation to the HAMR process, implemented for this body of research, essentially results in a Field Cooled Magnetisation (FCM). A FCM is achieved after an ensemble of magnetic particles are subjected to a high temperature and then cooled to ambient through the blocking temperature in the presence of an applied field. This approximation allows for a simple model to be applied, if it is assumed that the sample reaches thermal equilibrium immediately

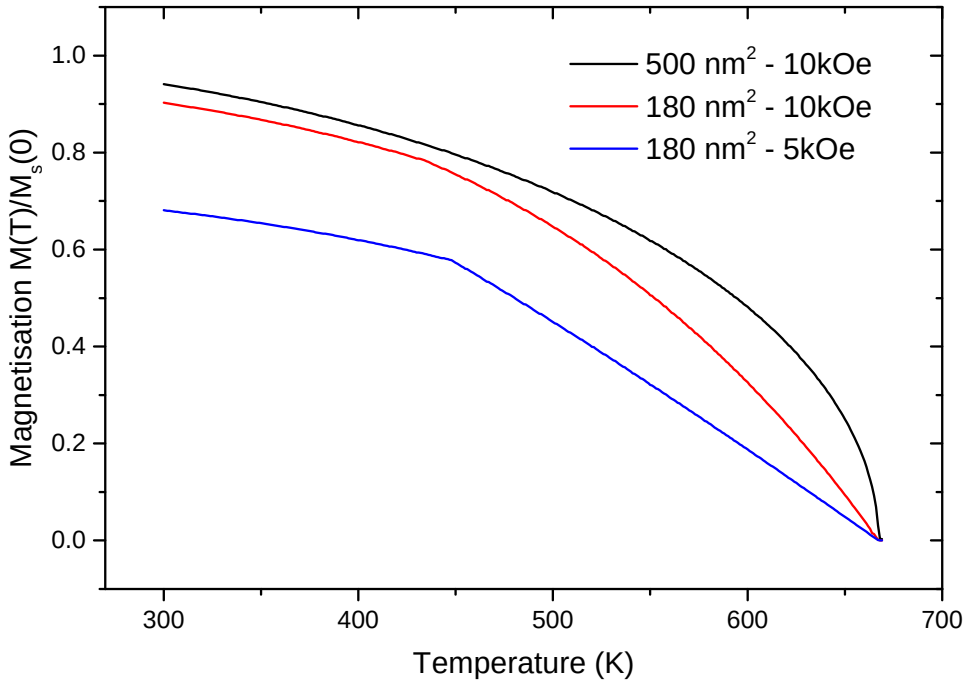

Figure. 5.10: The effect on the FCM due to an increase in the blocking temperature as a result of reduced grain volume and reduced applied field strength. The results where determined with a simple numerical approximation using the model of Chantrell and Wohlfarth[60]. The results from this simplistic model are in agreement with the data presented in 5.9.

after the temperature drops below the Curie point and is constantly at thermal equilibrium during the cooling process, where the temperature is above the blocking temperature, T_B. In this case the semi-analytic approach of Chantrell and Wohlfarth[60] can be applied if the saturation magnetisation and anisotropy are evaluated at a given temperature. In the work by Chantrell et al. it was shown that the magnitude of the FCM is dependent on the temperature cooling rate. Essentially this assumes that the magnetisation is in thermal equilibrium above a blocking temperature, T_B, which is cooling rate dependant and the magnetisation will be effectively fixed once the system temperature falls below T_B.

In the the work by Chantrell et al.[60] it was shown that the rate dependent blocking temperature is determined via the parameter Z_c, given as a solution of the following equation:

$$Z_c = ln\left(\frac{f_o \dot{T}^{-1} 25 T_K (1-h)^2}{Z_c^2}\right) \tag{5.1}$$

where Z_c = $\frac{K_v V}{k_B T_B}$(1 - h)^2 and T_K = K_vV/(25k_B) is the blocking temperature for quasi-static isothermal measurements and h = H/H_k is the applied field relative to the anisotropy field, H_k, known as the reduced field and $\dot{T}$ is the rate of change of the temperature. From equation 5.1 the blocking temperature is given by:

$$T_B = \left(\frac{K_v V}{k_B Z_c}\right)(1-h)^2 \tag{5.2}$$

The blocking temperature was calculated in an analytic approximation in the work by Chantrell et al., but it is used here as to determine a numerical solution to equation 5.2. A mono-disperse ensemble of particles are consider with the easy axis aligned for each particle. The analytic approximation determined within the blocking model, by Chantrell et al., assumes that the magnetisation is in thermal equilibrium when the temperature is greater T_B and makes the transition to a non-equilibrium state on cooling through T_B. As the magnetisation in thermal equilibrium, for an aligned system is M = tanh(β) where β = M_s(T)H/(k_BT), we therefore have the follow magnetisation approximately above and below T_B.

$$M = \tanh(\beta) \quad T > T_B \tag{5.3}$$

and

$$M = \tanh(\beta_c) \quad T \leq T_B \tag{5.4}$$

where β_c = M_s(T)V H/$k_B T_B$.

In this simple model, equation 5.4 shows that magnetisation becomes frozen on cooling through T_B and remains a that magnitude at temperatures below T_B. The temperature dependent magnetocrystalline anisotropy, K_v(T) is approximated using the Callen-Callen theory with S=3/2. Given the temperature dependencies of K_v and M_s it is straightforward to calculate M(T), both above and below the blocking temperature, by using equations 5.3 and 5.4.

Using this simple numerical model the field cooled magnetisation has been approximated as a function of both grain volume, 500nm^2 and 180nm^2, and field

strength, 5kOe and 10kOe, using a cooling rate of 500K/ns. For the relatively large system and with the larger field strength the magnetisation is seen to increase in magnitude smoothly as the temperature is cooled through T_B and further on to ambient, figure 5.10. For the smaller particle system and with the large field strength the situation is different; at approximately 450K the magnetisation exhibits a change in slope which is consistent with the effects of blocking. The effects of blocking are more pronounced for the case with the lower field strength, 5kOe, where the magnetisation is seen to freeze at a higher temperature. This shows that the effect of blocking are increased for smaller particle systems and further so with smaller applied fields.

This simple numerical model is limited in its scope, as it can clearly reproduces the form of the FCM on cooling, but it is not capable of reproducing the reduction of the switched magnetisation at the higher sweep rates, seen in figure 5.9. This is due to the assumption that the magnetisation is always in thermal equilibrium above the blocking temperature. When the system is subject to vary rapid cooling rates, this causes the system to go from a high temperature - low anisotropy regime, where magnetisation reversal can occur, to a low temperature - high anisotropy regime, where magnetisation reversal is forbidden, in a period of time which is too fast to allow the system to reach thermal equilibrium at each temperature.

The results produced by the simple numerical model are dynamic generalisation of the concept of 'thermal writability' which suggest that the cooling rates, used for the HAMR, process need to be sufficiently slow, at allow the magnetisation to always be in thermal equilibrium during the cooling process. This can be quantified in terms of the freezing time as a function of the cooling rate, R; τ_f = (T_c - T_B)/R. Therefore τ_f is essentially the time taken for the temperature to drop from the Curie point to the blocking temperature. For efficient switching in HAMR, $\tau_r > \tau_f$, where τ_r is the relaxation time of the magnetization during the cooling process. This stresses the importance of the linear reversal mechanism[61, 62] in HAMR, as the switching via the linear reversal mode gives access to relaxation times of the order of picoseconds[10].

5.6 Grain Volume Effects on the HAMR Process

A greater insight pertaining to HAMR can be gained by studying the reversal process as a function of grain volume and the temperature rise. The conventional picture of HAMR is as magnetisation reversal over a thermally reduced energy

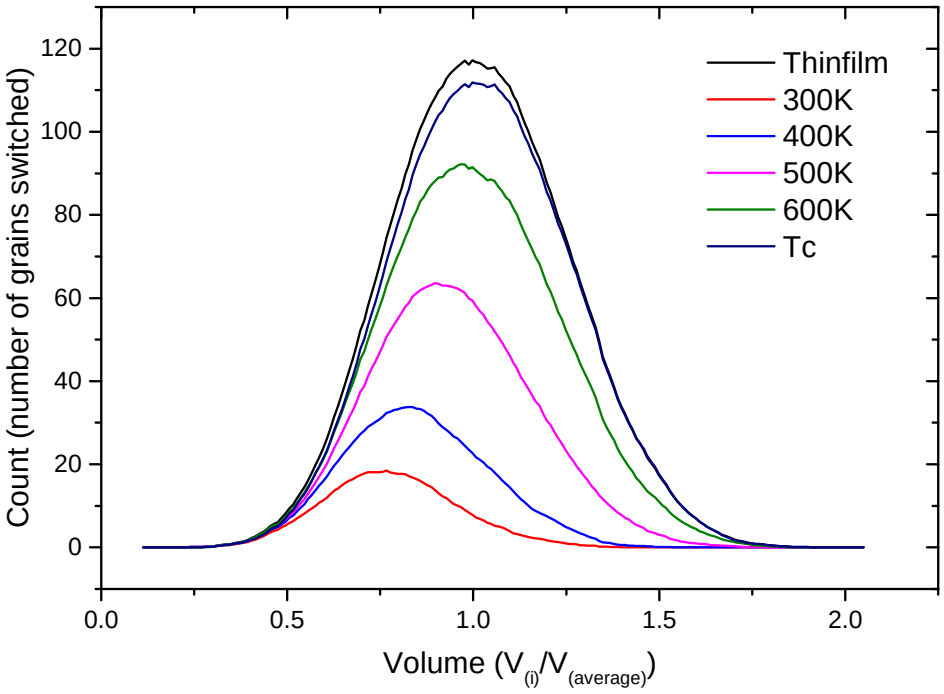

Figure. 5.11: Top: The count of grains that have switched after the HAMR process, as a function of relative volume and temperature, for 100% L_{10} FePt grains with an average volume of 2.16x10^{-25}m^3. The data shows an increase in the average volume of grains that switch with increasing temperature. Also the count of grains at each volume is also given for comparison.

barrier, this is well depicted for the lower temperature cases with the data presented in figure 5.11. The top panel in figure 5.11 shows the number of grains which have switched the magnetisation, as a function of grain volume and temperature, after the HAMR process. The data presented has been averaged over a number grain volumes to give a clearer picture. Effectively further increasing the temperature this further lowers the maximum anisotropy energy, K_v(T)V, allowing increasingly larger grains to switch the magnetisation, this is shown as the average volume of the grains that have switched increases with increasing temperature rise. However it is interesting to note that with above a temperature increase to 600K there is a marked increase in the number of grains that have reversed the magnetisation with virtually no corresponding increase in the average volume. This is likely due to a change in the reversal mechanism, as the system enters the elliptical and linear reversal regimes, which will allow the the magnetisation to reach thermal equilibrium faster.

It should also be noted that for the highest temperature cases the

magnetisation of the smallest grains are far less likely to reverse the magnetisation after the HAMR process. The lower temperature cases - 300K and 400K - show a picture consistent with the conventional view of HAMR, as further increasing the temperature induces larger grains to switch as the anisotropy energy is further lowered. But for the highest temperature cases - 600K and T_c the situation appears quite different. For both of these cases the smallest grains show a low or zero probability of reversing. This picture is consistent with the concept of 'thermal writability' introduced by Evans et al. [58, 59], which stipulates that the applied strength $M_v VH >> k_B T_f$ where T_f is the freezing temperature; ensuring the applied field strength is sufficient to reverse the magnetisation and overcome any thermally induced back switching. That being said, the results for the smallest and largest grains do contain a large error, due to the dispersion of the grain volume of the thin film; for the case of the smallest volume, there is only a single grain for that case and based on the error being approximated as N^2/N, where N is the number of grains of that approximated volume, this would give an error 1, which implies the data, in these cases, is non-reliable. The data does still hint at concept of 'thermal writabiliby', as these grains did switch for the lower temperature cases.

To gain a better insight in to this effect the calculation was repeated with a series of thin films with an identical structure, but where the average diameter was adjusted for each case, from 3nm - 10nm. In each case the system anisotropy is 100% L_{10} FePt and the temperature rise is to the Curie point, also the calculations were repeated with three applied field strengths: 6.0kOe, 8.0kOe and 10.0kOe. The data regarding switching of the magnetisation as a function of volume was captured for each case only if the volume of the grains was within one standard deviation of the mean value and the data from each calculation was then collated and the probability of a grain switching the magnetisation is represented as a function of particle volume, as is shown in figure 5.12. The top panel in figure 5.12 shows the data as was collated and the bottom panel shows the data modified by averaging over 40 data points, for clarity. The data presented clearly shows a reduction in the probability of a grain switching the magnetisation for the relatively smaller grains, for each applied field strength case. For the case with the lowest field strength 6kOe the probability of a grain switching is significantly reduced for grains with a diameter of less then approximately 6nm. Even with applied field strength of 10kOe the probability of a grain switching is significantly reduced below a diameter of approximately 5nm.

These results (figures 5.11 and 5.12) are consistent with the concept of 'thermal

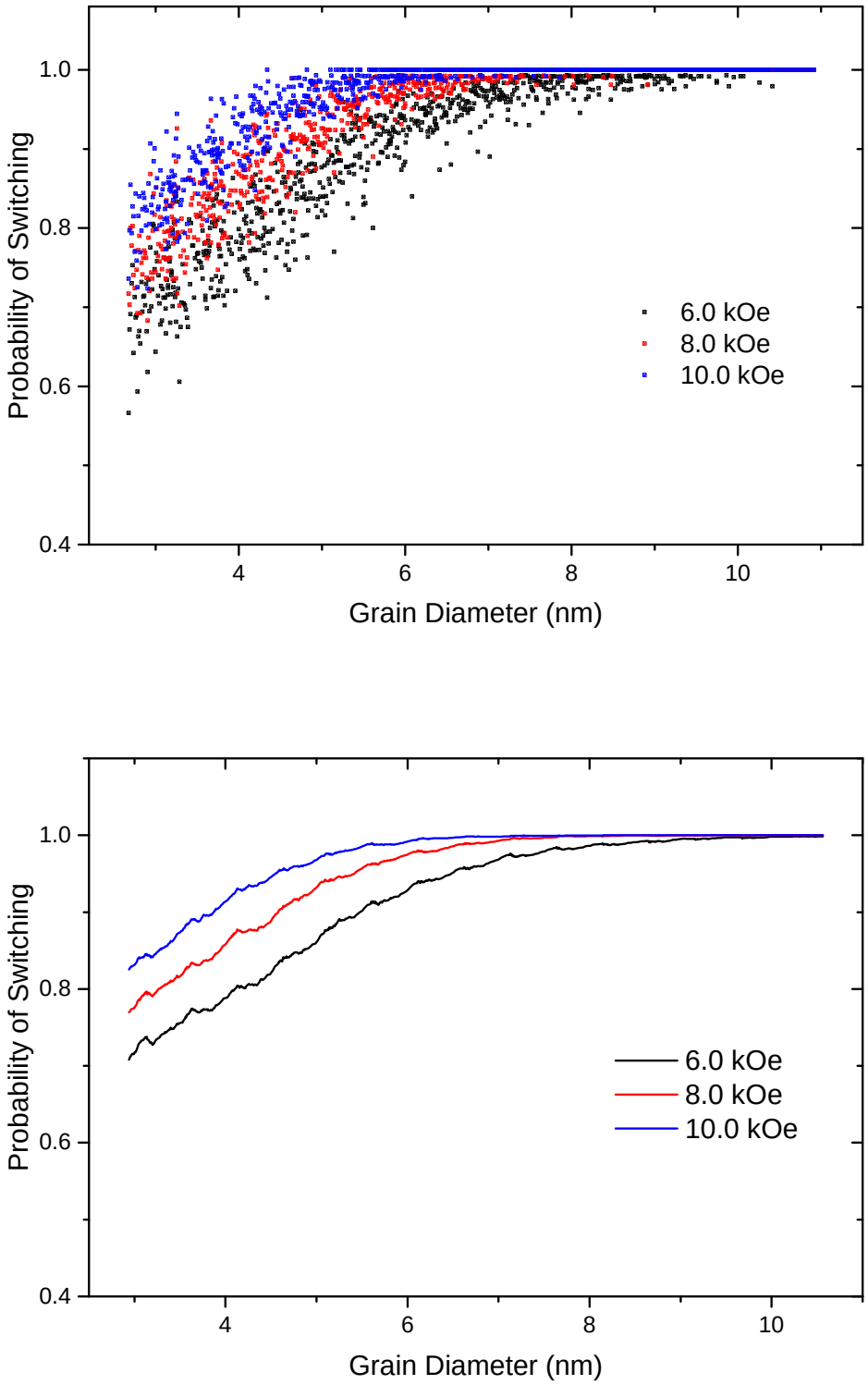

Figure. 5.12: Top: The reversal percentage for the 100% L_{10} ordered thin film, where the temperature was raised to T_c during the HAMR process. Below a critical grain size the probability of the magnetisation reversing is signicantly reduced for a given applied field strength, where the critical grain size is reduced with increased field strength. Bottom: The same results averaged over the volume for simplicity in reading the data.

writability', introduced by Evans et al.[58] and Richter et al.[59], which states the requirement that the applied field strength should be sufficiently large to ensure that there is no thermally induced back switching of the magnetisation, as the magnetisation rebuilds due to the temperature of the system cooling below T_c. The field strength must be sufficiently large to ensure the freezing temperature (T_f) of the grain with magnetisation M_sV is large enough to prohibit any back-switching.

In practical situations, such as HAMR, this effect could have significant consequences, as the probability of magnetisation reversal for the smaller grains is reduced this would suggest an increase in the dc noise on data read back, due to the reduced magnitude and thus strength of the magnetisation. Also, as predicted by Evans et al.[58], the the thermal stability criterion shown in chapter 1 - equation 1.2, where $K_vV/k_BT > 60$, which suggests that grains with a diameter as small as 3.3nm [63], with K_v equal to 100% L_{10} ordered FePt, could be used within the recording media for HAMR, is not the limiting factor and 'thermal writability' becomes the more stringent criterion, as shown in figure 5.12, where, with a 10kOe applied field the magnetisation is significantly reduced after the switching process, when the system is comprised of grains with an average diameter less 5nms.

5.7 Implications for HAMR

The final magnetic state of the system after the HAMR process is of vital importance in terms of recording applications. In this section the final state of the system is characterised as the fraction of the system magnetisation that has switched after the HAMR process. The fraction is taken as the magnitude of the reduced magnetisation relative to the saturation magnetisation at ambient temperature. The final state of the system is observed over the complete range for the anisotropy for partially ordered to fully L_{10} ordered FePt. The increase in anisotropy has a resultant increase in the temperature required to initiate and complete the reversal process, figure 5.13. Above an anisotropy of 60% of that of L_{10} ordered FePt and below a temperature rise to 600K the fraction of the reversed magnetisation is very low or even zero. The data presented also shows that for all anisotropy cases the desired level of magnetisation reversal is achieved when the maximum temperature rise is to T_c.

For the relatively lower anisotropy case, 20% FePt, the fraction of the reversed magnetisation has a relatively weak dependence on the maximum temperature

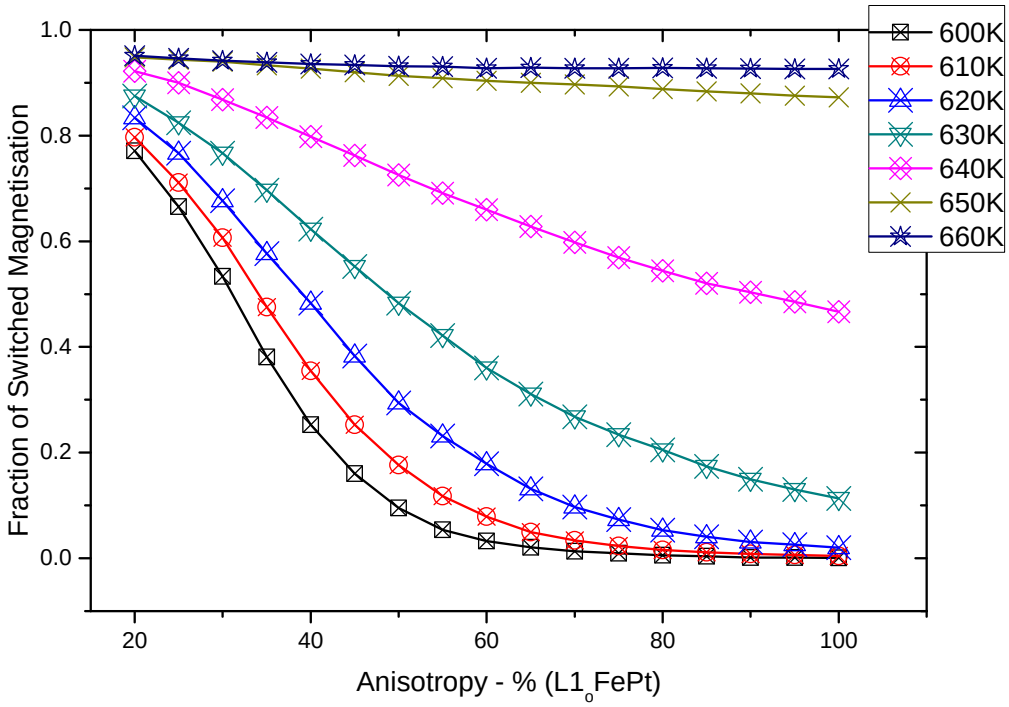

Figure. 5.13: The reversal probability for the thin lm magnetisation with a 6kOe applied field, over a range of maximum system temperatures (600K - T_c) and anisotropies (20% - 100%) of L_{10} ordered FePt. The data shows that for the desired level of magnetisation reversal the temperature must be to a minimum of T_c for all anisotropy cases.

reached during the HAMR process, although the fraction does increase as the temperature rise approaches T_c. There is a great dependence on the temperature for systems with a high anisotropy approaching that of fully L_{10} ordered FePt. In the highest anisotropy cases a peak temperature of 620K is insufficient to cause a significant amount of magnetisation switching, as in these cases the reversal path is only available via the linear reversal mechanism, which requires a temperature rise to very close to T_c. These suggest that the linear reversal mechanism will become the dominant reversal mechanism as the anisotropy values increase to maintain thermal stability for ultra high density systems.

These results suggest that two constraints will limit the HAMR process; the increasingly high anisotropy regime and the need for temperature approaching T_c. This implies that the switching window, i.e the temperature range where reversal of the magnetisation of any of the grains is significantly reduced. This narrowing of the switching window could lead to the possibility of incomplete reversal, as reversal must occur at T_c. Therefore, the intrinsically fast pico-second timescale of switching via linear reversal mechanism could be an important factor

in HAMR.

5.8 Summary

The physics of the HAMR process - a hard disk magnetic storage technology capable of continuing the historic increase in the areal density - has been investigated, concentrating on the thermodynamic aspects of the process. The data presented shows the field required to reverse the magnetisation is significantly reduced to a minimum value of approximately 6 - 7 kOe, with a temperature rise to the Curie point, for all anisotropy values investigated in the range available with L_{10} ordered FePt - 1.8×10^7ergs/cc to 9.0×10^7ergs/cc, for a system with an average grain diameter of 6nm. However, the investigation has also demonstrated that the HAMR process is not as simple as magnetisation reversal over a thermally reduced energy barrier, in the high temperature - low anisotropy regime, as the reversal process is far more complex. To reverse the magnetisation using the HAMR process requires that the temperature be raised to the Curie point, for all anisotropies investigated, and the magnitude of the applied field used to switch the magnetisation must be sufficient to overcome any thermally induced back-switching that may occur.

For the lower anisotropy and lower temperature rise cases - an anisotropy of 20% of L_{10} ordered FePt and a temperature rise of less than or equal to 600K i.e. sufficiently below the Curie point - the HAMR process can be split in two distinct stages. Firstly there is a rapid reduction in the magnitude of the magnetisation of each grain and the thin film as a whole, caused by the rapid increase in the temperature. There is also an equally rapid reduction in the magnetic anisotropy which allows for precessional magnetisation switching over a thermally reduced energy barrier, as in the conventional picture of HAMR. Finally as the temperature lowers toward ambient the rate of magnetisation switching is reduced and there is an ever slowing change in the magnetisation which can occur, depending on grain size, for a significantly extended period up to 10ns, which is caused by thermally activated reversal events. These three stages are anisotropy dependent and therefore the temperature range where these three stages occur is increased with increasing anisotropy and thus narrower, due to the onset of the elliptical and linear reversal mechanism. For the high anisotropy cases the temperature range where these processes occur is sufficiently higher and thus narrower; for the highest anisotropy investigated 100% of L_{10} ordered FePt no reversal events occur with a temperature rise as high as 600K, therefore the range of temperatures where the conventional picture of HAMR is applied is reduced to approximately 40K - 610K to 650K.

With a temperature rise greater than this, the elliptical and linear reversal mechanisms come in to play and the reversal process is far more complex than the conventional picture of HAMR.

We have demonstrated that for high density recording media the HAMR process is only possible via the linear reversal mechanism, where the magnetisation is entirely destroyed by raising the temperature to the Curie point and allowing the magnetisation to reform in the direction of the applied field on cooling below T_c, similar to a field-cooled magnetisation process, albeit at extreme levels for temperature cooling. In this case, if the magnetisation is to be reversed to the desired level the applied field must be sufficient to overcome the superparamagnetic freezing that may occur during the period of rapid temperature decrease.

It has also been demonstrated that the concept of 'thermal writability' may be a limiting factor for HAMR technologies. This investigation has shown that the magnetisation of grains with a diameter below approximately 5nm, are increasingly susceptible to thermally activated back-switching events. This represents a more stringent criterion than the limitations of thermal stability, which for the high anisotropy case of L_{10} ordered FePt would allow for sufficiently smaller grains to be implemented in the storage media, down to approximately 3.3nm in diameter. However, it should be noted that we are assuming an applied field of 10kOe, which is a realistic value with current write field technologies. Therefore if HAMR is to reach the full potential and achieve the ultra high densities originally thought possible, higher effective write fields will be required.

This study has highlighted and confirmed a number of areas of interest within the physical processes that will govern heat assisted magnetic recording. Therefore further to this study the effects of grain volume on the reversal process will be undertaken to better understand how smaller grain volume effects the reversal process; as a function of both reduced average grain volume and also how relatively smaller grains within the thin film are effected during the HAMR process. Also, a significant study in to the effects of parameter dispersion, such as: T_c, M_s, K_v, damping and the susceptibilities, should be undertaken to fully understand how this will impact the recording process. Also, the model will be further developed to include multilayered recording media. Beyond this the model will be developed to investigate the HAMR process in a more practical manner through the simulated recording of bits on the hard disk recording media. This will help ascertain the limits of HAMR in a more practical way.

6. Continuous Wave Laser Assisted Magnetisation Reversal Dynamics

As previously mentioned perpendicular recording techniques have been used for many years and have been investigated to a great extent over that period, with the technology having remarkable success in multiple commercial magnetic recording products [64, 65, 66, 67]. However the challenge still remains to meet the ever increasing demand for ultrahigh density recording products [68, 2, 69]. As mentioned in a previous chapter heat assisted magnetic recording (HAMR) is a promising candidate for one of the next generation of hard disk recording techniques, as HAMR is capable of overcoming the difficulties and physical barriers that are currently hindering further progress towards increasingly high density recording media[70, 71, 72, 73]. As previously stated the principle of the HAMR process is to make use of the thermal dependence of the magnetocrystalline anisotropy to allow recording to happen in the high temperature - low anisotropy environment, with the desired media stability in the ambient temperature - high anisotropy environment [74, 75, 76]. However, many challenges still remain before HAMR can become a viable alternative to current hard disk recording methods.

The magnetisation dynamics during the thermally-assisted magnetisation switching process have been extensively investigated over recent years by many research groups. However, the practical implementation of pulsed HAMR into hard disk technologies is extremely challenging and a more practical approach is necessary. In reality a continuous wave (CW) laser is more applicable to HAMR technologies, both practically and economically, and is now the standard method for heating in HAMR technologies.

In this chapter the principle and feasibility of using a continuous wave (CW) laser as a heating technique within HAMR technologies is investigated using the LLB granular model in a parallel investigation to an experimental study on GdFeCo by colleagues at The University of York; T.Y Cheng and J. Wu. In both cases an increase in temperature is shown to assist the magnetisation reversal process, by softening the magnetic properties and therefore reducing the energy barrier to reversal. The results determined via the two methods have a good qualitative agreement, but due to the nature of the parameterisation of the LLB model - currently the model is specific to FePt - there is a difference in the

temperature dependence of certain properties, such as the magnetisation and magnetocrystalline anisotropy, which may effect the magnetisation dynamics in a significant way at higher temperature. Although the broad features are common to the model calculations and experiment, the material differences preclude a direct comparison.

6.1 Numerical Model

To investigate the application of a continuous wave (CW) laser as a heating tool within the HAMR process a series of numerical calculation using the LLB granular model were undertaken. The exact form of the numerical calculations were prompted by a series of similar experiments undertaken by colleagues at The University of York - T.Y. Cheng and J. Wu which have been presented in [77]. These experiments suggested the calculations given in this chapter, so the simulations presented will study the response to the specific magnetic field profile used in the experiments. In the following we first of all describe the model and give the results of a systematic study of the response of the magnetisation to the temperature and field evolution. Subsequently we describe the experiments and make a comparison between theory and experiment.

To study the principle of using a CW laser, as a heating tool, in the HAMR process a simple numerical model of the HAMR process has been implemented, where the heat and field induced magnetisation dynamics can be observed. To observe the change in the magnetisation dynamics, due to raised temperature, the thin film was subject to a pulsed field, in the negative z direction, that induced the dynamics over a range of temperatures. For consistency with the experiments a bias field was applied in the positive z direction, so that the magnetisation was restored to a temperature dependent equilibrium configuration.

The GdFeCo thin film used in the experiments has a relatively low coercivity of 25 Oe, which suggests a low anisotropy and also that the thin film is comprised of relatively large domains, as the thermal fluctuations associated with smaller domains would easily overcome the energy barrier associated with the low anisotropy and the thin film would become demagnetised. Therefore the random thermal fields associated with the LLB equation, described in the model chapter, are set to zero for this part of the investigation. Also, the domain structures within the GdFeCo thin film are believed to be highly exchange coupled, as this partly explains the oscillation in the z-axis that was observed in the experimental results.

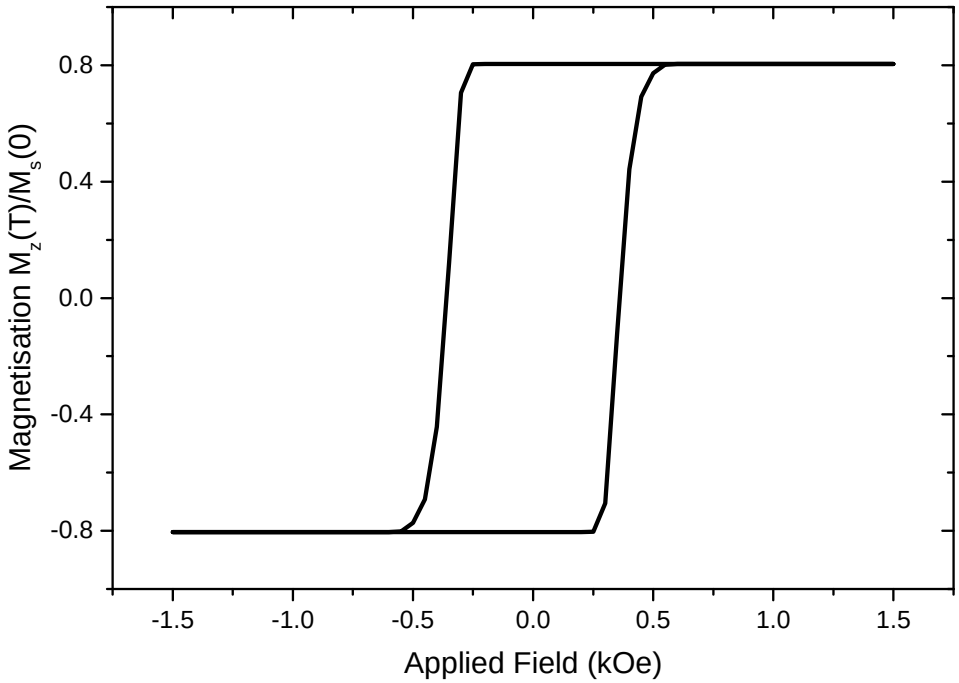

Figure. 6.1: A hysteresis loop generated with the GdFeCo thin film that was used to investigate the use of a continuous wave laser within the HAMR process.

6.2 Numerical Setup

The thin film simulated for the numerical calculations is approximately 1750nm by 1750nm in the x - y plane and 20nm thick and is comprised of 7558 grains with an average volume of $8.0\text{x}10^{-24}\text{m}^2$. To best approximate the thin film used in the experiments the magnetocrystalline anisotropy was set to $1.6\text{x}10^4$ ergs/cc, the saturation magnetisation was set to 150 emu/cc, with a damping constant of 0.07 and an average inter-domain exchange field of 20kOe. The high inter-domain exchange proved essential to the observed dynamics. The hysteresis loop produced with this thin film setup is shown in figure 6.1, where the coercivity, H_c, is approximately 0.35kOe, which is significantly larger than the thin film coercivity used in the experiments. The LLB model was unable to reproduce a system with a coercivity as low as 25Oe, with a saturation magnetisation of 150 emu/cc, as the effects of the magnetostatic field resulted in an in-plane magnetisation and therefore gave no hysteresis. Therefore the anisotropy is required to be significantly larger, to maintain a perpendicular magnetisation orientation, which results in an increased coercivity. This implies that an exact representation of the experiment can not be made and the results obtained with

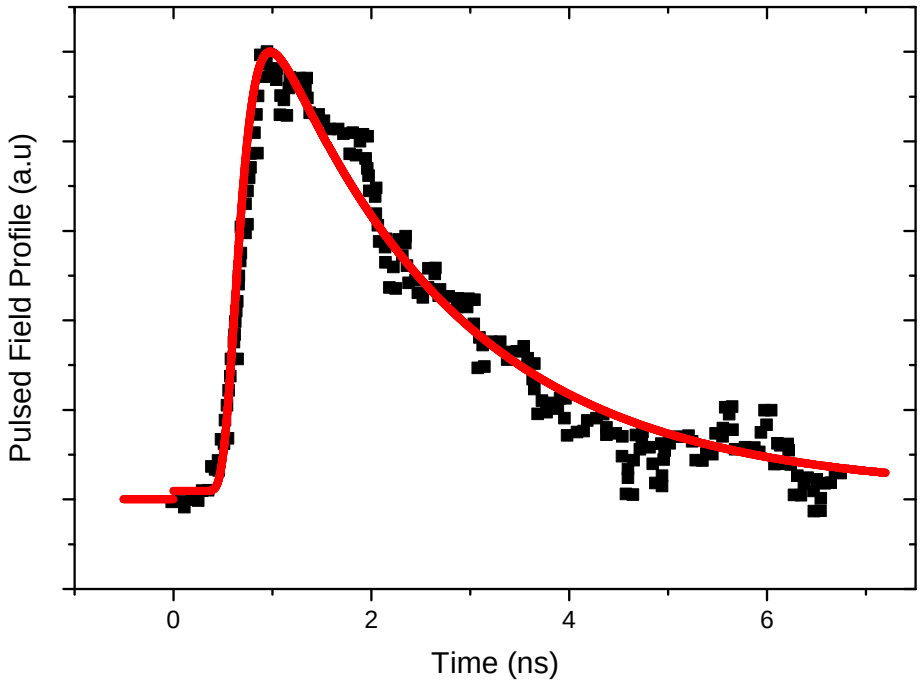

Figure. 6.2: A graphic showing the profile of the field pulse for both the experiment and LLB granular model cases. The pulsed field used in the experiment is shown in black and polynomial fit, used in the numerical calculations is shown in red.

the LLB granular model will only be able to show a similar trend.

Due to the increase in the coercivity, a larger bias field was applied in the numerical calculation; set to 1.66kOe. The form of the pulsed field used for the simulations was determined by fitting a polynomial to the form of the pulsed field used in the experiments; both are shown in figure 6.2. Also the set of temperature dependent parameters used for the LLB granular model are for FePt, which may alter the exact form of the results, when compared with the experimental case which were performed with a GdFeCo thin film, especially for the high temperature cases.

6.3 Numerical Magnetisation Dynamics

The simulations were initially set up so that both the pulsed and bias fields were set exactly anti-parallel and collinear with the anisotropy axis. The results produced in this situation showed no similarities with those observed experimentally. In this situation the magnetisation reduced in magnitude due to

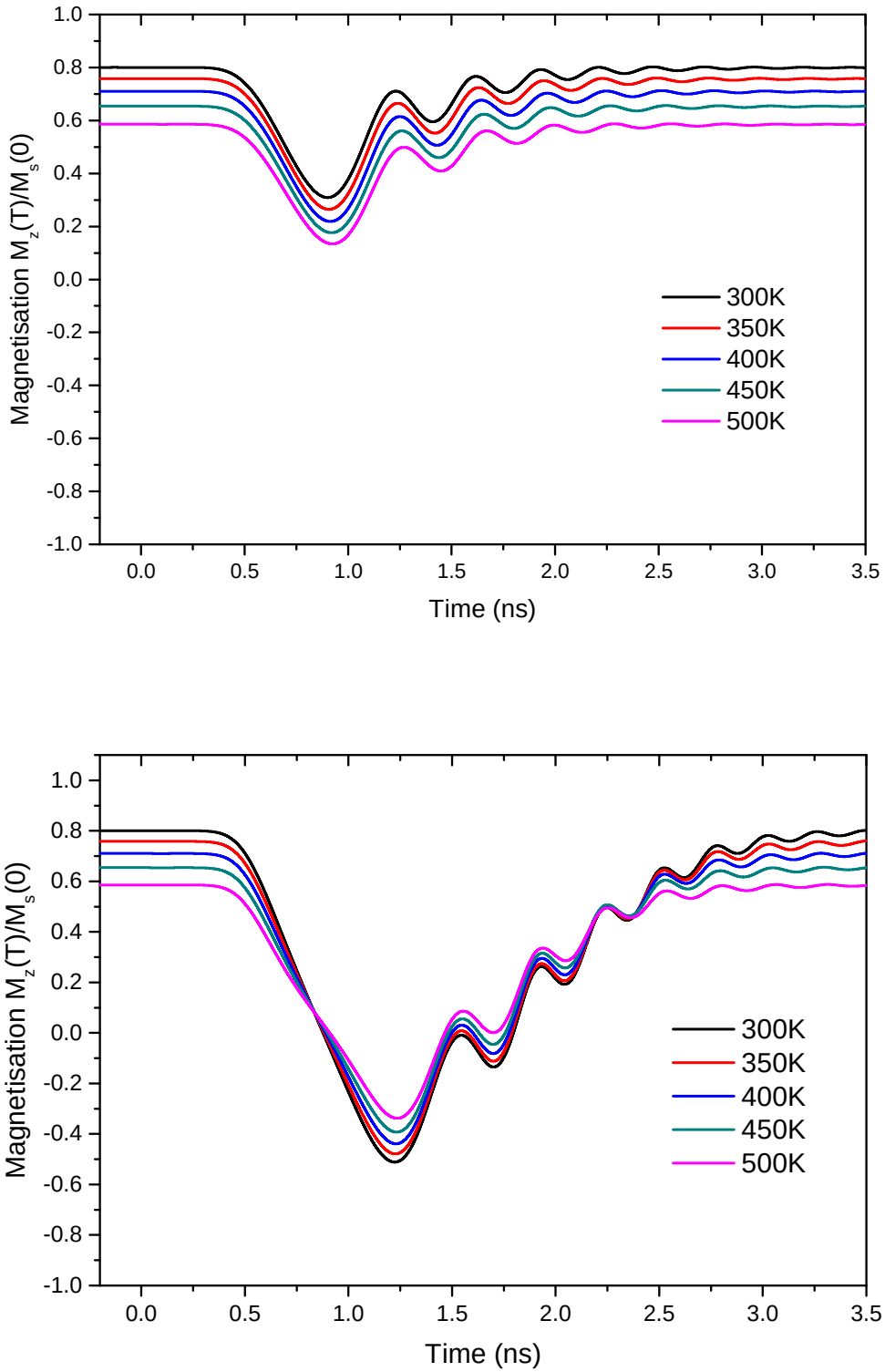

Figure. 6.3: The field and heat induced magnetisation dynamics determined with the LLB granular model where the results are in the form given by the LLB granular model. There are two cases shown. Top: The maximum field pulse strength is 1.8kOe, with a constant bias field of 1.66kOe, over a range of temperatures, 300K, 350K, 400K, 450K and 500K. Bottom: The maximum field pulse strength is 1.8kOe, with a constant bias field of 1.66kOe, over the same temperature range.

the interaction with the pulsed field, however the oscillation that was observed experimentally was not produced. To induce the oscillation a small angle between the pulsed field and biased field was required, which was found to be approximately 6 degrees. The offset in angle between the competing fields caused the magnetisation to precess around a point away from the anisotropy axis which resulted in the oscillation in the z component of the magnetisation observed in the experiment and the numerical results shown in figure 6.3. It is believed that the relatively large inter-domain exchange coupling causes the magnetisation of the system to precess as one, acting as a single spin, which allowed the magnetisation of the thin film to precess around a point between the anisotropy axis (z axis) and the bias field, which resulted in the observed oscillation in the z axis.

The change in the magnetisation dynamics due to raised temperature is difficult to quantify with the magnetisation data directly produced with the numerical model, as the relative level of magnetisation reversal is not apparent, due to the variation in the temperature dependent equilibrium configuration, as a result of the reduced magnetisation. The results obtained directly from the model are shown in figure 6.3.

To represent the data in a format that better highlights the impact on the magnetisation dynamics due to raised temperature and in a manner that is consistent with the results produced experimentally, which show the relative level of Kerr rotation, the magnetisation trace generated with the LLB granular model has been modified using a simple translation of the data given in equation 6.1 and the modified results are shown in figure 6.4.

$$M_z(r.u) = \left| \left(\frac{M_z}{M_{ze}} - 1 \right) \right| \tag{6.1}$$

In Eq.6.1, M_z(r.u), where M_z is given in reduced units, is the modified results for the magnetisation in the z-axis, M_z is the unmodified magnetisation data in the z-axis generated by the LLB model equal to $M_z(T)/M_s(0)$ and M_{ze} is the magnitude of z component of the magnetisation at equilibrium. This process results in a value that gives the magnitude of the reversal, where 0 represents the magnetisation in the initial orientation and 2 would represent a fully reversed system.

The effect of raised temperature on the magnetisation dynamics is well displayed in the modified data shown in figure 6.4. In all cases the change in the magnetisation follows the form of the pulsed field, which includes the effect of

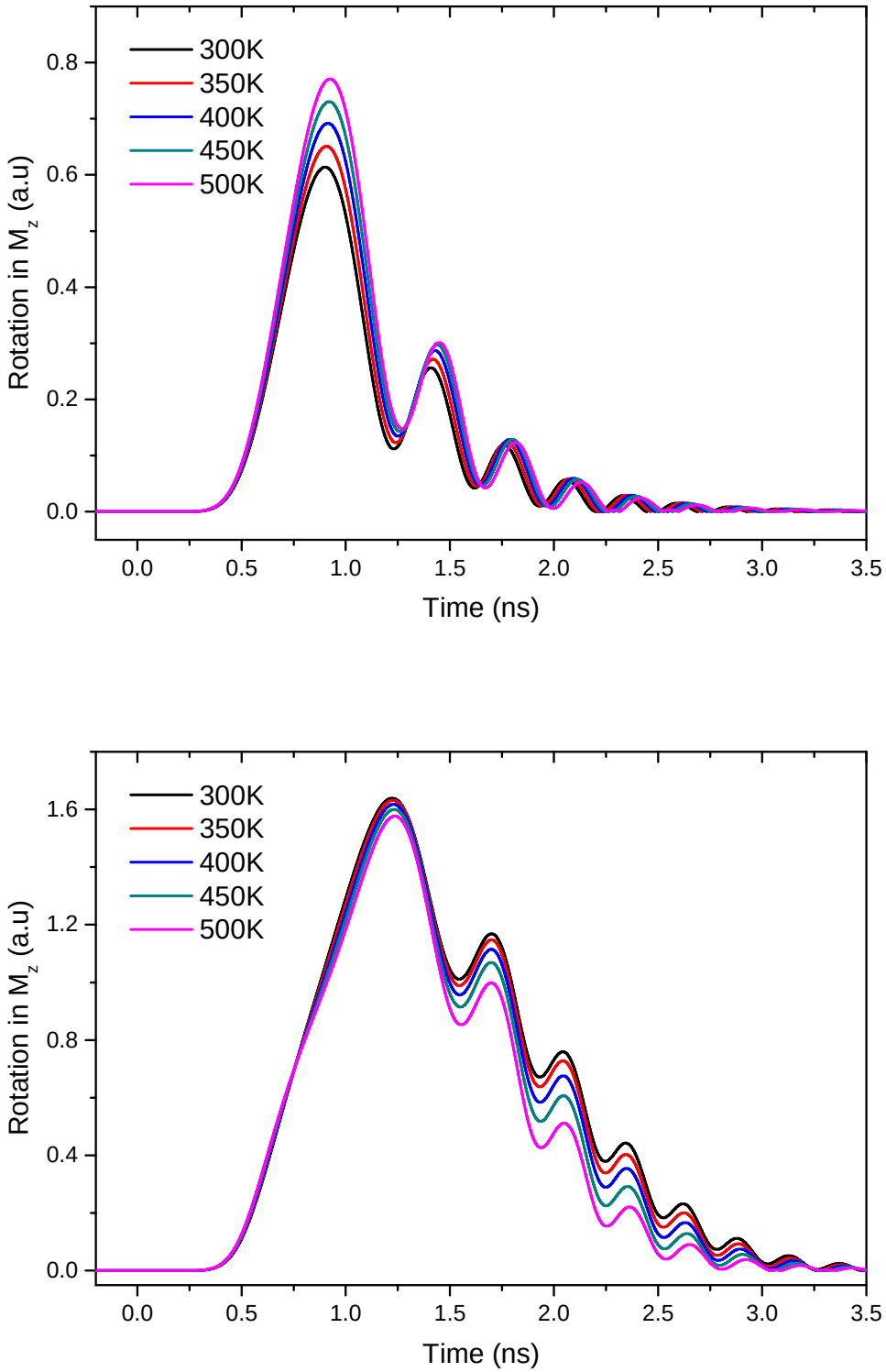

Figure. 6.4: The field and heat induced magnetisation dynamics determined with the LLB granular model where the results are modified using the translation shown in equation 6.1. There are two cases shown. Top: The maximum field pulse strength is 1.8kOe, with a constant bias field of 1.66kOe, over a range of temperatures, 300K, 350K, 400K, 450K and 500K. Bottom: The maximum field pulse strength is 1.8kOe, with a constant bias field of 1.66kOe, over the same temperature range.

the angle between the anisotropy and pulsed field, as the magnetisation further rotates away from the anisotropy axis, then returning back to the temperature dependent equilibrium configuration as the magnitude of the pulsed field decays.

For the minimum field pulse case, 1.8kOe, the maximum strength of the total field in the negative z direction - the bias field and the pulsed field - is negligible due to the maximum magnitude of the z component of the total field (approximately 10Oe) and the time period where the total field is negative (approximately 90 picosecond). Therefore the observed dynamics result from the transverse component of the pulsed field, which induces the magnetisation to oscillate around a point between the anisotropy axis and the direction of the pulsed field. This effect is increased with increasing temperature, as the reduction in the anisotropy field is having a reduced effect, causing the magnetisation to precess with an increased angle. This results in an increase in the reduction in the z component of the magnetisation at the peak amplitude of the pulsed field, figure 6.4. These results clearly show a softening of the magnetic properties - mainly the magnetocrystalline anisotropy - which is seen in the increased magnitude of the oscillations.

If the higher field pulse case is considered the change in the magnetisation is more significant, as the total field in the negative direction plays an increased role in the magnetisation dynamics. In this case the magnitude of the total field in the negative z axis is far greater than the previous case and for a significantly longer time period, which results in the magnetisation reversing for all temperature cases, figure 6.4. However, the magnetisation is reduced for the higher temperature cases, due to the the temperature dependence of the magnetisation. This indicated that the field pulse is the main factor that is dictating the magnetisation dynamics, although the reduction in the anisotropy is still apparent. Also, the transverse component of the pulsed field still plays a significant roll in the magnetisation dynamics, which causes the observed oscillation.

Also, there is a change in the way the magnetisation relaxes back to the temperature dependent equilibrium configuration as a function of raised temperature. For the lower field pulse case, 1.8kOe, where the change in the magnetisation is relatively low and the magnetisation does not switch, the magnitude of the oscillations, as the magnetisation relaxes toward the equilibrium configuration, is greater with increased temperature. Whereas, the opposite is true for the case with the larger pulsed field strength, 2.2kOe, where the system is seen to reverse the magnetisation. In this case the magnitude of the oscillations are reduced with increased temperature, figure 6.4.

Also the rate of relaxation back to the temperature dependent equilibrium configuration is similar for all cases shown in figure 6.4, independent of the temperature and maximum strength of the pulsed field.

6.4 Experimentally Observed Magnetisation Dynamics

To study the principle of using a CW laser as a heating tool in the HAMR process a simple experimental model of the HAMR process was implemented by colleagues at The University of York - T.Y. Cheng and J. Wu.

6.4.1 The Experiment

The experiment uses a field-induced time-resolved magneto-optical kerr effect setup in combination with a CW laser for heating, where a micro-coil is used to generate the required magnetic applied field pulse. A simple schematic of the optical experimental setup is shown in figure 6.5. Note that the experiments were carried out by TY Chen and J Wu and are described here for completeness.

A GdFeCo thin film with the easy axis orientated perpendicular to the plane was prepared for the experiment using a dc magnetron sputtering technique on a thermally oxidised Si substrate. The GdFeCo layer was approximately 20nm thick with a 10nm Ta base layer and a 4nm capping layer. The thin film had a material composition of Gd0.25Fe0.6Co0.15 which was achieved by using a composite target, by putting Gd and Co chips symmetrically of to the Fe target. The GdFeCo thin film exhibited a strong exchange coupling, as a very square hysteresis loop was obtained, at room temperature, showing a coercivity, H_c, of around 25Oe with a saturation field of approximately 60Oe, figure 6.6. The relatively small coercivity is necessary to allowing magnetisation switching within a short time and with the applied field pulse that the micro-coil is capable of generating. Also it is believed that the thin film is comprised of relatively large domains as the thermal fluctuations associated with relatively smaller domains would easily overcome the small anisotropy barrier and the thin film would quickly demagnetise. This is an important point to consider when attempting to simulate the experiments and is discussed in greater detail at a later stage in this chapter.

The GeFeCo sample was situated so that a permanent magnetic applied a bias field to insure that the sample was set to saturation before and after each

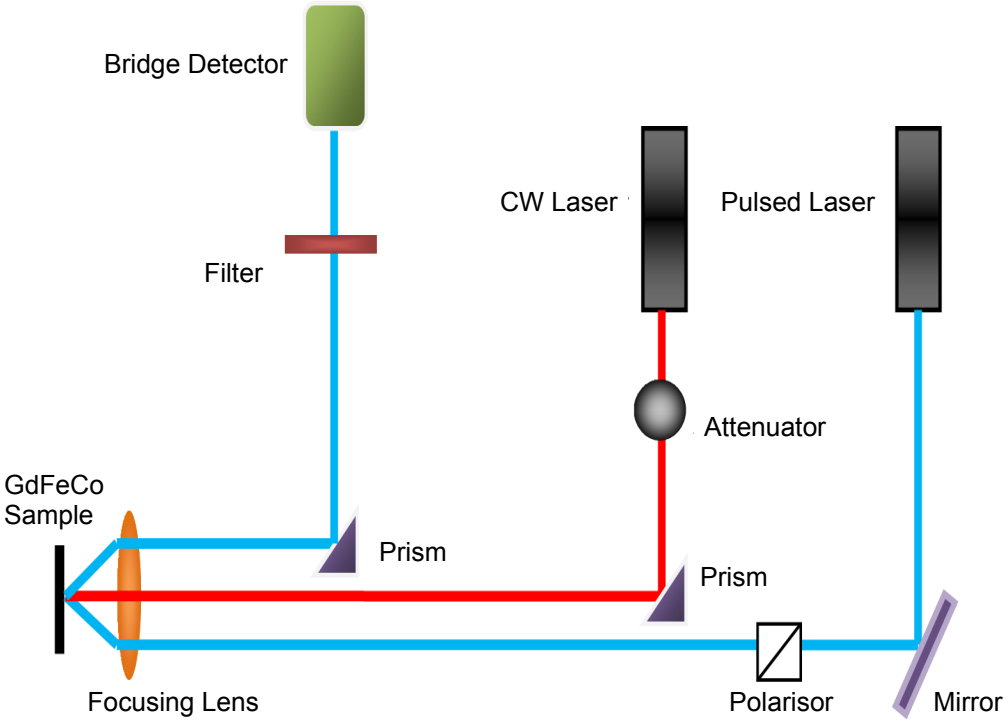

Figure. 6.5: A simple schematic of the experiment setup that was used to investigate the use of a continuous wave (CW) laser in the HAMR process.

field pulse excitation. The pulsed field was supplied by the micro-coil which had diameter of 600 micrometres and could supply a maximum field strength of 2.4kOe. The CW laser, with a wavelength of 660nm, was used to heat the sample throughout the period of the experiment. The dynamic change in the magnetisation was observed via the magnto-optical kerr effect (MOKE), using a pulsed semiconductor laser, with a repetition of 1KHz and a central wavelength of 409nm and a pulse width of 28ps, as the probe to detect the change in the magnetisation. As the GdFeCo sample has a perpendicular orientation for the anisotropy axis with the magnetisation point out of plane, a polar MOKE geometry was chosen. The optical observation setup is shown in figure 6.5. The system is set to guarantee a relatively large Kerr rotation, by keeping the incident angle of the laser small - no more than 5 degrees.

6.4.2 *Summary of Experimental Results*

A series of heat and field induced magnetisation dynamics experiments were performed over a range of field pulse strengths (1.35, 1.75, 2.16 and 2.4 kOe) and temperatures, produced by increasing the power of the CW laser from 0 - 180 mW. T.Y. Cheng and J. Wu were unable to give any precise information about the

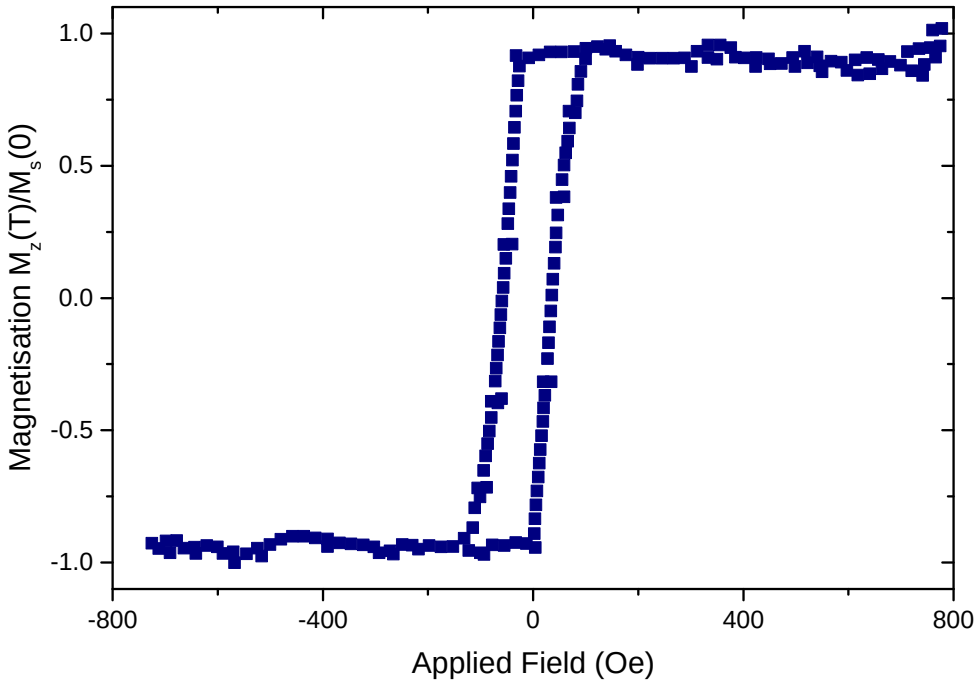

Figure. 6.6: A hysteresis loop generated with the GdFeCo thin film that was used to investigate the use of a continuous wave laser within the HAMR process. Courtesy TY Chen and J Wu.

temperature of the thin film during each experimental run. In all cases the bias field remained constant at 1.16 kOe.

The four cases presented in figure 6.7 show an increasing effect of the CW laser heating with reducing field pulse strength. The maximum field pulse strength of 2.4kOe, figure 6.7(a) shows virtually no change in the peak amplitude of the first oscillation in Kerr rotation for the different levels of heating. However, for the cases where the field pulse strength was lower there is an increasing effect due to CW laser heating for reduced field pulse strength, as with the lower field pulse strength used in the numerical investigation.

Consider first the case of the largest applied field in figure 6.7(a), it can be seen that there is a change in magnetisation on the timescale of the field pulse up to a peak which is independent of the temperature. This is followed by a temperature dependent precession. The increased temperature assisted the magnetisation to precess at an increased angle as the system relaxes to the temperature dependent equilibrium configuration. As mentioned above, there is an increased effect on the level of magnetisation reversal due to increased heating for lower field pulse cases. For the lowest levels of field pulse strength, figure 6.7 (c) and (d) there

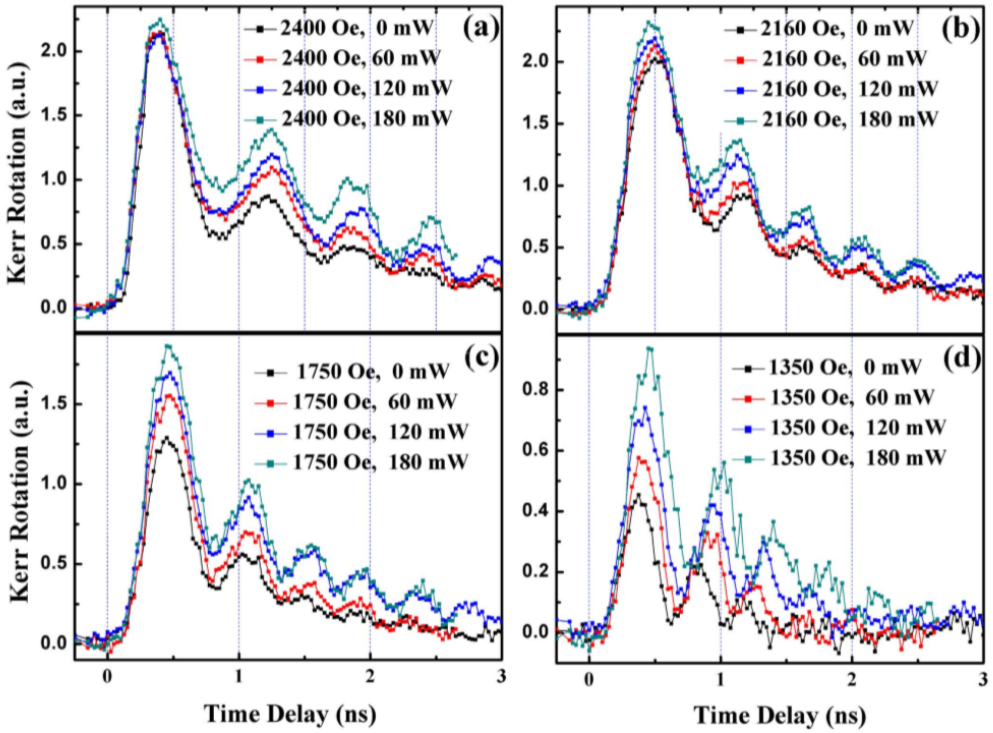

Figure. 6.7: The field and heat induced magnetisation dynamics determined experimentally for a range of maximum field pulse strengths, with a constant bias field of 1.16kOe, also of a range of temperature due to different power CW laser heating, 0, 60, 120 and 180 mW. The four field pulse cases are (a) 2.4kOe, (b) 2.16kOe, (c) 1.75kOe and (d) 1.35kOe. The effect on the magnetisation reversal, due to CW laser heating, is increased with lower field pulse strengths.

is marked increase in the increase in the magnetisation switching for increase temperature. This is consistent with the result of the numerical investigation.

In all cases shown in figure 6.7 the magnetisation relaxes to the temperature dependent equilibrium configuration in a similar time, independent of maximum field pulse strength and temperature, which is very close to what was seen in the numerical calculations. Also the magnetisation oscillates as the system relaxes in a similar was to the numerical results. However, the observed switch in the temperature dependence of the oscillation is not seen. This could indicate that the level of magnetisation is considerably less in the experimental case.

6.5 Comparison Between Theory and Experiment

The data obtained numerically with the LLB granular model and that obtained via experiment are qualitatively similar; they both show a softening of the magnetic properties and the magnetisation oscillates back towards the

temperature dependent equilibrium configuration in a similar way. However, there is a point of difference between the results produced. For the highest field pulse case in the numerical investigation there is a switch in the temperature dependence of the observed oscillation, as follows. In all the lower field pulse case, 1.8kOe, the magnitude of the oscillation is increased with increasing temperature. Whereas, with the largest field pulse used in the numerical calculations the, 2.2kOe, the opposite is true and the magnitude of the oscillation reduces with increasing temperature. In all the experimental cases this effect is never seen.

The results obtained with the numerical calculations and experimentally are difficult to compare as the experimental results are in terms of a relative Kerr rotation. To further quantify and obtain a comparable picture of the effect on the magnetisation dynamics as a result of raised temperature, for both the numerical and experimental results, the data from both investigated has been collated in manner that defines a reversal enhancement due to the change in the magnetisation dynamics as a function of raised temperature, as follows:

$$ReversalEnhancement = \frac{R_T}{R_A} \tag{6.2}$$

where R_T is the value of the rotation, at peak amplitude, with CW laser heating and R_A is the rotation, at peak amplitude, without CW laser heating.

For both sets of data there is a clear trend; when the maximum field strength is reduced the CW laser heating has an increased effect on the reversal enhancement, figure 6.8. However, there is a significant difference between the numerical and experimental data. The highest field pulse case, 2.2kOe, in the numerical study shows a reduction in the reversal enhancement with increased temperature. This is due to the level of magnetisation reversal at the peak amplitude in the magnetisation oscillation. The highest field pulse case in the numerical study showed that magnetisation to have switched orientation at the peak amplitude of the pulse field. In this situation the magnitude of the temperature dependent magnetisation, results in a decreased magnetisation, which effectively reduces the reversal enhancement, as defined in equation 6.2. This suggests that the dominant force driving the magnetisation dynamics is the field pulse, although the raised temperature is clearly softening the magnetic properties, as expected, as shown in figure 6.4.

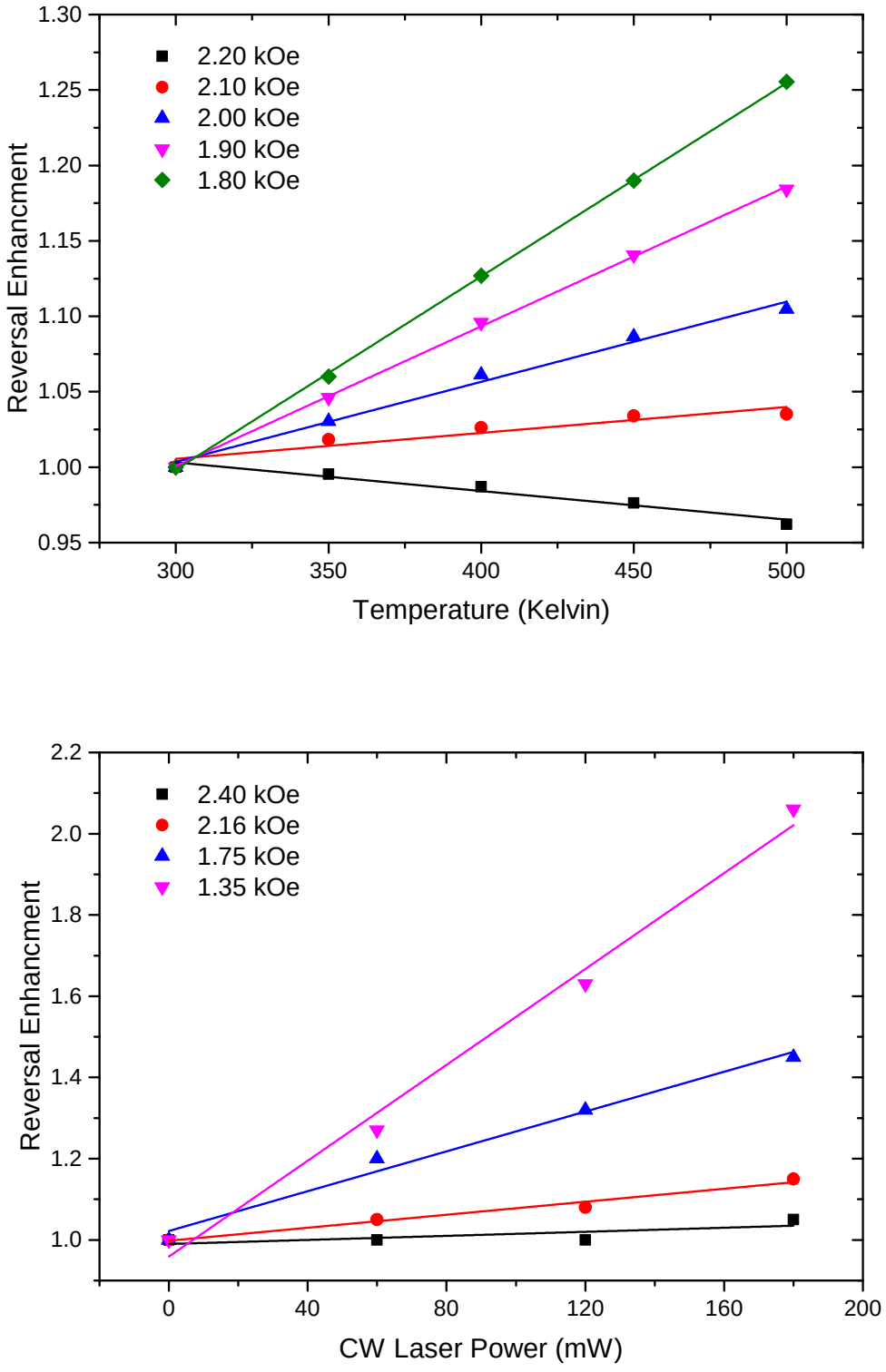

Figure. 6.8: Top: The relative reversal enhancement (peak amplitude at ambient/peak amplitude as elevated temperature), verses raised temperature, determined with the LLB granular model. Bottom: The relative reversal enhancement (Kerr rotation peak amplitude with CW laser heating/Kerr rotation peak amplitue without CW laser heating), versus the increasing CW laser power, determined experimentally.

Another significant conclusion can be drawn from the results presented in figure 6.8; namely that the magnetisation did not switch orientation in any of the experiments - the data shown in figure 6.7. These results, the change in the temperature dependent relaxation process with increasing field strength and the decrease in the reversal enhancement with increasing field strength, all suggest that the magnetisation did not switch in any of the experimentally observed cases, as these effects were not observed experimentally and the magnetisation never switched in the cases where these effect were observed numerically. The likely explanation for the discrepancy is the difference in material properties between the model calculations (for FePt) and experiments (GdFeCo). A more direct comparison is not possible without introducing the ferrimagnetic LLB equation into the granular model or repeating the experiments with FePt granular films.

6.6 Summary

The concept of using a continuous wave (CW) laser as a tool to heat the recording media during the heat assisted magnetic recording process has been investigated both numerically with the LLB granular model and also experimentally by colleagues at The University of York - T.Y. Cheng and J. WU. The thin films used in both cases have a coercivity which is significantly lower than are used in the high density recording media used in hard disk technologies, however the enhancement provided by the CW laser heating was significant and is consistent with a CW laser being used in HAMR technologies. Also the CW laser heating would not be constant in HAMR technologies as the laser would be moved over the region on the media where recording was happening, which would results in a momentary heating and consequent momentary lowering of the anisotropy to allow magnetisation reversal in the low anisotropy regime with the subsequent return of media stability as the temperature returned to ambient.

The numerical and experimental investigations showed good agreement over the full temperature range investigated, even though the two systems had different temperature dependent properties. The numerical and experimental results both showed a similar rate of relaxation toward the temperature dependent equilibrium configuration, which was independent of the temperature and the maximum pulsed field strength. Also, in both cases the magnetisation was seen to oscillate, as the system relaxed, which was found to be caused by an angle between the total applied field (pulsed field and the bias field) and the anisotropy axis. However, the numerical results showed

a situation where there was a switch in the temperature dependence of the observed oscillation. For the lowest field pulse used in the numerical study, 1.8kOe, the magnitude of the oscillation is increased with increasing temperature. Whereas, with the largest field pulse used in the numerical calculations, the 2.2kOe case, the opposite is true and the magnitude of the oscillation reduces with increasing temperature. This effect is due to the level of magnetisation reversal. In the lowest field pulse case the magnetisation was only perturbed away from the equilibrium configuration and the magnetisation never switched. Whereas, with the higher field pulse the magnetisation reversed in all temperature cases. This difference in the level of magnetisation reversal resulted in the switch in the nature of the observed oscillation. In all the experimental cases this effect is never seen. This indicates that the level of magnetisation reversal was sufficiently less in the experimental cases.

To further the understanding of CW laser heating as a tool in the HAMR process, the experiment should be modified to account for a situation where the magnitude of the total field - bias field and pulsed field - is more comparable with the coercivity of the thin film. This would enable a better understanding of the reversal enhancement could provide to the HAMR process. Also as a further experiment it would be interesting to see the level of reversal enhancement in the situation where there is no bias field and the CW laser heating is removed as the magnitude of field pulse decays, as in a field cooled magnetisation experiment. The rate of field pulse decay could be varied and the effect on the reversal enhancement observed. Also, the experiments should be repeated with an FePt high anisotropy thin film, as this is more applicable to the HAMR process and the current parameterisation of the LLB granular model.

7. Calculating the Magnetostatic Field - The Discrete Approximation (DA) Method

As mentioned in a previous chapter the dipole approximation makes assumptions and is therefore only applicable in certain situations. Here the applicability and inaccuracy of the dipole approximation is shown and a new method that better approximates the magnetostatic field, the discrete approximation (DA) method, is described and investigated. The method still calculates the field using the demagnetisation tensor, retaining the intrinsic speed of the method, but calculates the tensor elements accurately using the DA method.

Firstly a review of the dipole approximation is undertaken to show that the method is relatively accurate in certain situations, but can become increasingly inaccurate as the shape of the system in question becomes increasingly irregular. Secondly a complete description of the DA method is given. Finally the accuracy of the DA method is determined and compared with the dipole approximation. Also the computational runtime of the setup stage of the DA method is determined.

7.1 Dipole Approximation

The dipole approximation is an excellent approach for approximating the magnetostatic field in certain situations. As mentioned in an earlier chapter the derivation of the dipole approximation makes the assumption that the objects generating and subjected to the field are effectively point particles. These assumptions dictate the conditions where the dipole approximation is appropriate to use; in reality the field generated by a magnetic particle acting on another magnetic particle is a function of the size, shape and position of both interacting particles. Therefore the dipole approximation is most accurate when the effects of size and shape are minimised; effectively when the interacting particles are at a distance which is sufficiently larger than the particle size and also when the particles are uniform in shape.

To show the applicability of the dipole approximation a number of tests have been performed, using a number of different shaped interacting particles: a cubic

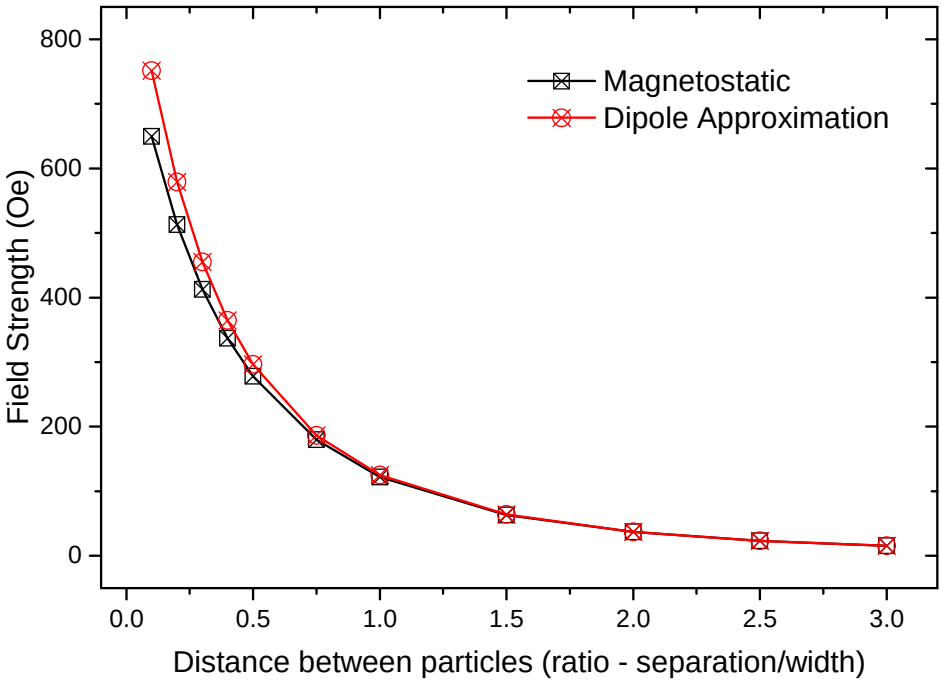

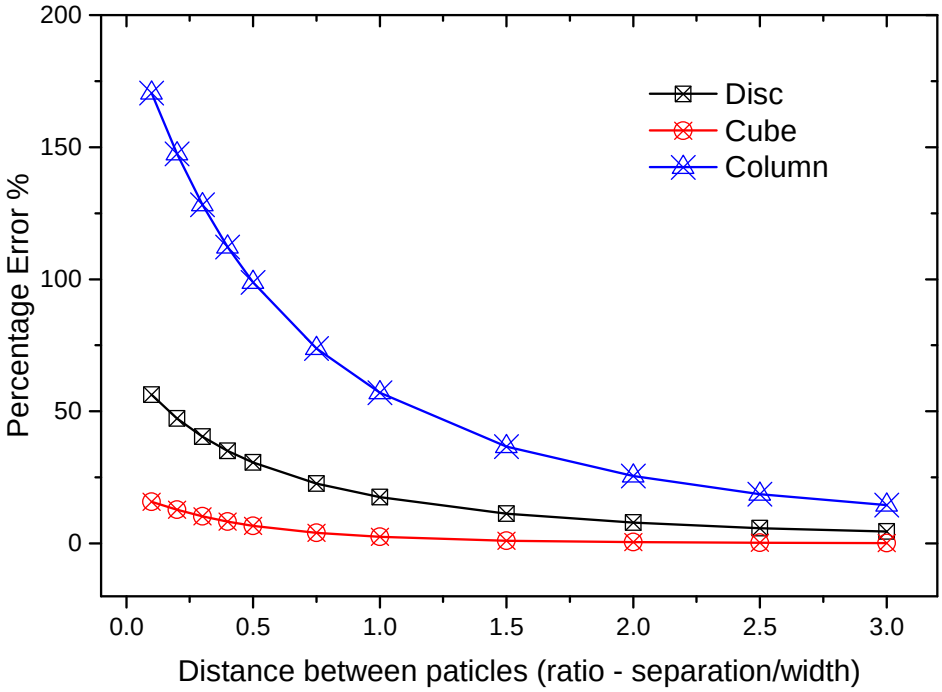

Figure. 7.1: Top: The field strength experienced by two interacting cubes as a function of particle separation, determined using the magnetostatic calculation and also the dipole approximation for comparison. Bottom: The percentage error of the dipole approximation, when compared with the magnetostatic calculation as a function of separation, for a number of different particle shapes: a cubic disc, a cube and a cubic column. The height of the particle is given as a ratio of height to width.

disc, where the dimensions are 5nm x 5nm x 1nm, a cube, where the dimensions are 5nm x 5nm x 5nm and also a cubic column with dimensions 5nm x 5nm x 10nm. It should be noted that for each test the interacting particles are alike. For simplicity the separation of the particle is always in the x axis and distance between interaction particles is given as a ratio of the separation distance between the particles to the particle width. Also the field determined is always in the z axis, due to a magnetisation vector being in the positive z axis with a magnitude of 1, (0,0,1), and the field is always given as a field strength rather than the actual field.

The data presented in the top panel of figure 7.1 gives an overview of the average field strength at the centroid of the particle, determined using both the correct magnetostatic calculation and the dipole approximation, for the case of the 5nm x 5nm x5nm cube, as a function of the distance between the interacting particles. Where the term 'magnetostatic calculation' is used; this means the correct answer has been determined, using the charge sheet method of Newell et al. [78], which was coded by a colleague S. Ruta at The University of York. As expected increasing the distance between the particles increases the accuracy of the result obtained using the dipole approximation; this is shown as the results obtained with the two methods tend towards the same value with increasing separation; when the particles are separated by great than one particle width the field determined using the two method are approximately the same.

The percentage error in the dipole approximation is given at the bottom of figure 7.1 and this also confirms the increase in accuracy of the dipole approximation as the separation between interacting particles is increased. For the cubic case with separation distance greater than 1 particle diameter (in this case 5nm's) the error in the dipole approximation is less than 2.5%. As expected, for cases where the distance between the interacting particles is low, the dipole approximation is most accurate for the shape that is most regular - i.e the cube. Also as expected, for all three shape types: disc, cube and column, the result obtained using the dipole approximation becomes increasingly accurate as the distance between the interacting particles is increased.

The effect on accuracy due to the shape of the particle is also apparent in figure 7.1, where the accuracy of the dipole approximation is reduced as the shape of the interacting particles is less uniform. As expected the cube gives the most accurate result, as this shape is most uniform; here the percentage error is approximately 15% when particle separation is 0.1 of the particle width. The disc and column cases are far less accurate at this separation distance: 56% for the disc and 170% for the column. This is partly due to the difference in the

particle volume, as the field determined with the dipole approximation directly scales with particle volume and therefore a two disc or two column system of equal volume where the centroid of the two particles are equally spaced would give the same result. That being said the shape of the interacting particle has a significant impact on the accuracy of the dipole approximation.

7.2 The Discrete Approximation Method

The aim of designing the discretised approximation (DA) method is to approximate the magnetostatic field with an acceptable level of accuracy for a range of arbitrary grain shapes, including those where the dipole approximation is highly inaccurate. Also the DA method should maintaining a realistic computational runtime that is similar to the dipole approximation in the case where only grains within a given cut-off distance are considered. The following sections describe how this is achieved, giving both a physical and mathematical description of the method.

7.2.1 A Physical Description of the DA Method

To accurately calculate the magnetostatic field the shape of both interacting particles must be considered, as shown above when comparing the results obtained with the dipole approximation and the exact magnetostatic calculation. The DA method considers the shape of both interacting particle by mapping the granular system on to a cubic grid of discretised cells, figure 7.2. This process is done by checking whether the centroid of a given discretised cell falls within the boundary of a given grain. This generates an approximation to the granular structure which is comprised of cubes, also shown in figure 7.2. It should be noted that the approximation of the granular system is in 3D in the x, y and z direction and not as a plane of squares as is shown in figure 7.2, it is only shown like this for simplicity. Also the size of the discretisation cells is chosen so that an exact number of these cells will fit within the z dimension of the elements. This is done to minimise any additional shape or volume effects that could arise due to cubic approximation of the granular structure.

The dipole approximation shown in equation 3.10, where only the field acting on grain i due to a single grain j is given, can be written in a tensor form, figure 7.1. The nine components of the tensor can be predetermined and this allows for the component of the dipole approximation acting on grain i due to grain j can be calculated by a simple matrix multiplication between the

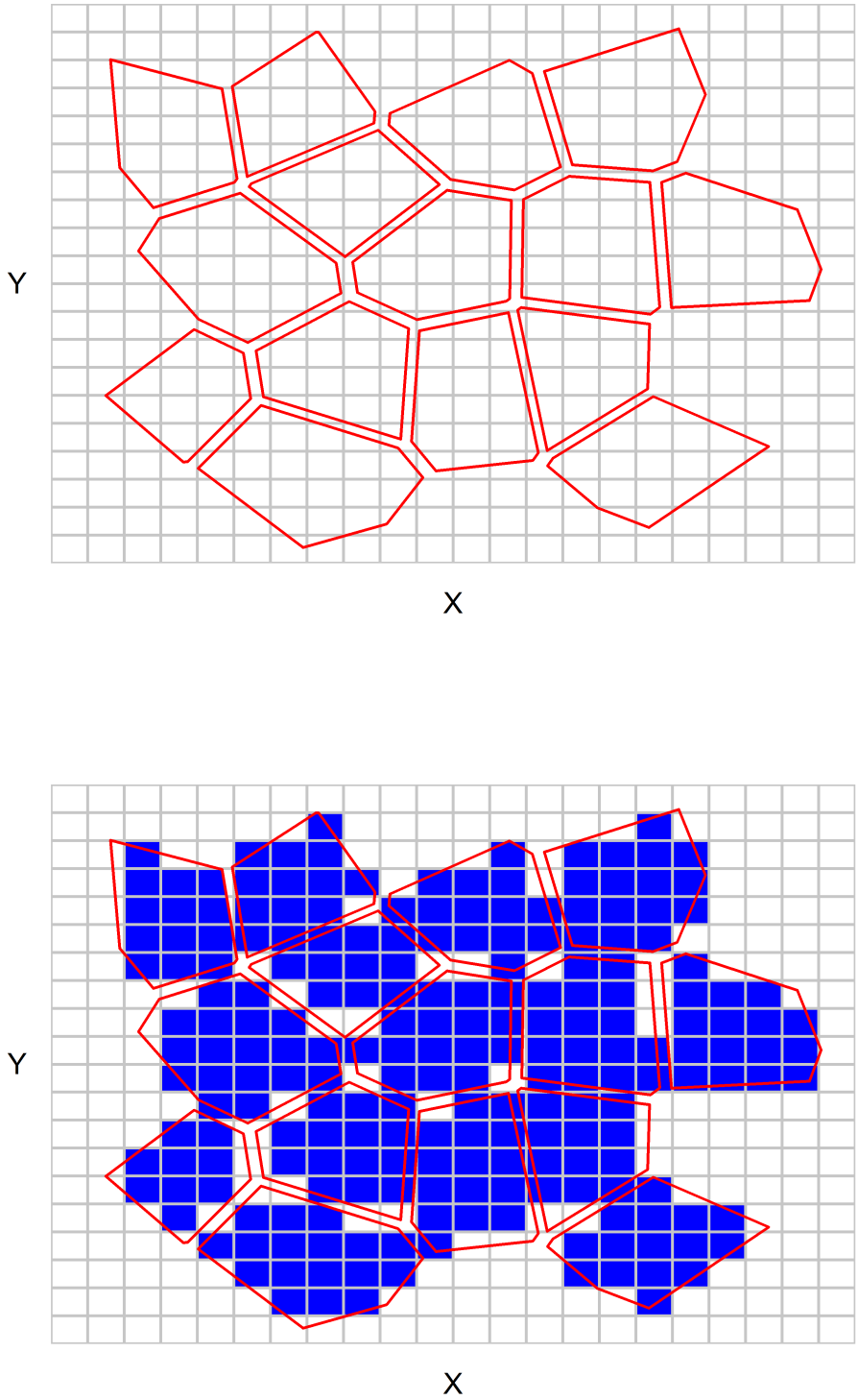

Figure. 7.2: Top: A schematic representation of a discretised grain patch in two dimensions. Bottom: A schematic representation of a discretised grain patch in two dimensions, showing which discretised cells are associated with which grains. Note the discretisation is three dimensional and is shown here in two dimensions for simplicity.

predetermined tensor and the magnetisation vector of grain j. The DA method uses a similar approach to predetermining the dipole tensor. To do this the dipole approximation is used to determine the nine field components of the tensor in the three principle axes - x, y and z, shown in figure 7.1 - acting on each discretised cell associated with a given grain i due to the interaction with all of the discretised cells associated with a given grain j. This generates a series of tensors, one associated with each discretised cell for grain i. The contributions to each tensor are given below, in equations 7.5 to 7.9. Each like component is then averaged to generate a series of tensors; one for each interaction between grain i and relevant grains j. This process is then repeated to account for all grains i. In doing so a series of tensors are generated which are used to determine the field acting on each grains i.

$$\begin{pmatrix} H_{dip}^{xi} \\ H_{dip}^{yi} \\ H_{dip}^{zi} \end{pmatrix} = \frac{M_s^j(0)V_j}{r_{ij}^3} \begin{pmatrix} 3\hat{r}_{xij}^2 - 1 & 3\hat{r}_{yij}\hat{r}_{xij} & 3\hat{r}_{xij}\hat{r}_{zij} \\ 3\hat{r}_{yij}\hat{r}_{xij} & 3\hat{r}_{yij}^2 - 1 & 3\hat{r}_{yij}\hat{r}_{zij} \\ 3\hat{r}_{zij}\hat{r}_{xij} & 3\hat{r}_{zij}\hat{r}_{yij} & 3\hat{r}_{zij}^2 - 1 \end{pmatrix} \begin{pmatrix} M_{xj} \\ M_{yj} \\ M_{zj} \end{pmatrix} \tag{7.1}$$

where $M_s^j(0)$ is the saturation magnetisation of grain j, V_j is the volume of grain j, r_{ij} is the distance between the centroids of grains i an j and M_j is the reduced magnetisation of grain j.

It can be seen in equation 7.1 that each part of the dipole tensor accounts for a contribution to the dipole field components acting on grain i due to the magnetisation of grain j and distance components between grains i and j.

The DA method that has been designed for this model modifies the pre-factor and each component of the tensor to account for the shape of both grain i and grain j. If grain i is divided into n cubes and grain j is divided into m cubes, then the tensor equates to this:

$$\begin{pmatrix} \tau(x)(100) & \tau(x)(010) & \tau(x)(001) \\ \tau(y)(100) & \tau(y)(010) & \tau(y)(001) \\ \tau(z)(100) & \tau(z)(010) & \tau(z)(001) \end{pmatrix} \tag{7.2}$$

where the form of each components of the tensor are given below:

The components that contribute to the x component of the field acting on grain i due grain j are:

$$\tau(x)(100) = \frac{1}{n}\sum_{n}\sum_{m}\frac{M_s^j(0)V_m}{r_{nm}^3}(3\hat{r}_{xnm}^2 - 1) \tag{7.3}$$

$$\tau(x)(010) = \frac{1}{n}\sum_{n}\sum_{m}\frac{M_s^j(0)V_m}{r_{nm}^3}(3\hat{r}_{ynm}\hat{r}_{xnm}) \tag{7.4}$$

$$\tau(x)(001) = \frac{1}{n}\sum_{n}\sum_{m}\frac{M_s^j(0)V_m}{r_{nm}^3}(3\hat{r}_{xnm}\hat{r}_{znm}) \tag{7.5}$$

The components that contribute to the y component of the field acting on grain i due grain j are:

$$\tau(y)(100) = \frac{1}{n}\sum_{n}\sum_{m}\frac{M_s^j(0)V_m}{r_{nm}^3}(3\hat{r}_{ynm}\hat{r}_{xnm}) \tag{7.6}$$

$$\tau(y)(010) = \frac{1}{n}\sum_{n}\sum_{m}\frac{M_s^j(0)V_m}{r_{nm}^3}(3\hat{r}_{ynm}^2 - 1) \tag{7.7}$$

$$\tau(y)(001) = \frac{1}{n}\sum_{n}\sum_{m}\frac{M_s^j(0)V_m}{r_{nm}^3}(3\hat{r}_{ynm}\hat{r}_{znm}) \tag{7.8}$$

The components that contribute to the z component of the field acting on grain i due grain j are:

$$\tau(z)(100) = \frac{1}{n}\sum_{n}\sum_{m}\frac{M_s^j(0)V_m}{r_{nm}^3}(3\hat{r}_{znm}\hat{r}_{xnm}) \tag{7.9}$$

$$\tau(z)(010) = \frac{1}{n}\sum_{n}\sum_{m}\frac{M_s^j(0)V_m}{r_{nm}^3}(3\hat{r}_{znm}\hat{r}_{ynm}) \tag{7.10}$$

$$\tau(z)(001) = \frac{1}{n}\sum_{n}\sum_{m}\frac{M_s^j(0)V_m}{r_{nm}^3}(3\hat{r}_{znm}\hat{r}_{ynm} - 1) \tag{7.11}$$

where $M_s^j(0)$ is the saturation magnetisation of grain j, V_m is the volume of discretisation cubes of both grains i and j, r_{nm} is the distance between the centroid of the discretised cubes n and m associated by grains i and j respectively.

It is not required to generated a series of tensors for each contribution, from the cells associated with grain j for each cell associated with grain i, as the magnetisation for each cell within grain j will always be equal and therefore the contributions can simply be summed and it is only required that individual tensors are generated for all the cells associated with grain i, which can then be averaged.

The tensor data can be stored and used in a manner similar to the standard dipole approximation, and therefore to apply the DA method it is computationally identical to the dipole approximation and is therefore equal in runtime. The methods differ only in the computational time that is taken to set up the stored tensors. This is investigated at a later stage within this chapter.

7.3 Testing the Discrete Approximation (DA) Method

We have shown that the dipole approximation to the magnetostatic field is only applicable in specific situations and can be highly inaccurate when implemented in the incorrect situation, figure 7.1. The aim of this section is to investigate how the size of the discretisation cells effect the accuracy of the result, with the aim of determining an optimised discretisation to maintain an acceptable level of accuracy and also minimise the computational runtime, when setting up the required series of interaction tensors. Throughout all further sections of this chapter all field strengths given are the field in the z axis due to a magnetisation vector equal to 1, which is always positive in the z axis (0,0,1).

7.3.1 Discretisation Requirements

As discussed earlier in this chapter the DA method represents each ferromagnetic particle, those that experience and generate the field, with a number of discretised cells. The number of cells that each particle is represented with will affect the accuracy of the result, and in the extreme case of a single unit cell per particle the approximation method would have limited success at accurately approximating the field, as this would effectively reproduce the dipole approximation. Firstly the method is applied to a system of two cubes, as this case is best suited to

the DA method due to the nature of the discretisation allowing for an exact representation of the cubic system in both the shape and the volume. Secondly the DA method is applied to a system of two non-identical grains to determine the discretisation requirements for a system that better approximates the granular systems where the method will be applied using the model.

Testing the DA method on a Simple Cubic System - Two Identical Cubes

To test the effect of the size of the discretisation cells on the accuracy of the method, a system of two 10nm cubes, i and j, separated by 1nm has been generated and the number of cells that each cube i and j are divided into is altered and the field strength acting on cube i is determined and compared to both the magnetostatic and dipole methods. The size of the discretised cubes that are used is such that they will always fit exactly within the volume of the 10nm cubes in all three axis.

The effect of altering the number of cells that the system is divided into is shown in figure 7.3. The graph at the top of figure 7.3 shows the field strength acting on cube i due to cube j, for a number of discretisation sizes from 10nm to 1/1.5nm. The result obtained with the DA method is compared with the values obtained using both the magnetostatic calculation and the dipole approximation. The DA method gives a good accuracy when the system is divided into greater than three cells along each axis, where the error is less than 1% for 4 or more cells along each axis. As the number of cells used to divide the system is reduced below three the value of the field determined approaches that of the dipole approximation and with a discretisation of one cell the two methods give exactly the same answer. This is expected as in this case the two methods are effectively identical.

The bottom of figure 7.3 shows the percentage error for the DA method when compared to the magnetostatic calculation. As mentioned above with a discretisation of 4 cells, along each axis, and above the accuracy is to within 1%, further reducing to less than 0.1% with a discretisation of 8 cells or greater. The maximum error of approximately 16% is when the system is divided into 1 cell, when the answer determined is the same as the dipole method.

The accuracy of the approximation method, in this situation, is expected to be high as the two interacting cubes can be divided exactly and the sum of the volume over the number of discretised cells will give the exact answer of the actual volume of the cubes.

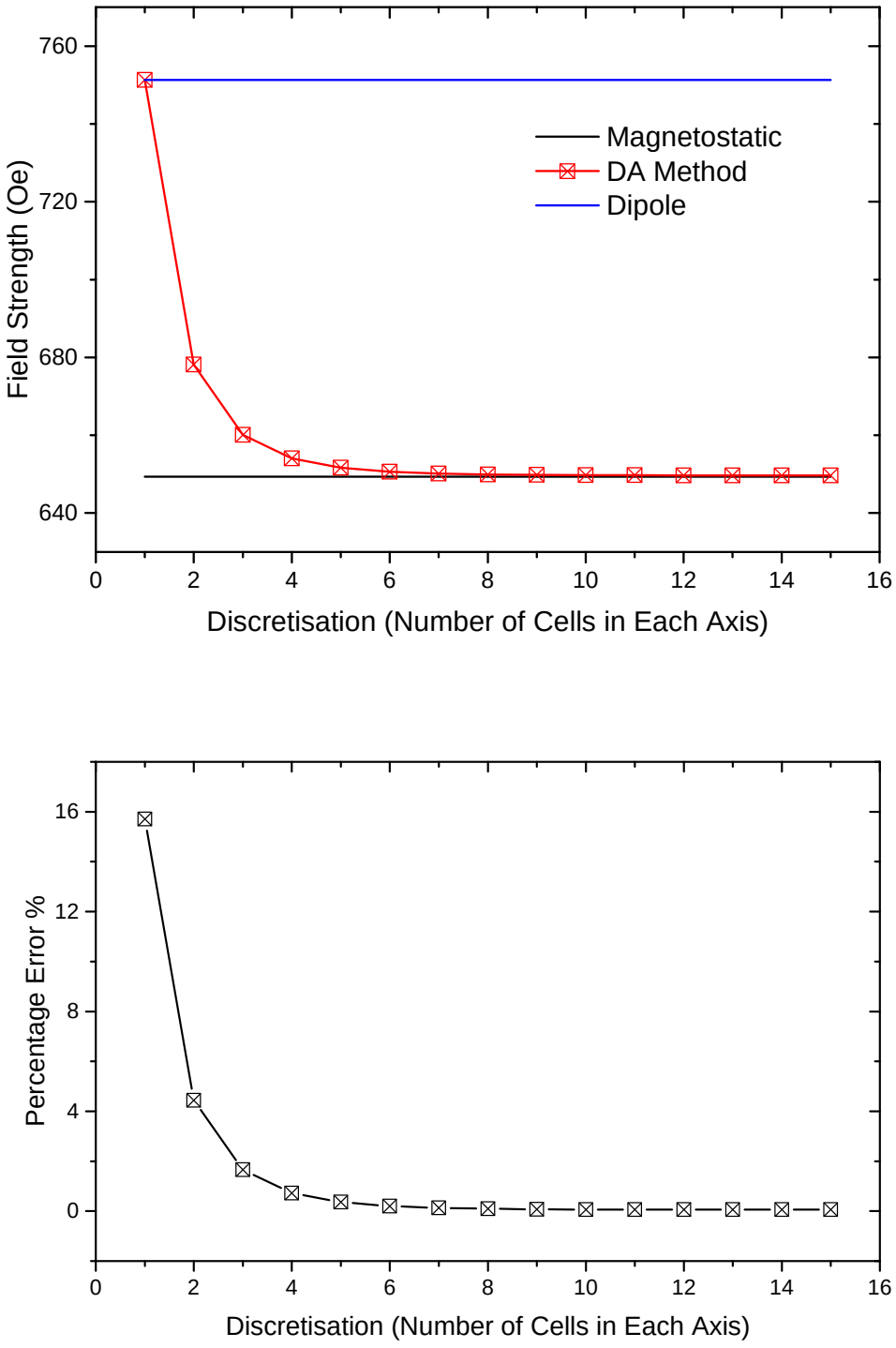

Figure. 7.3: Top: The field strength determined with the DA method, the magnetostatic calculation and the dipole approximation, for a system of two 10nm cubes separated by 1nm, over a range of size for the discretisation cells. Bottom: The percentage error of the DA method, when compared with the magnetostatic calculation, as a function of the number of discretisation cells in each axis.

Testing the DA method on a Simple Granular System - Two Identical Grains

The discretisation test was repeated with two grains, each having an average area in the plan view of approximately 100nm^2, but sufficiently different to give a good approximation of two interacting grains in a realistic granular system: 66.09nm^2 for grain i and 115.01nm^2 for grain j. As with the cubic case the two grains are also separated by approximately 1nm. In this system the size of the discetisation cells are such that they fit exactly within the dimension on the z axis, but not in the x and y axis.

To achieve a similar level of accuracy, as the with cubic case, it is expected that a greater number of discretisation cells will be required. This is due to the nature of the DA method, as the discretised cells do not map exactly to the shape of the grains and therefore there is both a shape and volume discrepancy, which is effectively greater with larger discretisation cells. This is confirmed in the data presented in figure 7.4. The graph at the top of figure 7.4 gives the field strength acting on grain j due to the interaction with grain i, again for a number of discretisation sizes from 10nm to 1/1.5nm and again the data is also compared to the value obtained using both the magnetostatic calculation and the dipole approximation. The DA method shows a similar trend for the two grain system, but in this case the number of discretisation cells must be larger to achieve a similar level of accuracy; requiring an average of at least ten cells along each axis. As mentioned above the two grains in this system are not identical in either size or shape and one grain is sufficiently smaller than the other and would therefore require a smaller discretisation cell to achieve a similar level of accuracy this would increase the total required for the overall system; essentially the required discretisation level is determined by the smaller grain.

In the case of the two grain system the percentage error shows a similar trend with respect to the discretisation cell size, as to what was seen with the cubic case, although the percentage error does not decrease as consistently. The bottom of figure 7.4 shows the percentage error for both grains, i and j. Clearly the error is far more susceptible to the size of the discretisation cells. The percentage error does not decrease in a consistent manner as the number of discretisation cells are increased, this is due to the cells not mapping exactly to the the granular structure. The discretisation cells have been mapped to each grain in a way that simplifies the computation, to reduce computational runtime. This has the effect of not consistently mapping the discretisation cells to the grain and can therefore alter both the shape and volume in a manner that does not closer approximate the grains, as the size of the discretisation cell is reduced. Also, this can have the effect of marginally shifting the centre of mass of each grain which will also alter

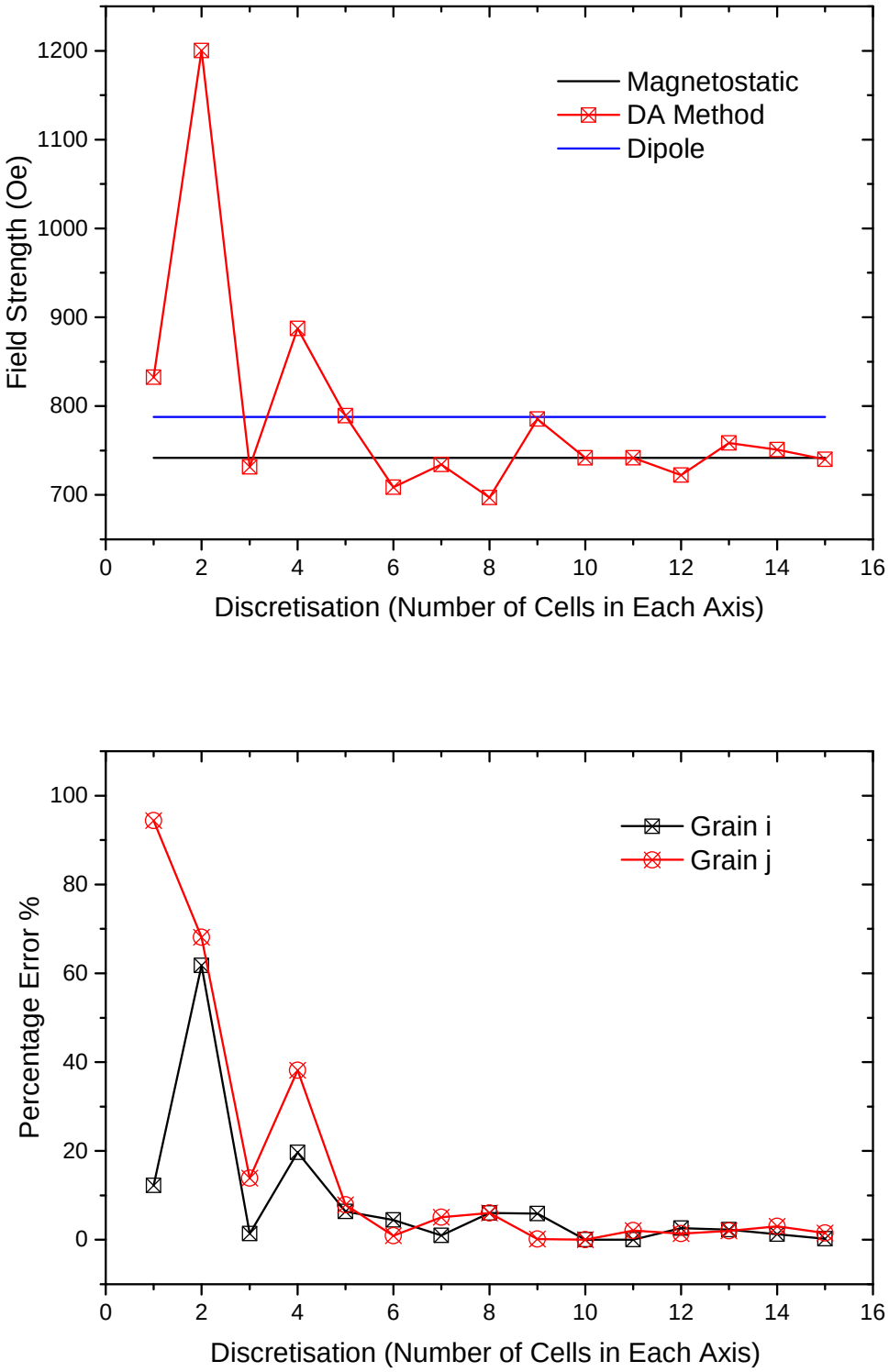

Figure. 7.4: Top: The field strength determined with the DA method, the magnetostatic calculation and the dipole approximation, for a system of two non identical grains separated by approximately 1nm, over a range of sizes for the discretisation cells. Bottom: The percentage error of the DA method, when compared with the magnetostatic calculation, as a function of the number of discretisation cells along each axis.

the field strength determined.

7.3.2 Accuracy as a Function of System Shape for Two Interacting Particles

As shown earlier in this chapter, changing the shape of the interacting particles can significantly alter the accuracy of the dipole approach and this effect is more significant when the interacting particles are less regular in shape and the particles are closer together. This section investigates the accuracy of the DA method as a function of the shape of the two interacting particles. There are three particle types investigated: again a cuboid system, a hexagonal system and also two non-identical grains and each interacting pair is studied as a function of the height of the particle verses the width. This effectively enables the study of discs, cubes and columns of differing shape. The area, when viewed in plan view, of each shape type is held constant throughout this part of the investigation: 100nm squared for the cuboid system, 10nm along the short axis for the hexagonal system and the two non-identical grains investigated have the same shape and area as those investigated in the previous section of this chapter. To test a more complex range of system shapes, the height of the systems is varied from 2nm to 20nm. Note both interacting particles are always the same shape and height. The discretisation cells are held constant at 1nm cubed, as this give approximately 10 cells along each axis in the x and y direction, as this gave an acceptable accuracy for the two interacting grains in a previous section of this chapter.

For each shape type investigated the DA method shows close agreement with the magnetostatic calculation for the full range of system heights investigated, figure 7.5. For all three system types the maximum error is for cases where the height is significantly less than the width. Unlike the dipole approximation, the disc like cases give the largest error using the DA method. The increase in the error for the disc like cases is due to relatively fewer discretisation cells approximating the systems, when compared with the cuboid and column like cases. The error is also marginally increased, verses the minimum error cases, when the system height is far greater than the width - i.e the column cases - but the error is still significantly less than in the disc cases. For both the column like and disc like cases the increase in error is partly due to the DA method relying on the dipole approximation and due to the size of the discretisation cells, as each component of the DA method, determined with the dipole approximation, will contain an error.

This being said, the DA method is still highly accurate compared with the dipole approximation. For both the cuboid and hexagonal cases the error is less

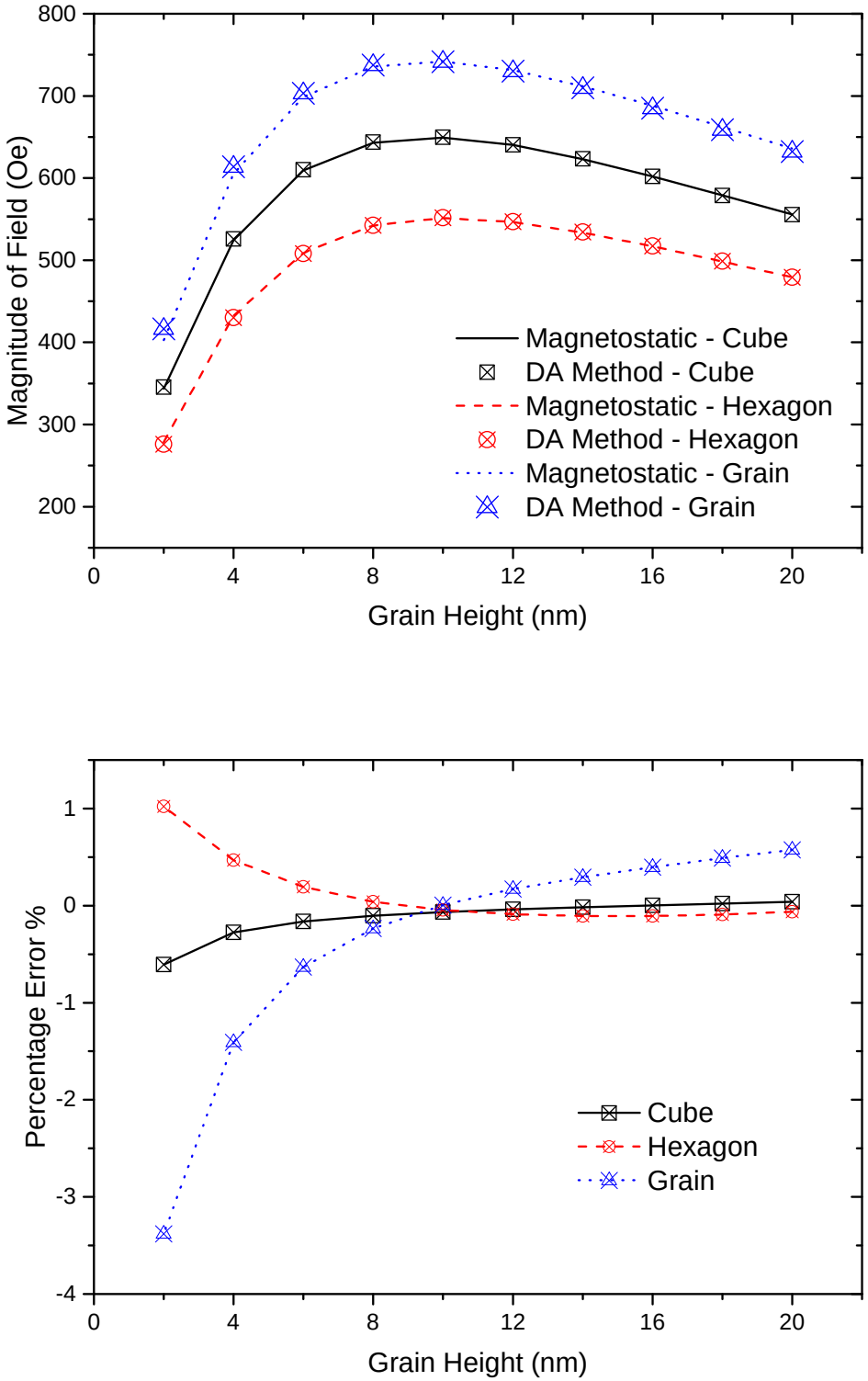

Figure. 7.5: Top: The field strength determined with the DA method for interacting shape pairs: cubic, hexagonal and granular, over a range of system heights. Each interacting shape pair is identical and are all approximately 10nm squared, when viewed in plan view. Bottom: The percentage error for each case, when compared with the magnetostatic calculation.

than a 1% for all system heights. As expected the system with the largest error is the two non identical grains, but the error only becomes relatively significant, greater than 1%, when the system height is 4nm or less. For two non-identical grains the size of the grain can have a significant affect on the accuracy of the DA method, as the accuracy of field generated by the smaller grain will be less than that of the larger grain, when using a fixed size for the discretisation cells. Clearly this can be overcome by setting the size of the discretisation cell as a function of the grain size.

7.3.3 Grain Patch

The DA method will be applied to realistic systems and in the case of this model it is a granular thin film, but the method can be applied to any system of interacting magnetic particles where the magnetostatic field could be a significant effect, such as the nano magnetic particles used for magnetic hyperthermia. Therefore the same set of tests have been applied to a small grain patch containing 15 grains, with an average area for each grain, in the plan view, of approximately 100nm squared. As before the test was repeated over a range of system heights, form 2nm to 20nm, but for simplicity of reading the data here only three system heights are shown: 10nm, 2nm and 20nm, figure 7.6.

In this situation the DA method again shows a good level of accuracy when compared with the exact magnetostatic calculation and far better than the dipole approximation. The top panel in figure 7.6 shows the field strength acting on each grain due to the interaction with all the other grains within the system, for the case where the grains are the most uniform in shape - i.e where the system height is roughly equal to the average grain width - 10nm. In this case the dipole approximation will give the highest level of accuracy. It is clear from the data presented in figure 7.6 that the DA method is still far more accurate that the dipole approximation, when comparing with the magnetostatic results. For the results obtained with the DA method the maximum error on any grain is approximately 2%, with an average error of approximately 0.66%. Whereas the field determined using the dipole approximation is far less accurate, having a maximum error on any grain of approximately 35.7%, with an average error of 19.75%. This shows that even in the best case scenario, the dipole approximation is a poor method for approximating the magnetostatic field in a granular system and the DA method is a far superior choice.

The accuracy of the DA method is further highlighted in the data presented in the bottom panel of figure 7.6, which shows the percentage error for each

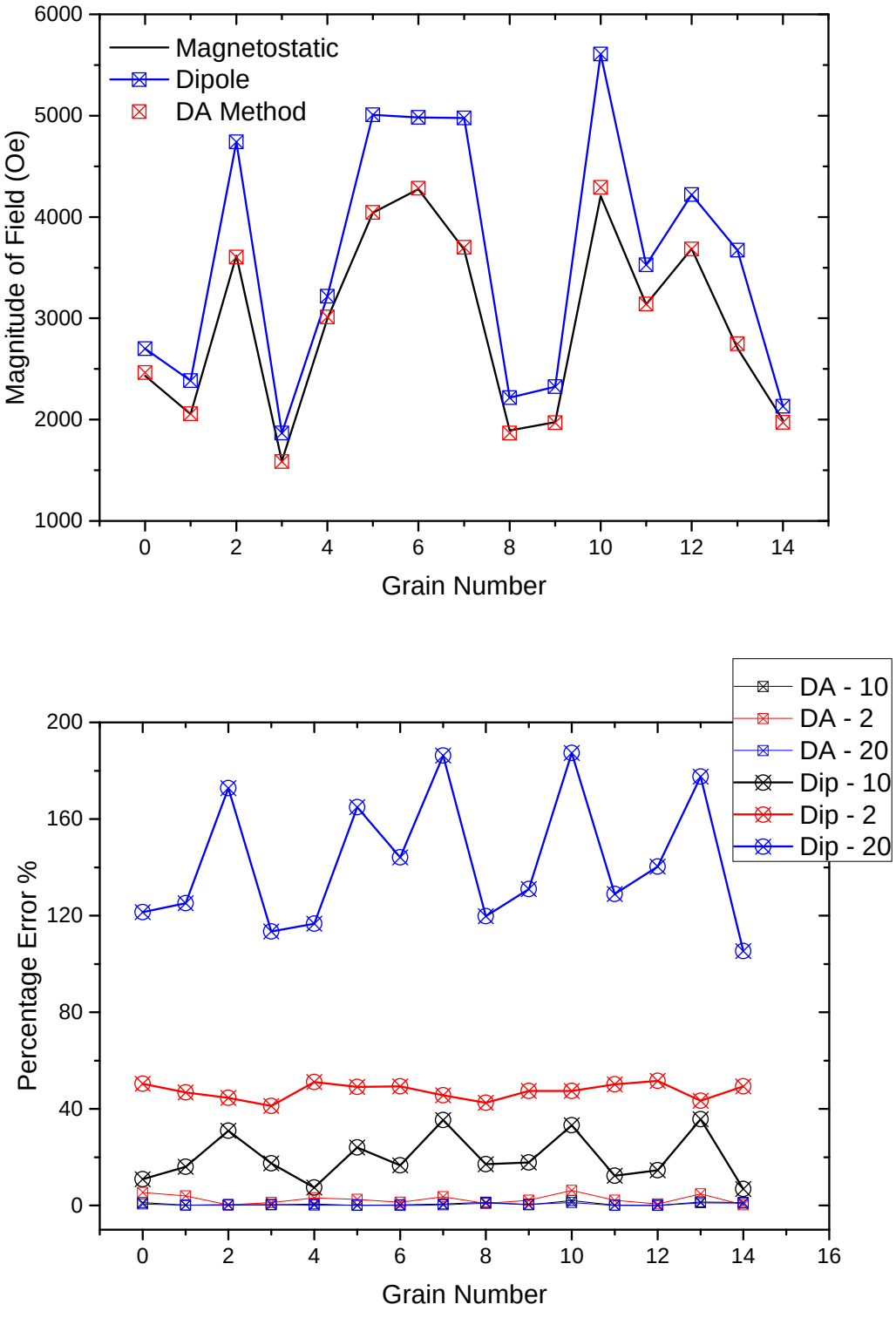

Figure. 7.6: Top: The field strength determined using the DA method, the magnetostatic calculation and the dipole approximation, for a grain patch containing 15 interacting grains, where the system height is 10nm. Bottom: The percentage error for a similar system with three different heights: 2nm, 10nm and 20nm, when compared with the magnetostatic calculation.

grain in the system for three different height systems: 2nm, 10nm and 20nm. The data shows the percentage error for both the DA method and the dipole approximation. The percentage error shows a similar story to what was seen for the two interacting particle cases; that the accuracy was reduced, when using the DA method, for the disc like case when the system height was 2nm. In this case the maximum error on any grain was approximately 6.2% with an average error of 2.6%. Although this is a marked increase when compared to the errors seen for the case where the system was 10nm high, it is still well within an acceptable level. Unlike in the previous sections, the level of accuracy was best for the 20nm high case, with a maximum error of 1.27% and an average of approximately 0.46%. This data clearly show the DA method as highly accurate, especially when compared with the level of accuracy of the dipole approximation. It is easy to see, in figure 7.6 that the dipole approximation overestimated the magnitude of the field in all cases presented.

7.3.4 Runtime Evaluation

As previously mentioned the DA method works by dividing the granular system in to a number of discrete cells of a given size; to maintain the desired level of accuracy each grain must be divided into approximately 100 cells in the plan view - the x-y plain - where the number of cells in the z axis is of less importance. Therefore the setup cost of determining the series on DA tensors that are required to calculate the DA methods approximation to the magnetostatic field is not simply a function of the number of grains and also scales with the height of the system. To put it simply, the DA method scales with the number of grains and also the total number of discretised cells.

The data given in figure 7.7 show the time taken to setup the series of DA tensors for a number of systems with an increasing number of grains. Also the data shows how the height of the system, effectively the number of discretisation cells, effects the runtime. The two system heights are 2nm and 10nm and the size of the discretisation cells is 1nm cubed. There is a clear difference in the runtime for the two systems; where the larger, 10nm high, system takes much longer to complete the setup for a comparable number of grains. For a system with approximately ten thousand grains the setup costs are approximately 136 seconds for the 2nm high system and approximately 1415 seconds for the 10nm high system. The large increase in time is due to the increase in the number of discretisation cells in both grains i and j.

When considering fixed height systems the setup cost scales linearly. It is apparent that the scaling is not linear for the smaller system; this is due to the

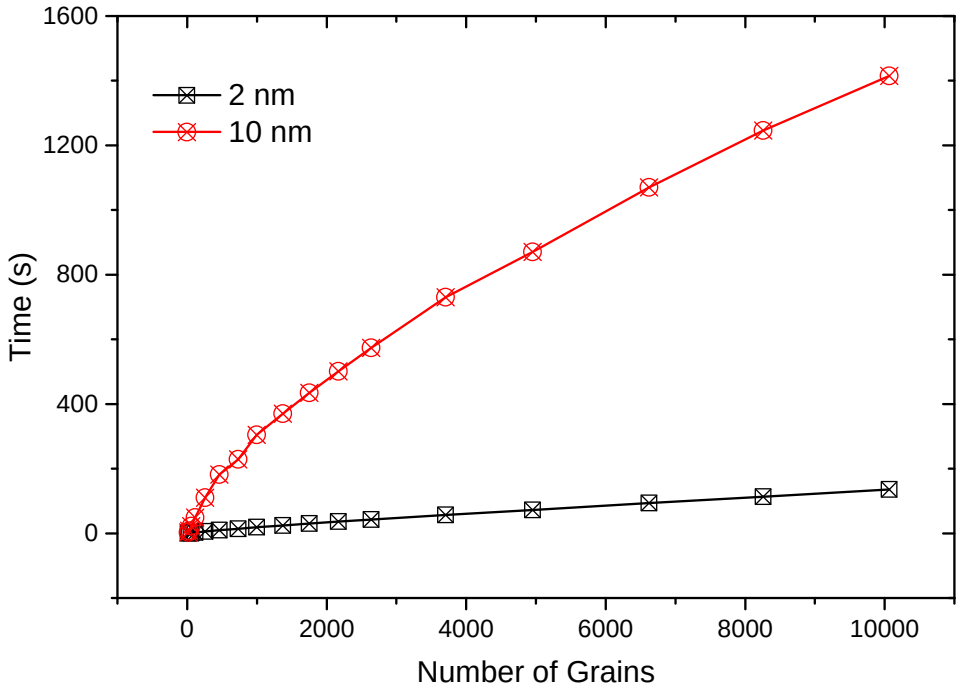

Figure. 7.7: The computational runtime required to setup the series of interaction tensors for the DA method. The data shows the time required for two different system sizes; both 10nm x 10nm, with different heights - 2nm and 10nm. The size of the discretisation cells is 1nm.

relative increase in the number of grains that each grain i must interact with. As previously stated the DA method includes, for interaction purposes, only grains that are within 8 grain diameters. Therefore for the smaller systems that are below this threshold the scaling is not linear and the scaling only becomes linear once each grain is interacting with approximately the same number of grains. For very large systems the setup runtime may become the majority of the overall runtime of a given simulation. If a like granular format is required for a number of simulations, the series of DA tensor should be output to a data file and read in at the begin of the simulations to increase the overall runtime simulations.

7.4 Summary

Firstly we have shown that the dipole approximation is only appropriate to use in situations where the particle that make up the system are approximately uniform in shape, although this method still has limited success even in this case due to the inaccuracy when determining the field between particles that are separated by a small distance.

Secondly the discrete approximation method has been described and evaluated: including the requirements for the method to give an accurate approximation to the magnetostatic field while maintaining a realistic computational runtime for the setup cost for the method, this was found to be approximately 10 discretisation cells along each axis in the x-y plain. Also the relative accuracy of the DA method when compared to the dipole approximation for number of different system type and finally an evaluation of the runtime for the setup cost of the method.

The work presented in this chapter has clearly shown that the discrete approximation method is far more accurate, at approximating the magnetostatic field between interacting magnetic nano particles, than the dipole approximation. In cases investigate the accuracy of the DA method is far superior to the dipole approximation, including: two identical cuboids of varying height, two identical hexagonal volumes of varying height, two non-identical grains of varying height and also a small grain patch consisting of 15 interacting grains. In all instances the DA method gave a good level of accuracy when compared to the magnetostatic calculation. The method was most inaccurate for cases where the system height was significantly less than the width of the particles. This is due to the these systems having relatively less descretisation cell compared with system with a larger height. Even though these systems gave a relatively reduced accuracy it was still within acceptable levels, generally far less than 6%, and far better than the dipole approximation.

8. Conclusions and Further Work

The final chapter of this thesis summarises the main results presented; drawing attention to the significant results and conclusions in each research area, including any areas that should be further investigated. Also, a summary of proposed further developments that are planned with the LLB granular model is given.

8.1 Damping as a Function of the Intergranular Interactions

The LLB granular model was used to investigated the effect of intergranular interactions - the intergranular exchange and magnetostatic interactions - on the effective damping in ultra-high density recording media. The effect of the magnetic interactions was determined using a simulated optical ferromagnetic resonance technique to probe the relaxation process; the technique is similar to what is commonly used in experiment. Both the intergranular exchange and magnetostatic fields are shown to affect the damping in a significant way, as follows. The effective damping is increased above the input value with increasing magnetostatic field, as the increased magnitude of the long range interaction perturbs the dynamics of the magnetisation and increases dissipation via the generation of spinwaves. The intergranular exchange field has the opposite effect; for increasing exchange the damping is seen to reduce towards the input value, as the effects of the magnetostatic field are minimised and the magnetisation of the thin film precesses in a more coherent manner. The results obtained with the LLB granular model are shown to be consistent with those obtained experimentally in the low intergranular exchange regime, with both sets of results exhibiting a similar non-monotonic downward trend. However, the model and experiment are in disagreement for the relatively large exchange regime where there was a significant increase in the damping observed experimentally. The increase is ascribed to a change in the magnetisation dynamics involving the formation domain structures and propagation via domain wall motion.

The damping dependence was found to arise from the magnitude of the degeneracy of the k-vectors with the frequency of the ferromagnetic resonance mode, k=0. A simple spinwave model was developed and implemented by

Dr T. Ostler using the methods of McMichael [13, 14, 51]. It was found that a larger magnitude for the magnetostatic field resulted in an increased degeneracy of the of k=0 vectors, which was reduced with increasing exchange. The results produced with the spin wave model showed a direct correlation with the results determined numerically for both increasing magnetostatic and exchange interactions. It was concluded that the two-magnon scattering process is the dominant term determining the damping dependence, as the LLB model does not consider scattering due to magnetic impurities, grain boundaries or domain structures within the grains, however the model does exhibit a distribution in the magnetostatic interaction due to the variation in grain size.

Switching time calculations, determined with the LLB granular model, as a function of increasing intergranular exchange and consequently reduced damping, gave a nontrivial relationship that is not consistent with the simple macrospin picture of single domain nano-particles, where a change in the damping is used to determine a subsequent change in the switching time and importantly the non-trivial relationship is for an exchange regime that is likely for high density magnetic recording media. The cause of this non-trivial nature of the transition time is not known and due to the significance in hard disk technologies should be considered an area for further investigation.

8.2 Heat Assisted Magnetic Recording

The thermodynamic aspects of the heat assisted magnetic recording (HAMR) process have been investigated with the LLB granular model, as the HAMR process is of particular interest as the technology is capable of the continue the historic increase in areal density. The HAMR process is shown to reduce the switching field to approximately 6 - 7 kOe, dependent on the magnitude of the anisotropy, with a temperature increase to the Curie point. However the investigation has shown that the HAMR process is not simply magnetisation reversal over a thermally reduced energy barrier, as the concept of 'thermal writability', introduced by Evans et al. [58], is of increasing importance as the grain size is further reduced.

For cases where the temperature rise is significantly below the Curie point the magnetisation of the thin film is never fully reversed after the HAMR process, as the switched magnetisation is below the remanent magnetisation. In this case the dynamic magnetisation processes are similar to the conventional picture of HAMR - magnetisation reversal over a thermally reduced energy barrier - which

can be split into two stages. There is an initial rapid reduction in the magnitude of both the magnetisation and magnetic anisotropy caused by the rapid increase in the temperature, which happens in hundreds of femto seconds. This allows precessional switching over the thermally reduced energy barrier. Secondly, as the temperature recover towards ambient the rate of switching events is reduced and the increase in the magnitude of the magnetisation slows. This process can be significant and extend for a period of up to 10ns dependent on the grain size, as a result of thermally activated switching events. The magnitude of the anisotropy is significant in this process. For the lower anisotropy regime, approximately 20% of L_{10} ordered FePt, a number of switching events are observed as the system relaxes without any heating effects, therefore any increase in temperature will instigate further switching events. Whereas for the high anisotropy case, 100% of L_{10} ordered FePt no switching events are observed with a temperature rise up to 600K. Therefore the temperature range where these processes occur is sufficiently higher, than in the low anisotropy case, and thus narrower. Consequently the temperature range where the conventional picture of HAMR is applied is reduced to approximately 40K - 610K to 650K. These results show that for successful switching via the HAMR process the magnetisation must reverse via the linear reversal mechanism, by raising the temperature to at least T_c, which is a more complex process than the conventional picture of HAMR.

It has been demonstrated that magnetisation reversal in ultra high density recording media, using the HAMR process, is only achievable via the linear reversal mechanism. In the case of the linear reversal mechanism the magnetisation is entirely destroyed by raising the temperature to or above the Curie point, where the magnetisation returns in the direction of the applied as the temperature is lowered to ambient. This process is similar to a field cooled magnetisation process, albeit at high levels of temperature and cooling. Also, it is apparent that to achieve the desired level of magnetisation reversal the applied field must be sufficient to overcome the superparamagnetic freezing that can occur during the period of rapid temperature decrease.

The concept of 'thermal writability' is demonstrated to be a significant limiting factor in HAMR with ultra high density recording media, as the magnitude of the magnetisation can be significantly reduced in the negative direction after the HAMR process, due to thermally activated back switching of individual grains. The effect of 'thermal writability' becomes increasingly significant when the average diameter of the grains is below approximately 5nm. Thermal stability has long been considered the limiting factor for hard disk technologies; with L_{10} ordered FePt allowing a minimum grain size of

approximately 3.3nm in diameter. However, thermal writability may be a more stringent criterion, limiting the maximum areal density capable with the technology. Although, a maximum applied field of approximately 10kOe was assumed in these calculations, as this is a realistic value with current write head technologies, therefore if HAMR is to achieve the ultra high areal densities originally thought possible there must be significant improvement in write field technologies.

The thermodynamic study of the HAMR process has highlighted and confirmed a number of physical processes that are of significant interest and must be better understood to see HAMR achieve its full potential; these include the linear reversal mechanism and thermal writability. Therefore a further study with the current LLB granular model and with additional developments to the model must be undertaken. The desired level of magnetisation reversal with the HAMR process requires the linear reversal mechanism, where the temperature is raised close to the Curie point. Therefore, a dispersion in parameters such as: T_c, M_s, K_v, damping and the susceptibilities could significantly impact the magnitude of the reversed magnetisation and further understanding how a dispersion in these parameters effects HAMR is essential. The effects of thermal writability are not well understood on the macro-scale and further understanding is necessary for the development of HAMR. Beyond this the model will be further developed to investigate the HAMR process in a more practical manner through simulating the recording of bits on the recording media. This will enable a better understanding of how these thermodynamic limits effect the recording process and help ascertain the limits of HAMR in a more practical way.

8.3 Continuous Wave Laser Assisted Magnetisation Reversal Dynamics

A continuous wave (CW) laser has been investigated as a tool for heating the recording media during the HAMR process. The benefit of CW laser heating has been investigated numerically with the LLB granular model and also experimentally by a colleague at The University of York (Dr T.Y. Cheng), with both sets of results being in reasonable qualitative agreement. The CW laser heating gives an increased enhancement to the magnetisation reversal process with increasing temperature, although the temperature in both investigations remained significantly below the Curie point. The method employed in both investigations was attempting to observe an enhancement in the level of reversal due to a reduction in the anisotropy, which has been shown. However, the

investigation method was significantly different from the HAMR process, as the temperature remained constant throughout and the magnetisation was returned back to its initial temperature dependent equilibrium configuration after each run. Whereas, in HAMR technologies the laser would be moved over the region on the media where recording was to happen, resulting in a momentary heating and consequent momentary lowering of the anisotropy to allow the magnetisation to align with the direction of an applied field as the temperature returned to ambient.

The numerical investigation was also able to determine the origin of the experimentally observed oscillation in the z component of the magnetisation. The oscillation was found to be caused by a 6 degree angle between the anisotropy axis and the total applied field, a combination of the bias and pulsed fields. The angle and the high intergranular exchange interaction caused the magnetisation to precess around a point between the anisotropy axis and direction of the total applied field. In the experiments the angle is a attributed to a non-uniform distribution in the pulsed field and the relatively small size of the components used in the experiment making it difficult to gain a good alignment.

To further understand the concept of CW laser heating as a tool in HAMR, the calculation should be modified to account for the situation where the magnitude of the total field, at peak amplitude for the pulsed field, is more comparable with the coercivity and reversal fields, which would give a better picture of the possible enhancement that a CW laser can deliver. Also, it would be interesting to determine the level of reversal enhancement in the situation where there is no bias field and the CW laser heating is momentary, as in a field cooled magnetisation process. The rate of field pulse decay and peak temperature could be varied and the effect on the reversal enhancement observed.

8.4 The Discrete Approximation Method

A method for approximating the magnetostatic field, to a high level of accuracy far beyond the capabilities of dipole approximation, has been developed and tested - the discrete approximation (DA) method. The DA method maps the granular system to a number of discretised cells; allowing a magnetostatic interaction tensor to be generated, similar to the dipole approximation, but where the coefficients of the tensor account for the shape of the interacting grains.

The accuracy of the DA method is increased with an increasing number of discretised cells. It was shown that approximately 10 cells in each axis in the

x-y plane gives a good balance between accuracy and the computational cost of setting up the series of interaction tensors, as the setup runtime increases with the number of discretisation cells. However, as the method employs a series of interaction tensors, similar to the dipole approximation, the runtime of the two methods are computationally similar. Also the accuracy of the DA method is shown to be far superior, when it is compared with the dipole approximation, for a number of different system configurations.

The DA method is clearly far more accurate than the dipole approximation and the setup cost is acceptable considering the level of accuracy. For all system configurations investigated the DA method results in an accuracy greater than 94%, but more generally greater than 99%. The DA method was most inaccurate for cases where the system height was significantly less than the width of the particles, as this resulted in far less discretisation cells approximating the systems.

To further develop the DA method a different system for discretising the granular system will be investigated, as the current method using the minimum x and y values of the grain vertices for setting the positions of the discretisation cells gives a non consistent trend for improving the accuracy with and increase number of discretised cells. The current method marginally shifts the centroid of the approximation of the granular system, which changes the determined field and therefore the accuracy. The new discretising method will set the positions of the cells using the centroid of the grain, which should improve the accuracy of the method. However, this will impact the runtime for setting up the series of interaction tensors, so this should also be investigated.

8.5 Further Development of the LLB Granular Model

The LLB granular model has been implemented in a manner that makes it extremely adaptable, and is capable of simulating many domain based magnetic systems. The model used for this research is capable of simulating a granular thin film with a single layer of single domain grains, where the magnetic parameters that govern the magnetic properties, such as the Curie point (T_c) and saturation magnetistion (M_s), are able to have a chosen dispersion, although for this research there was no dispersion in the magnetic parameters. In addition to this the model will be modified to simulate recording bits of information on the media using a realistic write head field profile and temperature profile associated with a pulsed and a continuous wave laser.

The next step in the model development is to allow for multi-layer systems

such as exchange coupled composite (ECC) media, where all the layers are ferromagnetic. Beyond this a kinetic Monte Carlo (KMC) solver will be implemented to allow for antiferromagnetic layers within the media, such as the the magnetic materials used in the read heads for hard disk technologies.

Appendix 1 - Spinwave Model

The following gives a brief description of the spin wave model developed and implemented by a colleague at The University of York, Dr T. Ostler, based on the method of McMichael [13, 14, 51].

In the work of McMichael [14, 13, 51] the Landau-Lifshitz-Gilbert (LLG) equation is linearised, with the magnetisation and fields written in Fourier space using the following:

$$b(\mathbf{r}) = \int \frac{d\mathbf{k}}{(2\pi)^2} b(\mathbf{k}) \exp(i\mathbf{k}\cdot\mathbf{r}) \tag{8.1}$$

where b represents the magnetisation and / or the fields. The effective field is a combination of the Zeeman, magnetostatic, anisotropy and exchange fields and is written in terms of a sum over the magnetisation multiplied with a kernel, G, which is translationally invariant. Due to the $\mathbf{r} - \mathbf{r}'$ term, on-site terms are represented by delta functions multiplied by a scalar. The Fourier components of the field are then written as:

$$\mathbf{H}_{eff}(\mathbf{r}) = \int d\mathbf{r}' G(\mathbf{r} - \mathbf{r}')\mathbf{m}(\mathbf{r}'). \tag{8.2}$$

where $h_{\mathbf{k}}$ are the elements of the normalised stiffness tensor:

$$\begin{aligned}
h_{\theta\theta,\mathbf{k}} &= M_s^{0\,-1}\big[H_i + Dk^2 \\
&\quad + M_s^0(1 - N_k)\sin^2(\theta_k)\big] && \text{(8.3a)}\\
h_{\phi\phi,\mathbf{k}} &= M_s^{0\,-1}\big[H_i + Dk^2 + M_s^0 N_k \cos^2(\phi)\big] \\
&\quad + M_s^0(1 - N_k)\sin^2(\phi)\cos^2(\theta_k) && \text{(8.3b)}\\
h_{\theta\phi,\mathbf{k}} &= M_s^{0\,-1}\big[M_s^0(1 - N_k)\cos(\theta_k) \\
&\quad \times \sin(\theta_k)\sin(\phi)\big] && \text{(8.3c)}\\
h_{\phi\theta,\mathbf{k}} &= h_{\theta\phi,\mathbf{k}} && \text{(8.3d)}
\end{aligned}$$

where $Dk^2 = (2A/\mu_0 \mathrm{M}_s)k^2$ is the exchange field for a spinwave with wavevector $\mathbf{k}$, assuming that the wavelengths of interest are much larger than the lattice space, A is the exchange stiffness and $H_i = B\cos(\phi - \phi_H) - (M_s^0 - H_k)\sin^2(\phi)$ is the 'internal field' consisting of the component of the applied field B (at an angle ϕ_H to the plane) parallel to the magnetisation, which is at an angle, ϕ, to the static part of the anisotropy field (H_k),the demagnetising field and the anisotropy field H_k and the plane. The k-dependent demagnetisation factor for a film of thickness d is given by:

$$N_k = \frac{1 - e^{-kd}}{kd} \tag{8.4}$$

The susceptibility tensor, $\chi_{\mathbf{k}}(\omega)$, can be obtained from the linearised LLG equations. For an applied field with spatial frequency $\mathbf{k}$ and angular frequency ω, the transverse susceptibility tensor is given by:

$$\chi_{\mathbf{k}}(\omega) = \frac{1}{Z_{\mathbf{k}}} \begin{bmatrix} h_{\phi\phi,\mathbf{k}} + \frac{i\alpha\omega}{\omega_M} & -h_{\theta\phi,\mathbf{k}} + \frac{i\alpha\omega}{\omega_M} \\ -h_{\phi\theta,\mathbf{k}} - \frac{i\alpha\omega}{\omega_M} & h_{\theta\theta,\mathbf{k}} + \frac{i\alpha\omega}{\omega_M} \end{bmatrix} \tag{8.5a}$$

$$\begin{aligned} Z_{\mathbf{k}} = {} & h_{\theta\theta,\mathbf{k}} h_{\phi\phi,\mathbf{k}} - h_{\theta\phi,\mathbf{k}} h_{\phi\theta,\mathbf{k}} - (1+\alpha^2)\left(\frac{\omega}{\omega_M}\right)^2 \\ & + i\alpha\left(\frac{\omega}{\omega_M}\right)(h_{\theta\theta,\mathbf{k}} + h_{\phi\phi,\mathbf{k}}), \end{aligned} \tag{8.5b}$$

where $\omega_M = \gamma M_s^0$. The dispersion relation is obtained by noting that the $\mid Z_{\mathbf{k}} \mid$ is a minimum and susceptibility is at resonance when:

$$\omega = \omega_{\mathbf{k}} = \frac{\omega_M}{\sqrt{1+\alpha^2}} \left[h_{\theta\theta,\mathbf{k}} h_{\phi\phi,\mathbf{k}} - h_{\theta\phi,\mathbf{k}} h_{\phi\theta,\mathbf{k}} \right]^{1/2}. \tag{8.6}$$

References

[1] J. Frenkel and J. Dorfman. Spontaneous and induced magnetisation in ferromagnetic bodies. *Nature*, 126:274–275, 1930.

[2] T. W. McDaniel. Ultimate limits to thermally assisted magnetic recording. *J. Phys. Cond. Matt.*, 17(7):R315, 2005.

[3] R. Wood. The feasibility of magnetic recording at 1 terabit per square inch. *IEEE Trans. Magn.*, 36(1):36–42, 2000.

[4] L. Neel. *Selected Works of Louis Néel*. Gordon and Breach, New York, 1988.

[5] J.D. Bean, C. P. Livingston. Superparamagnetism. *J. Appl. Phys*, S30:120S–129S, 1959.

[6] D. Suess, T. Schrefl, R. Dittrich, M. Kirschner, F. Dorfbauer, G. Hrkac, and J. Fidler. Exchange spring recording media for areal densities up to 10 tbit/in2. *J. Magn. Magn. Mater.*, 290291, Part 1:551 – 554, 2005.

[7] Ohashi and Y. Yasue. Newly developed inductive write head with electroplated conife film. *IEEE Trans. Magn*, 34:1462, 1998.

[8] E. Callen H. B. Callen. The present status of the temperature dependence of magnetocrytalline anisotropy, and the z(z+1)/2 power law. *J. Phys. Chem. Solids*, 27:1271–1285, 1966.

[9] Steven D. Granz and Mark H. Kryder. Granular $l1_o$ fept (0 0 1) thin films for heat assisted magnetic recording. *J. Magn. Magn. Mater*, 324(3):287 – 294, 2012.

[10] R. F. L. Evans and W. J. Fan. Atomistic simulation of sub-nanosecond non-equilibrium field cooling processes for magnetic data storage applications. *Appl. Phys. Lett.*, 105(19), 2014.

[11] Vincent Sokalski, David E. Laughlin, and Jian-Gang Zhu. Experimental modeling of intergranular exchange coupling for perpendicular thin film media. *Appl. Phys. Lett.*, 95(10):102507, 2009.

[12] G. Hrkac T. Schrefl Y. Ikeda et al C. Morrison, L. Saharan. Inter/intra granular exchange and thermal activation in nanoscale granular magnetic materials. *Appl. Phys. Lett*, 99:132507, 2011.

[13] R. D. McMichael. Ferromagnetic resonance linewidth models for perpendicular media. *J. Appl. Phys.*, 95(11):7001, 2004.

[14] R.D. McMichael and P. Krivosik. Classical model of extrinsic ferromagnetic resonance linewidth in ultrathin films. *IEEE Trans. Magn.*, 40(1):2–11, Jan 2004.

[15] P. Krone, M. Albrecht, and T. Schrefl. Micromagnetic simulation of ferromagnetic resonance of perpendicular granular media: Influence of the intergranular exchange on the Landau-Lifshitz-Gilbert damping constant. *J. Magn. Magn. Mater.*, 323(5):432–434, 2011.

[16] A. Butera. Ferromagnetic resonance in arrays of highly anisotropic nanoparticles. *EPJ B*, 52(3):297–303, 2006.

[17] Nan Mo, Julius Hohlfeld, Misbah ul Islam, C. Scott Brown, Erol Girt, Pavol Krivosik, Wei Tong, Adnan Rebei, and Carl E. Patton. Origins of the damping in perpendicular media: Three component ferromagnetic resonance linewidth in co-cr-pt alloy films. *App. Phys. Lett.*, 92(2):022506, 2008.

[18] D. A. Garanin. Fokker-planck and landau-lifshitz-bloch equations for classical ferromagnets. *Phys. Rev. B*, 55:3050–3057, 1997.

[19] O Chubykalo-Fesenko D Hinzke, U Nowak and RW Chantrell. Llb micromagnetic models for ultrafast magnetisation processes. *HYSTERESIS MODELING AND MICROMAGNETICS*, page 101, 2009.

[20] P. Asselin, R. F. L. Evans, J. Barker, R. W. Chantrell, R. Yanes, O. Chubykalo-Fesenko, D. Hinzke, and U. Nowak. Constrained monte carlo method and calculation of the temperature dependence of magnetic anisotropy. *Phys. Rev. B*, 82:054415, Aug 2010.

[21] M. F. Toney J. A. Hedstrom J. U. Thiele, K. R. Coffey and A. J. Kellock. Temperature dependent magnetic properties of highly chemically ordered fe55xnixpt45l10 films. *J. Appl. Phys.*, 91:6595, 2002.

[22] O. Kitakami T. Miyazaki Y. Shimada S. Okamoto, N. Kikuchi and K. Fukamichi. Chemical-order-dependent magnetic anisotropy and exchange stiffness constant of fept (001) epitaxial films. *Phys. Rev. B*, 66:024413, 2002.

[23] W. F. Brown. Thermal fluctuations of a single-domain particle. *Phys. Rev.*, 130:1677–1686, Jun 1963.

[24] W. F. Brown. Thermal fluctuation of fine ferromagnetic particles. *IEEE Trans. Magn.*, 15(5):1196–1208, Sep 1979.

[25] R. F. L. Evans, Q Coopman, S. Devos, W. J. Fan, O. Hovorka, and R. W. Chantrell. Atomistic calculation of the thickness and temperature dependence of exchange coupling through a dilute magnetic oxide. *J. Phys. D*, 47(50):502001, 2014.

[26] V. M. Kalita A. F. Lozenko P. A. Trotsenko et al A. A. Timopheev, S. M. Ryabchenko. The influence of intergranular interaction on the magnetization of the ensemble of oriented stonerwohlfarth nanoparticles. *J. Appl. Phys.*, 105:083905, 2009.

[27] P Erdos. Theory of ion pairs coupled by exchange interaction. *Phys. Chem. Solids*, 27:1705–1720, 1966.

[28] James H. Giusti Lei Wang, Shaoping Li and Juan Fernandez de Castro. Micromagnetic study of effect of media intergranular exchange interaction in perpendicular recording. *J. Apl. Phys.*, 91:8381–8381, 2002.

[29] N. Kazantseva, D. Hinzke, R. W. Chantrell, and U. Nowak. Linear and elliptical magnetization reversal close to the curie temperature. *EPL*, 86(2):27006, 2009.

[30] O. Chubykalo-Fesenko, U. Nowak, R. W. Chantrell, and D. Garanin. Dynamic approach for micromagnetics close to the curie temperature. *Phys. Rev. B*, 74:094436, 2006.

[31] Jessada Chureemart. Orientation and thermal stability of advanced recoding media. *The Univeristy of York*, page 41, 2013.

[32] D. A. Garanin and O. Chubykalo-Fesenko. Thermal fluctuations and longitudinal relaxation of single-domain magnetic particles at elevated temperatures. *Phys. Rev. B*, 70:212409, 2004.

[33] R. F. L. Evans, D. Hinzke, U. Atxitia, U. Nowak, R. W. Chantrell, and O. Chubykalo-Fesenko. Stochastic form of the landau-lifshitz-bloch equation. *Phys. Rev. B*, 85:014433, 2012.

[34] U. Atxitia, O. Chubykalo-Fesenko, N. Kazantseva, D. Hinzke, U. Nowak, and R. W. Chantrell. Micromagnetic modeling of laser-induced magnetization dynamics using the landau-lifshitz-bloch equation. *Appl. Phys. Lett.*, 91(23), 2007.

[35] Y. Peng, X. W. Wu, J. Pressesky, G. P. Ju, W. Scholz, and R. W. Chantrell. Cluster size and exchange dispersion in perpendicular magnetic media. *J. Appl. Phys.*, 109(12), 2011.

[36] T.W. Clinton, N. Benatmane, J. Hohlfeld, and E. Girt. *J. Appl. Phys.*, 103:075546, 2008.

[37] E Beaurepaire, J.-C. Merle, A Daunois, and J.-Y. Bigot. Ultrafast spin dynamics in ferromagnetic nickel. *Phys. Rev. Lett.*, 76(22):4250–4253, 1996.

[38] I Radu, K Vahaplar, C Stamm, T Kachel, N Pontius, H A Dürr, T A Ostler, J Barker, R F L Evans, R W Chantrell, A Tsukamoto, A Itoh, A. Kirilyuk, Th Rasing, A. V. Kimel, and H a Dürr. Transient ferromagnetic-like state mediating ultrafast reversal of antiferromagnetically coupled spins. *Nature*, 472(7342):205–8, 2011.

[39] K Vahaplar, A. Kalashnikova, A. V. Kimel, D Hinzke, U Nowak, R Chantrell, A Tsukamoto, A Itoh, A. Kirilyuk, and Th Rasing. Ultrafast path for optical magnetization reversal via a strongly nonequilibrium state. *Phys. Rev. Lett.*, 103(11):117201, 2009.

[40] T A. Ostler et al. Ultrafast heating as a sufficient stimulus for magnetization reversal in a ferrimagnet. *Nat. Comm.*, 3:666, 2012.

[41] U. Atxitia, J. Barker, R. W. Chantrell, and O. Chubykalo-Fesenko. Controlling the polarity of the transient ferromagneticlike state in ferrimagnets. *Phys. Rev. B*, 89(22):224421, 2014.

[42] J. Becker, O. Mosendz, D. Weller, A. Kirilyuk, J. C. Maan, P. C. M. Christianen, Th. Rasing, and A. Kimel. Laser induced spin precession in highly anisotropic granular $l1_o$ fept. *Appl. Phys. Lett.*, 104(15):152412, 2014.

[43] Thomas A Ostler, Matthew O A Ellis, Denise Hinzke, and Ulrich Nowak. Temperature-dependent ferromagnetic resonance via the landau-lifshitz-bloch equation: Application to fept. *Phys. Rev. B*, 90(9):094402, 2014.

[44] Sangita Kalarickal, Nan Mo, Pavol Krivosik, and Carl Patton. Ferromagnetic resonance linewidth mechanisms in polycrystalline ferrites: Role of grain-to-grain and grain-boundary two-magnon scattering processes. *Phys. Rev. B*, 79(9):094427, 2009.

[45] A. Mekonnen, M. Cormier, A. V. Kimel, A. Kirilyuk, A. Hrabec, L. Ranno, and Th. Rasing. Femtosecond laser excitation of spin resonances in amorphous ferrimagnetic $Gd_{1-x}co_x$ alloys. *Phys. Rev. Lett.*, 107(11):117202, 2011.

[46] X. Zou, J. Wu, P. K. J. Wong, Y. B. Xu, R. Zhang, Y. Zhai, C. Bunce, and R. W. Chantrell. Damping in magnetization dynamics of single-crystal fe3o4/gan thin films. *J. Appl. Phys.*, 109(7):07D341, 2011.

[47] H. Nemoto, I. Takekuma, H. Nakagawa, T. Ichihara, Araki R., and Hosoe Y. *J. Magn. Magn. Mater.*, 320:3144, 2008.

[48] J.K. Chen, D.Y. Tzou, and J.E. Beraun. A semiclassical two-temperature model for ultrafast laser heating. *Int. J. Heat Mass Transfer*, 49(1-2):307–316, 2006.

[49] I. Radu, C. Stamm, A. Eschenlohr, F. Radu, R. Abrudan, K. Vahaplar, T. Kachel, N. Pontius, R. Mitzner, Holldack, K. Fhlisch, T. A. A. Ostler, J.H. Mentink, R.F.L. Evans, R. W. Chantrell, A. Tsukamoto, A. Itoh, A. Kirilyuk, A.V. Kimel, and Th. Rasing. *J. Spin*, 5:1550004, 2015.

[50] Lei Lu, Zihui Wang, Griffin Mead, Christian Kaiser, Qunwen Leng, and Mingzhong Wu. Damping in free layers of tunnel magneto-resistance readers. *Appl. Phys. Lett.*, 105(1):012405, 2014.

[51] R. D. McMichael, D. J. Twisselmann, and Andrew Kunz. Localized ferromagnetic resonance in inhomogeneous thin films. *Phys. Rev. Lett.*, 90(22):227601, 2003.

[52] Yuri P. Kalmykov, William T. Coffey, Unai Atxitia, Oksana Chubykalo-Fesenko, Pierre-Michel Déjardin, and Roy W. Chantrell. Damping dependence of the reversal time of the magnetization of single-domain ferromagnetic particles for the néel-brown model: Langevin dynamics simulations versus analytic results. *Phys. Rev. B*, 82(2):024412, 2010.

[53] M O A Ellis and R W Chantrell. Switching times of nanoscale fept: Finite size effects on the linear reversal mechanism. *Appl. Phys. Lett.*, 106:1–5, 2015.

[54] O. Heinonen and K. Z. Gao. Extensions of perpendicular recording. *J. Magn. Magn. Mater*, 320:2885–2888, 2008.

[55] G.P. Ju and et.al. High density heat-assisted magnetic recording media and advanced characterization-progress and challenges. *IEEE Trans. Magn.*, 51:3201709, 2015.

[56] X. D. Liu, Z. Xu, R. X. Gao, Z. F. Chen, T. S. Lai, J. Du, and S. M. Zhou. Single laser pulse induced dynamic magnetization reversal mechanism of perpendicularly magnetized l10 fept films. *J. Appl. Phys.*, 106(5), 2009.

[57] J. Barker, R. F. L. Evans, R. W. Chantrell, D. Hinzke, and U. Nowak. Atomistic spin model simulation of magnetic reversal modes near the curie point. *Appl. Phys. Lett.*, 97(19), 2010.

[58] R. F. L. Evans, R. W. Chantrell, U. Nowak, A. Lyberatos, and H.J. Richter. Thermally induced error: Density limit for magnetic data storage. *Appl. Phys. Lett.*, 100(10), 2012.

[59] H. J. Richter, A. Lyberatos, U. Nowak, R. F. L. Evans, and R. W. Chantrell. The thermodynamic limits of magnetic recording. *J. Appl. Phys.*, 111(3), 2012.

[60] R. W. Chantrell and E. P. Wohlfarth. Rate dependence of the field-cooled magnetisation of a fine particle system. *Phys. Status Solidi A*, 91(2):619–626, 1985.

[61] N. Kazantseva, D. Hinzke, R. W. Chantrell, and U. Nowak. Linear and elliptical magnetization reversal close to the curie temperature. *EPL*, 86(2):27006, 2009.

[62] J. Barker, R. F. L. Evans, R. W. Chantrell, D. Hinzke, and U. Nowak. Atomistic spin model simulation of magnetic reversal modes near the curie point. *Appl. Phys. Lett.*, 97(19), 2010.

[63] D. Weller and A. Moser. Thermal effect limits in ultrahigh-density magnetic recording. *IEEE Trans. Magn.*, 35(6):4423–4439, 1999.

[64] S. N. Piramanayagam. Perpendicular recording media for hard disk drives. *J. Appl. Phys.*, 102(1), 2007.

[65] Y. Honda, A. Kikukawa, Y. Hirayama, and M. Futamoto. Effect of soft magnetic underlayer on magnetization microstructure of perpendicular thin film media. *IEEE Trans. Magn.*, 36(52):2399–24012, 2000.

[66] B. R. Acharya, J. N. Zhou, M. Zheng, G. Choe, E. N. Abarra, and K. E. Johnson. Anti-parallel coupled soft under layers for high-density perpendicular recording. *IEEE Trans. Magn.*, 40(4):2383–2385, 2004.

[67] G. Choe, M. Zheng, E.N. Abarra, B.G. Demczyk, J.N. Zhou, B.R. Acharya, and K.E. Johnson. High-performance coptcro perpendicular media: optimizing exchange coupling and anisotropy orientation dispersion. *J. Magn. Magn. Mater.*, 287:159 – 166, 2005.

[68] A. Lyberatos and J. Hohlfeld. Model of thermal erasure in neighboring tracks during thermomagnetic writing. *J. Appl. Phys.*, 95(4):1949–1957, 2004.

[69] Sharat Batra, Werner Scholz, and Thomas Roscamp. Effect of thermal fluctuation field on the noise performance of a perpendicular recording system. *J. Appl. Phys.*, 99(8), 2006.

[70] R. E. Rottmayer, S. Batra, D. Buechel, W. A. Challener, J. Hohlfeld, Y. Kubota, L. Li, B. Lu, C. Mihalcea, K. Mountfield, K. Pelhos, C. Peng, T. Rausch, M. A. Seigler, D. Weller, and X. M. Yang. Heat-assisted magnetic recording. *IEEE Trans. Magn.*, 42(10):2417–2421, 2006.

[71] T. W. McDaniel, W. A. Challener, and K. Sendur. Issues in heat-assisted perpendicular recording. *Joint NAPMRC 2003. Digest of Technical Papers Perpendicular Magnetic Recording Conference*, page 66, 2003.

[72] K. Waseda, R. Doi, B. Purnama, S. Yoshimura, Y. Nozaki, and K. Matsuyama. Heat-assisted magnetization reversal using pulsed laser irradiation in patterned magnetic thin film with perpendicular anisotropy. *IEEE Trans. Magn.*, 44(11):2483–2486, 2008.

[73] C. Bunce, J. Wu, G. Ju, B. Lu, D. Hinzke, N. Kazantseva, U. Nowak, and R. W. Chantrell. Laser-induced magnetization switching in films with perpendicular anisotropy: A comparison between measurements and a multi-macrospin model. *Phys. Rev. B*, 81:174428, 2010.

[74] D. Atkinson and R. P. Cowburn. Heat-assisted magnetization switching in elongated submicrometer permalloy structures. *Appl. Phys. Lett.*, 85(8):1386–1388, 2004.

[75] M. H. Kryder, E. C. Gage, T. W. McDaniel, W. A. Challener, R. E. Rottmayer, G. Ju, Y. T. Hsia, and M. F. Erden. Heat assisted magnetic recording. *Proc. IEEE*, 96(11):1810–1835, 2008.

[76] W. A. Challener, Chubing. Peng, A. V. Itagi, D. Karns, Wei. Peng, Yingguo. Peng, XiaoMin. Yang, Xiaobin. Zhu, N. J. Gokemeijer, T. HsiaY, G Ju, Robert E. Rottmayer, Michael A. Seigler, and E. C. Gage. Heat-assisted magnetic recording by a near-eld transducer with efcient optical energy transfer. *Nat. Photon.*, 3(4):220–224, 2009.

[77] T. Y. Cheng, L. Atkinson, J. Wu, R. W. Chantrell, J. Sizeland, Y. M. Lu, J. W. Cai, and Y. B. Xu. Heat-assisted magnetization dynamics in gdfeco using field-induced tr-moke. *IEEE Trans. Magn.*, 50(11):1–4, 2014.

[78] A. J. Newell, W. Williams, and D. J. Dunlop. A generalization of the demagnetizing tensor for nonuniform magnetization. *J. Geophys. Res.*, 98(B6):9551–9555, 1993.